ON PHYSICAL PROCESSES OCCURRING IN THE HYDRODYNAMIC AND MAGNETOHYDRODYNAMIC ASTROPHYSICAL AND LABORATORY FLOWS

David Tsiklauri

Thesis presented for the degree of Doctor of Philosophy at the Physics Department of the

University of Cape Town
August 1996

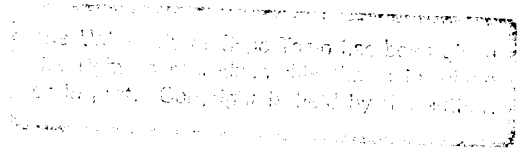

Papers contributing to the Ph. D. thesis

1. Rogava A.D. and Tsiklauri D.G., "The structure of the accretion disc boundary layer around a rotating, non-magnetized star", Astrophys. and Space Sci., **204**, 9, (1993).

2. Tsikarishvili E.G., Rogava A.D. and Tsiklauri D.G., "Relativistic, hot stellar winds with anisotropic pressure" Astrophys. J., **439**, 822, (1995).

3. Tsiklauri D. and Viollier R.D., "On possible signatures of heavy neutrino balls in active galactic nuclei", Mon. Not. Roy. Astron. Soc., **282**, 1299, (1996)

4. Chagelishvili G. D., Rogava A.D. and Tsiklauri D.G., "On effect of coupling and linear transformation of waves in shear flows", Phys. Rev. E, **53**, 6028, (1996).

5. Chagelishvili G. D., Rogava A.D. and Tsiklauri D.G., "compressible hydromagnetic shear flows with anisotropic thermal pressure: non-modal study of waves and instabilities", (submitted to Phys. Plasmas).

6. Tsiklauri D.G., "On the conical refraction of hydromagnetic waves in plasma with anisotropic thermal pressure", Phys. Plasmas, **3**, 800, (1996).

7. Tsiklauri D.G., "On the conical refraction of hydromagnetic waves in plasma with anisotropic thermal pressure: General consideration", Phys. Plasmas, **3**, 3902, (1996).

Contents

I. Abstract

Physics of hydrodynamic and magnetohydrodynamic flows is extensive, rapidly growing and important part of the physical science. It appears that in many cases space and laboratory plasma can be well described in the framework of the hydrodynamics or magnetohydrodynamics. In the present study we shall investigate several types of hydrodynamic and magnetohydrodynamic astrophysical and laboratory flows such as accretion disks and stellar (pulsar) winds and magnetized analog of the Couette flow, besides we also study certain basic plasma phenomena occurring in the medium under study.

The structure of the thesis is following:

In section II we study structure of a boundary layer of an accretion disk around non-magnetized, rotating stellar object. In particular (Rogava & Tsiklauri, 1993), we derive the most general equations governing structure of the boundary layer and investigate the system of the equations numerically. We proposed a method for determination of the initial conditions for the system, which gave us opportunity to obtain the numerical solutions. Basing on our model we quantitatively confirmed various statements about particular features and properties of the boundary layer scattered in the literature.

In section III we formulate our model (Tsikarishvili, Rogava & Tsiklauri, 1995) for relativistic, stellar (pulsar) wind with ultrarelativistic temperature basing on novel equations of state obtained in (Tsikarishvili et al., 1992). We were able to find analytical solutions of the set of relativistic hydromagnetic equations which govern the flow under consideration.

In section IV, basing on the standard theory of geometrically thin accretion disks, we investigate possible observational signatures of massive balls composed by heavy, degenerate neutrinos in the vicinity of the active galactic nuclei. Using our model (Tsiklauri & Viollier, 1996) we find that if a ball of heavy neutrinos, supported by degeneracy pressure, does exist in the vicinity of the active galactic nuclei, it will cause a bump in IR region of the emitted spectrum which is observed for several AGN (Malkan, 1989). We also find that if the bump at $\sim$1000K in the typical radio loud quasar 3C 273 spectrum is due to a neutrino ball, then our model implies mass of the black hole $10^8 M_\odot$, a ball mass of $4 \times 10^9 M_\odot$ and in turn, a neutrino mass of ~ 3 keV$/c^2$.

In section V we switch to investigation of magnetized shear flows. Although we do not constrain ourselves with application of our results to any concrete astrophysical object, it is evident that the results of our study (Chagelishvili, Rogava & Tsiklauri, 1996a; Chagelishvili, Rogava & Tsiklauri, 1996b) are applicable and relevant for a variety of the astrophysical and laboratory flows where presence of the shear is important. Basing on the novel mechanism of transformation of the magnetohydrodynamic waves in shear flow (Chagelishvili, Rogava & Tsiklauri, 1996a), we mainly focus our attention on the case when thermal pressure of the medium is anisotropic and investigate interplay of effect of presence of the shear with firehose

and mirror instabilities and demonstrate a novel phenomenon — double transformation (Chagelishvili, Rogava & Tsiklauri, 1996b).

In section VI we continue consideration of problems related with basic plasma phenomena. In particular, we show theoretically (Tsiklauri, 1996a; Tsiklauri, 1996b) that in the magnetized plasma with anisotropic thermal pressure under certain conditions there should occur novel phenomenon — phenomenon of the conical refraction, which as we shall see below is quite similar to the effect well known before in crystaloacoustics and crystalooptics. We also discuss possible ways of experimental corroboration of the predicted phenomenon and address a question about its feasible usage in plasma diagnostics.

II Geometrically Thin Disk Accretion Flows

II.1 introduction

It is widely known that accretion phenomenon is of great importance for various astrophysical problems. One of the reasons is that accretion is very effective and powerful mechanism for the generation of electromagnetic type radiation from the space objects. Conventional demonstration of the latter fact is given by the estimate the gravitational energy released via accretion of unit mass of the matter upon the object with mass M and radius R. Which apparently is $E_{\rm accretion} = GM/R$. For a typical neutron star (object of our special interest in the context of the present study) with $R \approx 10^6$cm and $M \approx M_\odot$ one gathers that $E_{\rm acc}$ is roughly 10^{20} ergs per gram of the accreted matter. In astrophysics alternative energy source of the radiation normally is the nuclear fusion reactions. For the most typical fusion reaction i.e. conversion of hydrogen into helium one can write that the energy yield per gram of matter is $E_{\rm nuclear} = 0.007c^2 = 6 \times 10^{18}$ erg/gram. Thus, even this crude order of magnitude estimate shows that accretion onto a neutron star is at least twenty times more efficient than the typical nuclear fusion reaction for the same amount of mass converted into the electromagnetic radiation. However, this is not the case for the white dwarfs ($R \approx 10^9$cm and $M \approx M_\odot$) for which the ratio $E_{\rm nuclear}/E_{\rm acc}$ can be 25–50. Of course, this is a consequence of a trivial fact that energetical yield from accretion crucially depends on the ratio R/M which is, basically, measure of the compactness of a particular astrophysical object.

Another essential point in the accretion process onto the compact objects, is importance of angular momentum of the accreting matter. In numerous cases, accreting matter cannot effectively get rid of its angular momentum which leads to the formation of the accretion disc around the central object. Vast amount of previous contributions revealed that an accretion disc is a kind of astrophysical flow which very efficiently extracts gravitational binding energy of the accreting matter and converts it into the radiation.

Besides, it is known (Pringle, 1981) that approximately half of the accretion luminosity may be generated in so called boundary layer (BL) of the disc. Therefore, study of this important fragment of the accretion disc should be of a particular interest. Below, we focus our attention on the investigation in some detail BL of the accretion disc around a rotating, non-magnetized neutron star. Further results of this section are mainly based on the paper by Rogava and Tsiklauri (1993).

First of all let us note what motivation one can have why the BL should do exist. In the standard accretion disc theory angular velocity is normally assumed to be Keplerian. However, it is clear that if an accretion disc is formed around a stellar object with weak

enough magnetic field, then its innermost part cannot be Keplerian since the angular velocity of the stellar object itself Ω_0 is always less then corresponding Keplerian value $\Omega_k(R) = \sqrt{GM/R^3}$. Where R stands for the radius of the star. Basically, under Ω_0 we mean angular velocity of the stellar surface (in principle, it is not necessary for a star to rotate as a rigid body). Typical maximal values of the Ω_0 for example for neutron stars are $0.77--0.90\,\Omega_k(R)$ (Friedman, Ipser & Parker, 1986). For larger values of Ω_0 the star simply will be destroyed by centrifugal forces or by gravitational instability to nonaxisymmetric perturbations. Then, it is obvious that when the accreting matter is close to merge the stellar object its angular velocity should decelerate from its Keplerian value to that one of the surface of the star i.e. Ω_0. Normally, the region where this deceleration process takes place is referred as a BL. Despite of its geometrical narrowness BL is very important constituent part of the accretion disc since, as we mentioned above, energy liberation process is exceedingly intense there. Before, we turn to the brief review of previous contributions to the study of the BL, its worth of mentioning why do we constrain ourselves with consideration only weakly magnetized stellar objects. The reason is that in the case of the strong enough magnetic fields at the surface of the star, accretion process occurs with more complicated geometrical form namely, the accretion column which of course needs separate consideration and is beyond the scope of the present study.

Importance of the BL in the accretion process was acknowledged almost at the same time as the accretion paradigm appeared itself. Lynden-Bell and Pringle (1974) considered relatively simple model of the BL assuming constant turbulent viscosity law and zero pressure in the BL. Pringle (1977) and Pringle and Savonije (1979) studied BL features in order to explain X-ray emission from the dwarf novae and proposed existence of strong shocks in the BL. Afterwards various authors investigated BL of the accretion discs around different types of astrophysical objects. In the context of the present study we must particularly mention contributions by Papaloizou and Stanley (1986) and by Stanley (1988) where authors introduced novel viscosity law. The latter one appears to be more relevant in the description of the BL rather than usual α viscosity law proposed by Shakura and Sunyaev (1973) which was and is widely used to describe outer regions (up to the BL) of an accretion disc. Besides, the former authors found certain instabilities in the BL and demonstrated their possible relevance in the treatment of quasi periodic oscillations in the low mass X-ray binaries (Stanley, 1988).

In general accretion disc theory is well developed and established. Traditional paradigm is use of equations of conservation of momentum and energy basing on the framework of hydrodynamics or hydromagnetics. However, one of the most important problem still remains to be unresolved — nature of viscosity in an accretion disc. Several phenomenological ideas were put forward. The most commonly used one is α viscosity law introduced by Shakura and Sunyaev (1973). However, in the region of the accretion disc like BL where we deal

with sharp gradients of the physical quantities the viscosity law must be modified. Following this reasonings we adopt modified viscosity prescription due to Papaloizou and Stanley (1986). Which was widely used in the subsequent literature (e.g. Lioure and Le Conte, 1994) including its further slight modifications (Popham and Narayan, 1992; Gordon, 1996).

Since general treatment of the BL is rather complicated task (partially from the mathematical point of view), further we make a number of simplifying assumptions which in fact are quite common for accretion disc theory. Namely, in order to avoid full thermodynamical treatment we adopt polytropic relationship between a surface density and vertically integrated pressure. Besides, we assume that the accretion takes place in a steady way i.e we drop all time derivatives. In the next subsection we derive the most general equations which govern accretion process in the BL and in the subsequent subsection present our numerical results. We also determine behaviour of the radiation intensity of the BL using the equation of the conservation of the energy. Finally, we discuss our results and compare them with existing qualitative notions.

II.2 main consideration

In the present study we consider stationary and axisymmetric disk around central stellar object with mass M and radius R. In what follows we neglect self gravity of the disk. We employ cylindrical coordinates (r, φ, z) choosing the rotational axis along z axis.

Further, we may write the equations for conservation of mass, radial momentum, angular momentum and energy for a geometrically thin disc as following (e.g. Straumann, 1984):

$$\dot{M} = -2\pi r S v_r = \text{const}, \tag{II.1}$$

$$v_r \frac{\partial v_r}{\partial r} = r\left(\Omega^2 - \Omega_k^2\right) - \frac{1}{S}\left(\frac{\partial W}{\partial r}\right), \tag{II.2}$$

$$S v_r \frac{\partial r^2 \Omega}{\partial r} = \frac{1}{r}\frac{\partial r^2 W_{\varphi r}}{\partial r}, \tag{II.3}$$

$$S v_r \frac{\partial}{\partial r}\left(\frac{v_r^2}{2} + \frac{r^2\Omega^2}{2} + (A+1)\frac{W}{S} + \Phi\right) = \frac{1}{r}\frac{\partial}{\partial r}\left(r^2 \Omega W_{\varphi r}\right) - Q^- \tag{II.4}$$

where all notations are standard. Namely, $\dot{M}$ stands for the accretion rate; v_r is the radial velocity and $\Omega \equiv v_\varphi / r$ is the angular velocity of the accreting matter; W, S and $W_{\varphi r}$ are vertically integrated (over z coordinate) pressure, surface density and turbulent viscosity tensor non-zero component accordingly; $\Omega_k \equiv \sqrt{GM/r^3}$ represents the Keplerian angular velocity; $\Phi \equiv -r^2\Omega_k^2$ is the gravitational potential; Q^- is the energy flux per unit area emitted from the disk surface; as regards constant A we give its definition below.

For the sake of completeness we present here the general equation of state which normally takes into account contributions from a gas and radiation pressures simultaneously

$$P = P_{\rm gas} + P_{\rm radiation} = \frac{k}{\mu m_{\rm H}}\rho T + \frac{aT^4}{3}. \tag{II.5}$$

The internal specific energy is given by equation

$$\varepsilon \equiv c_{\rm v}T + \frac{aT^4}{\rho} \equiv A(P/\rho)$$

where constant A is defined by the expression

$$A \equiv \frac{\beta}{\gamma - 1} + 3(1-\beta). \tag{II.6}$$

In the latter formula $\beta \equiv P/P_{\rm gas}$, $\gamma \equiv c_{\rm p}/c_{\rm v}$ (ratio of specific heats for constant pressure and volume accordingly). Note that in the regime when radiation pressure dominates in the BL then $A = 3$, whereas in the case of $P \simeq P_{\rm gas}$ (which, actually will be used throughout this study) $A = 3/2$.

For the only non-zero component of the turbulent viscosity tensor $W_{\varphi r}$ we use standard expression (Straumann, 1984)

$$W_{\varphi r} = rS\nu_t \frac{\partial \Omega}{\partial r} \tag{II.7}$$

where ν_t stands for the kinematic coefficient of the turbulent viscosity.

As far as at the later stage we use polytropic equation of state, we now adopt definition of the sound speed as following (Frank, King & Raine, 1992)

$$c_s^2 \equiv \frac{W}{S} \tag{II.8}$$

Further, using the latter definition and eqs.(II.1) and (II.7) we can rewrite the system of equations (II.2–II.4) in the following form

$$v_r\left[1 - \frac{c_s^2}{v_r^2}\right]\frac{\partial v_r}{\partial r} = r\left(\Omega^2 - \Omega_k^2\right) - \frac{\partial c_s^2}{\partial r} + \frac{c_s^2}{r}, \tag{II.9}$$

$$v_r\left(r^2\Omega - L_m\right) = r^2\nu_t\frac{\partial \Omega}{\partial r}, \tag{II.10}$$

$$v_r\frac{\partial v_r}{\partial r} + r\left(\Omega_k^2 - \Omega^2\right) - \left(r^2\Omega - L_m\right)\frac{\partial \Omega}{\partial r} + (A+1)\frac{\partial c_s^2}{\partial r} = \frac{2\pi r}{\dot{M}}Q^-, \tag{II.11}$$

where L_m is some integration constant which appeared after integration of the eq.(II.3).

We see that the equations (II.9–II.11) contain five unknown functions v_r, Ω, c_s, ν_t and Q^-. Therefore in order to obtain solution of the system it is necessary to impose at least two conditions relating some of the unknown physical quantities. For this purpose, normally, one admits some phenomenological expression for the viscosity law (i.e. for ν_t) and for

"cooling function" Q^-. The latter two steps can be recognized as the most weak points of the accretion disk paradigm. At one hand the accretion disks should be well described by the equations of motion for fully ionized plasma in a fixed gravitational field. On the other there is a poorly understood essential detail: In order to make it possible for a gas to accrete on a central object a stress is needed to remove the angular momentum form a particular fluid element. Therefore, transport of angular momentum is a central issue for accretion disk theories. In general two possible sources of the stress are proposed (Hawley and Balbus, 1995) — internal and external torques. External torques could be tidal forces (e.g. in binary systems) and/or magnetohydrodynamic winds. As regards internal torques these are normally atributted to the molecular and radiative viscosities. However, these viscosities are thought to be too small in the disks and their time scales can be comparable with the age of the universe. That is why an idea of some sort of "anomalous viscosity" was put forward. Traditionally, the anomalous viscosity is ascribed to the turbulent stress. However, origin of the turbulence in the disks always has been a problem because of their stability in the linear regime in respect to the hydrodynamic perturbations according to the Rayleigh's criterion. The latter inspired Shakura and Sunyaev, 1973 to assume that the disks can be turbulized at nonlinear stage of evolution of the perturbations. It is known that such kind of instabilities do exist in laboratory flows like, for instance, Couette flow. Nevertheless, it is questionable whether we can extrapolate this knowledge to the accretion disks. In a laboratory, flow always experiences effects from its boundaries, whereas in the case of accretion disk boundary effects (which are of considerable importance in terrestrial flows) are non-existent. In the present study we will pay no emphasis to this issue and will assume rather phenomenological treatment of the viscosity. In the same paper Shakura and Sunyaev proposed α-law for description of the turbulent viscosity, which afterwards became widely accepted in this field. However, as we mentioned above, Papaloizou and Stanley, 1986 introduced new viscosity prescription which is more relevant for the BL. Shakura & Sunyaev's α law for the kinematic viscosity due to turbulence reads as following:

$$\nu_t = \alpha c_s H \tag{II.12}$$

where α is a free parameter (usually assumed to vary in the range $0.01 \leq \alpha \leq 1$) and H is the half-thickness of the disk. The latter formula is based on the assumption that the turbulent eddies move with root mean square speed αc_s and have a mean free path roughly equal to the H. Eq.(II.12) can be reasonable for the outer, i.e. Keplerian parts of the disk. However, basing on general physical grounds it was argued in Papaloizou & Stanley, 1986 that in the BL region the mean free path of the turbulence should be taken as pressure-scale height in the radial direction rather than H. The natural measure of the former quantity can be represented by the following expression:

$$H_p = -W\frac{\partial W}{\partial r} \approx \frac{c_s^2}{r|\Omega_k^2 - \Omega^2|}.$$

When $\Omega \ll \Omega_k$ then $H_p \approx H^2/r \ll H$. Therefore, ν_t can be written as

$$\nu_t = \frac{\alpha c_s H}{1 + \beta r |\Omega_k^2 - \Omega^2| / (\Omega_k c_s)}$$

where β stands for a constant of order unity. The latter formula implies that in Keplerian part of the disk (where $\Omega = \Omega_k$) ν_t tends to the usual α-law (II.12). Whereas in the BL $\nu_t \sim \alpha c_s H_p/\beta$, which basically accounts for the fact that H_p was taken as mean free path of the turbulent eddies. In this study we use slightly modified form of the ν_t, namely, we have just eliminated H using the usual expression $H \approx c_s/\Omega_k$, which results in

$$\nu_t = \frac{\alpha c_s^3}{c_s \Omega_k + \beta r (\Omega_k^2 - \Omega^2)}. \tag{II.13}$$

As we already mentioned above, we adopt polytropic relationship between the vertically integrated pressure W and the surface density S

$$W = K S^{1+1/n} \tag{II.14}$$

where K and n stand for a polytropic constant and polytropic index respectively. The latter step has the following advantage: the adoption of the polytropic relationship makes it possible to solve the system of equations without usage of the energy equation (Stanley, 1988). Thus, we do not restrict ourselves by any kind of assumptions normally imposed on the "cooling function" Q^-. Just contrary to that after we find numerically the main kinematic physical quantities Ω, v_r and c_s we recover behavior of the Q^-, which turned out to be in accordance with general physical grounds.

Combining Eqs.(II.1), (II.8) and (II.14) we can get following algebraic relationship between v_r and c_s

$$|v_r| = \left(\frac{\dot{M} K^n}{2\pi}\right) \frac{1}{r c_s^{2n}}. \tag{II.15}$$

Further, using the latter equation in the Eq.(II.2) we arrive at

$$c_s \frac{\partial c_s}{\partial r} = -\frac{r (\Omega_k^2 - \Omega^2)}{2(n+1)}. \tag{II.16}$$

The next step we undertake is to substitute Eqs.(II.15) and (II.13) into Eq.(II.10) which results in

$$\frac{\partial \Omega}{\partial r} = -\left(\frac{\dot{M} K^n}{2\pi}\right) \frac{(r^2\Omega - r_m^2 \Omega_m)\,[c_s \Omega_k + \beta r (\Omega_k^2 - \Omega^2)]}{\alpha r^3 c_s^{2n+3}} \tag{II.17}$$

where instead of L_m [introduced in Eq.(II.10)] we put $L_m \equiv r_m^2 \Omega_m$. In the latter definition r_m and Ω_m denote respectively the values of radial distance from the stellar object and the angular velocity at the point where Ω attains its maximal value. Such choice of the integration constant L_m has a lucid physical explanation: at the distance r_m the derivative of angular velocity should vanish.

Let us mention that equations (II.16) and (II.17) already have a solvable form since they contain only two unknown physical quantities Ω and c_s.

Further on we introduce following dimensionless variables:

$$x \equiv r/R, \quad \omega \equiv \Omega/\Omega_k(R), \quad c \equiv c_s/\left(R\Omega_k(R)\right), \quad v \equiv v_r/\left(R\Omega_k(R)\right). \tag{II.18}$$

Here we recall that by R we denoted radius of the stellar object.

Taking into account the latter definitions we can rewrite Eqs.(II.16) and (II.17) in the dimensionless form

$$\frac{\partial c}{\partial x} = \frac{x\left(\omega^2 - 1/x^3\right)}{2(n+1)c} \tag{II.19}$$

and

$$\frac{\partial \omega}{\partial x} = -\left(v_0 c_0^{2n}\right) \frac{\left(x^2\omega - \varepsilon\right)\left[c/x^{3/2} + \beta x\left(1/x^3 - \omega^2\right)\right]}{\alpha x^3 c^{2n+3}} \tag{II.20}$$

where $v_0 \equiv v(x=1)$ and $c_0 \equiv c(x=1)$ denote values of the dimensionless radial velocity and sound speed at the surface of the stellar object. Besides, we introduced another constant ε which is defined by $\varepsilon \equiv \left(r_m/R\right)^2\left(\Omega_m/\Omega_k(R)\right)$. Before we turn to the presentation of our numerical work, it is useful at this stage to have an idea what reasonable value the newly introduced constant ε can have. We mentioned above that BL constitutes a narrow region of the disk. We can simply justify this statement by following simple, order of magnitude estimate (Pringle, 1977; Frank, King & Raine, 1992). In the Keplerian region of a geometrically thin accretion disk dominating terms in the radial component of the Eulers equation [Eq.(II.2)] are centrifugal term ($r\Omega^2$) and gravity term ($r\Omega_k^2$). But, in the BL as we know $\Omega < \Omega_k$ (or even in the vicinity of the star's surface $\Omega \ll \Omega_k$ if it rotates slowly). Therefore, the gravity term in the BL must be compensated either by $v_r\frac{\partial v_r}{\partial r}$ or by the pressure gradient $\frac{1}{S}\frac{\partial W}{\partial r}$. We can set roughly $\frac{\partial}{\partial r} \sim \frac{1}{b}$, where under b we imply width of the BL. Therefore, the former term can be estimated as v_r^2/b and the latter one (pressure gradient) as c_s^2/b (here we used straightforward relation $W = c_s^2 S$). The next step is usage of fact that radial velocity of the accreting flow should be less then the sound speed in the BL, otherwise the presence of the central star cannot be communicated outwards (Pringle, 1977). Thus, we conclude that the gravity term from the Eq.(II.2) can be compensated by the pressure gradient

$$\frac{c_s^2}{b} \sim R\Omega_k^2 = \frac{GM}{R^2}.$$

Note that we used R instead of r since the latter estimate is valid only in the BL or roughly at the stellar surface. On the other hand we know from the standard theory of the geometrically thin accretion disks that $H \approx c_s/\Omega_k$. Finally, we can incorporate our above statements in the following formula (Pringle, 1977; Frank, King & Raine, 1992)

$$b \sim \frac{R^2}{GM}c_s^2 \sim \frac{H^2}{R} \ll H \ll R \tag{II.21}$$

Therefore, since we just have shown that the BL is quite narrow we may imply that $r_m \sim R$ (in other words r_m, the point where Ω attains its maximal value, can be taken as outer boundary of the BL and this distance is approximately equal but slightly *more* than the radius of the stellar object). The same reasonings apply to the Ω_m: it is slightly *less* but approximately equal to the $\Omega_k(R)$. Therefore, as regards the parameter ε which we introduced before we can safely take it as $\varepsilon \equiv (r_m/R)^2 (\Omega_m/\Omega_k(R)) = x_m^2 \omega_m \approx 1$.

Further, as we said above, we use equation of the energy conservation to obtain expression for radiation intensity Q^- in terms of kinematical physical quantities whose behavior can be found numerically. Since we are in possession of the solvable system Eqs.(II.19) and (II.20) we write Q^- in terms of ω and c. Introducing dimensionless radiation intensity q^- as

$$q^- = \frac{2\pi R^3}{GM\dot{M}} Q^- \tag{II.22}$$

finally we can obtain

$$q^- = \left(\frac{n-A}{n+1}\right)\left(\frac{1}{x^3-\omega^2}\right) - \frac{(x^2\omega - \varepsilon)}{x}\frac{\partial \omega}{\partial x}. \tag{II.23}$$

In the next subsection we outline method which we have used for the determination of the initial conditions for the system of Eqs.(II.19) and (II.20), and represent and discuss results of our numerical work.

II.3 numerical calculations and discussion of the results

In the previous subsection we obtained closed system of equations for ω and c. To solve the system it is needed to specify the initial conditions which should have reasonable physical sense. First step of this task is specification $\omega(x = 1)$ i.e. angular velocity of the accreting matter at the stellar surface which should be essentially the angular velocity of the star. We know that the there is an upper limit for the latter physical quantity, since any star (even most rapidly rotating neutron star) will be disrupted by centrifugal forces if its angular velocity exceeds some threshold value. It was found (Friedman, Ipser & Parker, 1986) that the threshold value varies in the range $\omega_0^{\max} \approx 0.77 - -0.90$. On the other hand it is also clear that effect of the BL is more significant for slowly rotating stars (since the accreting matter ends up with the angular velocity of the stellar object, as less the latter quantity than the $\Omega_k(R)$ is as stronger shear forces are experienced by the matter). Therefore, it is useful to investigate the case when stellar object is rotating slowly. In our numerical calculations we choose as initial conditions three values of the of the angular velocity, namely $\omega_0^{(1)} = 0$, $\omega_0^{(2)} = 0.2$ and $\omega_0^{(3)} = 0.4$. Since in the BL ω is less than Keplerian angular velocity (which in dimensionless units is just $1/\sqrt{x^3}$) then it is evident from the Eq.(II.19) that the derivative

of sound speed $\partial c/\partial x$ should be negative. If we introduce dimensionless width of the BL according to the Eq.(II.21) as $\Delta \equiv (H/R)^2 \simeq c^2(x=1)$ then it is reasonable to parameterize the derivative of the sound speed in the interval $1 \leq x \leq \Delta$ as $\partial c/\partial x \simeq -kc/x$. In the latter expression we introduced some positive constant k which essentially will be used to parameterize the slope of the $c(x)$ at the initial point $x = 1$. Therefore, using Eq.(II.19) we can obtain following expression for $c(x=1) \equiv c_0$

$$c_0 \simeq \sqrt{\frac{1-\omega_0^2}{2k(n+1)}}. \tag{II.24}$$

In our numerical calculations we used following representative values for n and k: $n = 1$ and $k = 100$. Hence, in this case we can obtain initial values for the sound speed $c_0^{(1)} = 0.0500$, $c_0^{(2)} = 0.0490$, $c_0^{(1)} = 0.0458$.

Finally, we can acquire initial values for the radial velocity making use of the Eq.(II.20). For this purpose, bearing in mind narrowness of the BL, we shall estimate the derivative of the angular velocity at point $x = 1$ as

$$\left(\frac{\partial \omega}{\partial x}\right)_{x=1} \simeq \frac{\omega_m - \omega_0}{x_m - 1} \tag{II.25}$$

Taking into account the estimates $x_m \simeq 1 + \Delta \simeq 1 + c_0^2$ and $\omega_m = \varepsilon/x_m^2 \approx 1/(1+c_0^2)^2$ we can rewrite Eq.(II.25) as following

$$\left(\frac{\partial \omega}{\partial x}\right)_{x=1} \simeq \frac{1-\omega_0(1+c_0^2)^2}{c_0^2(1+c_0^2)^2} \tag{II.26}$$

Further, substituting Eq.(II.26) into Eq.(II.20) and writing the latter one in the point $x = 1$ we arrive at

$$v_0 = \frac{\alpha c_0 \left[1-\omega_0(1+c_0^2)^2\right]}{(1+c_0^2)^2(1-\omega_0)[c_0+\beta(1-\omega_0^2)]}. \tag{II.27}$$

Substituting in the Eq.(II.27) previously obtained values for ω_0 and c_0; and choosing reasonable values for the viscosity parameters α and β as $\alpha = 0.1$ and $\beta = 1$ (recall that usual range for alpha is $0.01 \leq \alpha \leq 1$ and beta should be of order of unity) we finally acquire initial values for the radial velocity $v_0^{(1)} = 0.0047$, $v_0^{(2)} = 0.0048$, $c_0^{(1)} = 0.0051$.

Results of our numerical calculations for kinematic physical quantities using initial conditions obtained above are presented on the Figs. II.1–II.3. In particular, On the Fig. II.1 we plot the angular velocity curves along with the curve of the Keplerian angular velocity which looks like a straight line due to the narrowness of the BL. We gather from the graph that the behavior of the angular velocities is in accordance with general physical grounds, namely, in the outer part of the BL the curves deviate from the Keplerian angular velocity curve then attain certain maximal value and finally end up in the points corresponding to

the appropriate values of the stellar angular velocity. This fact can be considered as a proof that our method for the determination of the initial conditions is fairly relevant.

In the Fig.II.2 we present our results for the sound speed. Again we may state that the behavior of the curves is in consonance with previous contributions, in particular, we see that the sound speed is increasing by its magnitude as accreting matter comes closer to the stellar surface. On the other hand dimensionless half-thickness of the disk is related to the sound speed via formula $H/R \simeq c(x)$, which essentially means that the shape of the half-thickness of the disk is roughly the same as one of the sound speed curves. Widening of the BL to its base was qualitatively pointed out by Shakura and Sunyaev (Shakura & Sunyaev, 1988) which is in accordance with our results.

Fig. II.3 represents the set of curves for the radial velocity of the accreting inflow of the matter. We gather form the graph that in the BL the matter decelerates all the way until the stellar surface. Similar kind of behavior was also obtained by Papaloizou and Stanley (Papaloizou & Stanley, 1986) which clarifies relevance of our treatment of the BL.

On the Fig.II.4 we plot radiation intensity q^- calculated by Eq.(II.23) versus the distance from the stellar surface using the same set of initial conditions. It can be clearly seen from the graph that radiation intensity increases rapidly and attains highest value at inner edge of the BL. Besides, we see that the maximal radiation intensity is achieved in the case of non rotating stellar object and it drops with increase of angular velocity of the star. This is in accordance with results from (Pringle, 1981) and with general physical grounds indeed.

Finally, we would like to emphasize that there were many assumptions adopted while formulating our model for the BL. However, obtained results clarify that previous qualitative treatments and notions of the BL (e.g. Frank, King and Raine, 1992; Shakura & Sunyaev, 1988) where correct in their basis. We can state that we achieved main goal of this study — basing on our model we confirmed *quantitatively* various statements about particular features of the BL around a rotating, non-magnetized stellar object scattered in the literature.

III Relativistic, Hot Stellar Winds with Anisotropic Thermal Pressure

III.1 introduction

In this section we consider yet another problem which is related with physics of magneto-hydrodynamic flows, namely basing on the model (Tsikarishvili, Rogava and Tsiklauri, 1995) we shall investigate properties of the relativistic, hot stellar (pulsar) winds. It can be stated that problem of stellar winds is quite natural continuation of the study presented in the previous section. Essentially, the winds are yet another class of solutions of the Euler's hy-

drodynamic (hydromagnetic) equation. It is well-known (e.g. Frank, King and Raine, 1992) that classification of the solutions (we shall mention only physical solutions and ones of the astrophysical interest) of the equation is as following: (i) inflow of the accreting matter; (ii) stellar wind; and (iii) stellar breeze. The term for the latter class of solutions comes from the fact the it always remains subsonic and essentially represents slowly sinking atmosphere of a star. Whereas, type (ii) solution passes through sonic point (besides, if the magnetic field is present it passes through the points where radial velocity becomes coincident with slow and fast magnetosonic velocities as well). These general statements apply to all kinds of stellar winds but our aim is to investigate physical processes occurring in the relativistic pulsar wind with ultrarelativistic temperature and anisotropic thermal pressure employing magnetohydrodynamical treatment. Therefore, we should take into account specific features characteristic for such a plasma medium. Namely, we make use of novel equations of state relevant for the case of ultrarelativistic temperature obtained in Tsikarishvili et al., 1992. But at first we shall briefly review previous contributions to this topic.

Generally speaking, stellar winds belong to the type of astrophysical flows which were extensively studied for quite a long time. The basis of the theory of the hydrodynamic expansion of extended stellar atmospheres (thermally driven winds) was constructed by Parker (1963). Considering a stationary and spherically symmetric thermal wind, Parker has demonstrated the existence of a sonic critical point, where the radial flow speed reaches the local speed of sound and the flow becomes hypersonic. However, it was evident that for stars with fast rotation and strong magnetic fields the azimuthal motion of the plasma and the corresponding angular momentum transfer cannot be neglected. Weber and Davis (1967) have considered stellar winds taking into account these effects for a nonrelativistic stellar wind in the star's equatorial plane. Three critical points (sonic, Alfven and supersonic) were found and the solutions passing through these points where constructed. Mestel (1968) studied stellar wind with the poloidal magnetic field, which is approximately dipolar at the star surface. The strength of the field is sufficient to force the flow to corotate with the star. At the large distances, beyond the light cylinder, the plasma flow carries outward the field lines, almost conserving the angular momentum of the flow elements.

The discovery in the late sixties of pulsars, quasars and relativistic bipolar outflows (jets) stimulated theoretical studies of relativistic stellar winds. Michel (1969) made a generalization of the paper by Weber and Davis for the case of a wind, flowing with a relativistic velocity out of a fast rotating neutron star with an extremely high magnetic field and zero temperature. Michel neglected pressure and gravity, and hence sonic and magnetosonic points did not appear in his work. A solution was obtained by assuming a "minimum torque critical condition", which essentially means that the pulsar wind adjusts to minimize the torque to the star. Goldreich and Julian (1970) extended the analysis for the case of finite, but nonrelativistic temperatures. They found a solution by means of the requirement of

smooth passing of the flow through the three critical points and obtained the results of Michel's (1969) "Minimum torque" solution as a special subcase of their own ones.

Further generalization of the theory was presented in Kennel et al. (1983) where Michel's (1969) cold relativistic wind model was generalized to finite temperatures and relativistic injection speeds; and Goldreich and Julian's (1970) cool isothermal wind model was replaced by a more realistic hot adiabatic one. The authors investigated a fully relativistic MHD model of a stationary hot stellar wind with a monopole magnetic field. It was clearly shown that relativistic temperatures seriously affect the MHD solutions established in the preceding considerations. In particular, high Mach numbers were reached only for hot relativistic stellar winds. Authors of Gedalin et al. (1991) considered a two dimensional MHD model of a relativistic hot stellar wind and generalized the results of Kennel et al. (1983) and Okamoto (1978) for the outflow along the poloidal field lines. They investigated the flow topology and studied the asymptotical θ-dependence of the solution.

Most of the expanding astrophysical flows are highly magnetized. Note that in *collisionless* plasma outflows from the star, the influence of the field considerably increases. In such a medium, the Lorentz force $eZ\vec{v}\times\vec{B}$ acts on charged particles. The force is exerted only in the plane normal to the field lines. Hence, the particles do not have equal freedom in moving along or transverse to the field lines. This leads to the anisotropy of thermal pressure and temperature. One should note that the anisotropy will be maintained due to the lack of collisions in the plasma. The medium will be reduced, in turn, to two independent subsystems (transverse and parallel in respect to the field lines) which will not be in thermodynamical equilibrium with each other. The thermal anisotropy plays an important role in the consideration of outflows from astrophysical objects like the Sun, highly magnetized pulsars, jets etc.

Tan and Abraham (1972) studied solar wind properties taking into account the pressure anisotropy effect. In their paper, the following polytropic laws were adopted:

$$P_{\|} = C_{\|}\rho\left(\frac{\rho}{B}\right)^{2\alpha}, \quad P_{\perp} = C_{\perp}\rho B^{\delta}$$

where $C_{\|}$ and $C_{\perp}$ are constants and α and δ are polytropic indices for the parallel and transverse components of pressure. A case $\alpha = \delta = 1$ corresponds to the well-known equations of state by Chew, Goldberger and Low (1956). When $\alpha = \delta = 0$ then this case represents an isothermal process. In the paper of Tan & Abraham (1972) numerical simulations where carried out for $0 \leq \alpha \leq 0.19$ and $0.08 \leq \delta \leq 0.302$ for best fitting of the observational data. Asseo and Beauflis (1983) have considered relativistic, anisotropic pulsar wind with non relativistic temperature i. e. they used the Chew, Goldberger and Low (1956) equations of state contrary to the case considered in this study.

It is widely acknowledged that a strong magnetic field exists at the surface of a neutron star and in the relativistic magnetospheric plasma surrounding the star. The plasma particles

flow along open magnetic field lines and lead to the formation of the magnetized relativistic wind. It is known that synchrotron-radiation losses considerably change the properties of the strongly magnetized collisionless plasmas of pulsar winds. Radiative losses lead to the noticeable reduction of the plasma particles momentum transverse components $p_\perp$. The process, in turn, leads to the establishment of a pressure anisotropy $P_{||} \gg P_\perp$ in these flows. Pressure anisotropy leads to the changes of the overall properties of such a medium. Its consideration must be based on the magnetohydrodynamical model of relativistic plasma with the anisotropic pressure tensor. When the plasma temperature is nonrelativistic, the magnetohydrodynamical model of Chew, Goldberger and Low (1956) is fully relevant. For ultrarelativistic temperatures, as was shown in Tsikarishvili et al. (1992) the canonical equations of state from Chew, Goldberger and Low (1956) are replaced by new equations of state. In particular,

$$P_{||} = \begin{cases} const\rho^3/|h|^2, & \text{for nonrelativistic temperatures;} \\ const\rho^2/|h|, & \text{for ultrarelativistic temperatures ;} \end{cases} . \qquad (III.1a)$$

$$P_\perp = \begin{cases} const\rho|h|, & \text{for nonrelativistic temperatures;} \\ const\rho\sqrt{|h|}, & \text{for ultrarelativistic temperatures ;} \end{cases} . \qquad (III.1b)$$

where $|h|$ is defined below by eq. (III.5).

It is interesting to note that if we rewrite covariant quantities in ultrarelativistic temperature limit from (III.1) into its classical form, we get that this will be equivalent to the case $\alpha = \delta = 0.5$.

In the present study we consider the ultrarelativistic region of a relativistic pulsar wind with a strong magnetic field. We assume that the temperature becomes ultrarelativistic beyond the light cylinder and restrict our consideration to this region. Using the explicit form of the stress-energy tensor for such a medium obtained in Tsikarishvili et al. (1992) we have written a closed set of conservation equations and analyze their properties. A representative analytic solution is also found and compared with the one of the existing in conventional models.

Our present study is a further generalization of Asseo & Beauflis (1983) to ultrarelativistic temperatures and Kennel et al. (1983) to anisotropic pressures.

III.2 main consideration

We shall work in a conventional Minkowskian space-time metric, writing its spatial part in spherical polar coordinates (r, θ, φ):

$$ds^2 = -c^2dt^2 + dr^2 + r^2(d\theta^2 + \sin^2\theta d\varphi^2). \qquad (III.2)$$

General-Relativistic corrections should be essential *nearby* the pulsar surface. However in the present paper we intend to consider a pulsar wind mostly *beyond* the light cylinder, i.e. at large enough radial distances, were metric (III.2) describes space-time geometry with sufficient accuracy.

Hereafter we shall use the following notations: (a) greek indices will range over t, r, θ, φ and represent space-time coordinates, components, etc.; (b) latin indices will range over r, θ, φ and represent coordinates in the three-dimensional spatial part of the metric (III.2). Note that the signature of the metric is +2.

The stress-energy tensor for collisionless, strongly magnetized plasma of the pulsar wind with anisotropic pressure may be written in the following way (Tsikarishvili et al. 1992):

$$T^{\alpha\beta} = \left[e + P_\perp + \frac{|h|^2}{4\pi}\right] u^\alpha u^\beta + \left[P_\perp + \frac{|h|^2}{8\pi}\right] g^{\alpha\beta} + \left[\frac{(P_\parallel - P_\perp)}{|h|^2} - \frac{1}{4\pi}\right] h^\alpha h^\beta. \qquad \text{(III.3)}$$

Here all notations are standard: u^α denotes the components of the plasma particles 4-velocity ($g_{\alpha\beta} u^\alpha u^\beta = -1$); $P_\parallel$ and $P_\perp$ are the parallel and transverse components of the plasma pressure (in respect to the magnetic field direction); e is the total specific energy density; and h^α are components of Lichnerowicz 4-vector of magnetic field, defined as (Lichnerowicz 1967, Tsikarishvili et al. 1992):

$$h^\alpha \equiv \frac{B^m}{\gamma}[\delta^\alpha_m + u^\alpha u_m], \qquad \text{(III.4)}$$

$$|h|^2 = B^2/\gamma^2 + (\vec{v}, \vec{B})^2, \qquad \text{(III.5)}$$

where δ^α_β is usual Kronneker symbol, while B^m are components of the spatial (3-dimensional) vector of the magnetic field. Note that the four-vector h^α is orthogonal to the vector of 4-velocity $h^\alpha u_\alpha = 0$. It is worthwhile to point out here that Maxwell equations

$$F_{\alpha\beta;\gamma} + F_{\beta\gamma;\alpha} + F_{\gamma\alpha;\beta} = 0, \qquad \text{(III.6)}$$

may be written by means of h^α as (Lichnerowicz 1967):

$$(u^\alpha h^\beta - u^\beta h^\alpha)_{;\alpha} = 0. \qquad \text{(III.7)}$$

In order to construct a model for a pulsar wind we shall write down the closed set of special-relativistic MHD equations describing a strongly magnetized, collisionless plasma of a pulsar wind with anisotropic pressure tensor. Such a set of equations were outlined by Tsikarishvili et al. (1992) in the framework of general-relativistic MHD. Consideration was based on the "3+1" formalism of Thorne & Macdonald (Thorne & Macdonald 1982, Macdonald & Thorne 1982) and the orthonormal tetrad technique (Rogava 1992). The same approach may effectively be used for special-relativistic kind of plasma flow – pulsar wind. Following Weber & Davis (1967), Michel (1969) and Goldreich & Julian (1970) we shall adopt a number of

simplifying assumptions: consider steady ($\partial/\partial t = 0$), two dimensional pulsar wind located in the equatorial plane ($\theta = \pi/2$) and having an angular symmetry ($\partial/\partial\varphi = 0$). Mass loss and decreasing of pulsar rotation rate will be neglected. Under these conditions, defining the spatial vector of the momentum flux as $S^i \equiv T^{ti}$ and writing the steady state equation of energy conservation as

$$div\vec{S} = 0, \tag{III.8}$$

we can immediately integrate (III.8) owing to the spatial symmetries of the flow and get:

$$r^2 S_r = r^2\left(\left[e + P_\perp + \frac{|h|^2}{4\pi}\right]\gamma^2 v_r + \left[\frac{(P_\parallel - P_\perp)}{|h|^2} - \frac{1}{4\pi}\right]h^t h_r\right) = const. \tag{III.9}$$

Quite in an analogous way, defining the spatial stress tensor as $\hat{T} \equiv T_{ik}$ and bearing in mind that a steady state equation of momentum conservation may be written simply as

$$div\hat{T} = 0, \tag{III.10}$$

we can, again, integrate it straightforwardly and obtain an algebraic equation describing the conservation of the pulsar wind azimuthal momentum:

$$r^2 T_{\varphi r} = r^2\left(\left[e + P_\perp + \frac{|h|^2}{4\pi}\right]\gamma^2 r v_\varphi v_r + \left[\frac{(P_\parallel - P_\perp)}{|h|^2} - \frac{1}{4\pi}\right]h_\varphi h_r\right) = const. \tag{III.11}$$

The continuity equation leads to the well-known expression (Goldreich & Julian 1970):

$$r^2\gamma v_r \rho \equiv f, \tag{III.12}$$

while from (III.7) one can also get equally well-known algebraic equations for the components of the magnetic field vector $\vec{B}$:

$$r^2 B_r = \Phi, \tag{III.13}$$

$$B_\varphi / B_r = (v_\varphi - \Omega r)/v_r. \tag{III.14}$$

where f is a mass flux, Φ is a magnetic field flux per unit volume angle and Ω is the star rotation frequency.

Conservation equations (III.9) and (III.11) may be simplified if we use (A.6) and (A.8) (see appendix) and will express h^α appearing in these equations through components of $\vec{B}$. Doing so, we can finally derive the following pair of important equations:

$$\gamma\left(\frac{e + P_\parallel}{\rho c^2}\right) - (1 - \beta)\frac{\Omega\Phi r B_\varphi}{4\pi f c^2} = \mu, \tag{III.15}$$

$$\gamma r v_\varphi\left(\frac{e + P_\parallel}{\rho c^2}\right) - (1 - \beta)\frac{\Phi r B_\varphi}{4\pi f} = L, \tag{III.16}$$

where μ and L are an energy flux per unit mass and angular momentum of unit mass respectively. We have also introduced the following useful dimensionless parameter:

$$\beta \equiv \frac{4\pi(P_{\|} - P_{\perp})}{|h|^2}. \tag{III.17}$$

For convenience of the forthcoming consideration we shall rewrite (III.15–III.16) in a slightly different form. Let us introduce the following dimensionless parameters (Asseo & Beauflis 1983):

$$\xi \equiv \frac{(e + P_{\perp})}{c^2 \rho}, \tag{III.18}$$

$$\delta \equiv \frac{(P_{\|} - P_{\perp})}{c^2 \rho \xi}. \tag{III.19}$$

Note that in these notations $(1 + \delta)\xi = (e + P_{\|})/c^2\rho$, and hence:

$$(1 + \delta)\xi\gamma - (1 - \beta)\frac{\Omega \Phi r B_{\varphi}}{4\pi f c^2} = \mu, \tag{III.20}$$

$$(1 + \delta)\xi\gamma r v_{\varphi} - (1 - \beta)\frac{\Phi r B_{\varphi}}{4\pi f} = L, \tag{III.21}$$

Equations (III.12–III.14) and (III.17–III.21) together with the relation (III.5) constitute a set of algebraic equations describing two-dimensional special-relativistic steady pulsar wind. The system is written in notations as similar as possible with the ones from Goldreich & Julian (1970). It must be noted that the system exactly reduces to the corresponding one from Goldreich & Julian (1970) for the isotropic pressure case ($P_{\|} = P_{\perp} = P$, $\delta = \beta = 0$) and further reduces to Michel's (1969) equations when $P = 0$. In addition the nonrelativistic limit of our equations reduce to the corresponding ones from Tan & Abraham (1972) as it, certainly, should be. Actually, our equations, except for the equation of state, coincide with the ones from Asseo & Beauflis (1983), which were written in different notations. In the latter publication the authors demonstrated that synchrotron-radiation losses considerably change the thermodynamical properties of the strongly magnetized collisionless plasma of the pulsar winds in such a way that their temperature (and pressure) become highly anisotropic. In particular, the radiative losses in a relativistic pulsar wind, where the transverse component of the plasma particles chaotic momentum is noticeably reduced, lead to the establishment of the regime $P_{\|} \gg P_{\perp}$ on characteristic time scales $t_0 = 3m^3c^5/2e^4B^2$ (Asseo & Beauflis 1983). On larger time-scales ($t \geq t_0$) the influence of synchrotron radiation becomes negligible and a relativistic collisionless, magnetized plasma with $P_{\|} \gg P_{\perp}$ may be described in the framework of the MHD theory discussed in Tsikarishvili et al. (1992), where it was found that when the plasma temperature is ultrarelativistic the specific energy density is equal to:

$$e = P_{\|} + 2P_{\perp}, \tag{III.22}$$

so that, evidently, $e \approx P_{\|}$, when $P_{\|} \gg P_{\perp}$. Equation of state (III.1a) gives a connection between $P_{\|}$, ρ and $|h|$. As regards to ξ and δ, from (III.18–III.19) we can immediately get:

$$\xi \approx P_{\|}/c^2\rho, \tag{III.23}$$

$$\delta \approx 1. \tag{III.24}$$

The expression for $|h|^2$ (III.5) may be rewritten as:

$$|h|^2 = B_{\varphi}^2 + \left(1 - \frac{\Omega^2 r^2}{c^2}\right) B_r^2, \tag{III.25}$$

which, if we take into account (III.13) and (III.14), leads to the following equation:

$$|h|^2 = \frac{\Phi^2}{r^4}\left[1 - \left(\frac{\Omega r}{c}\right)^2 + \left(\frac{v_{\varphi} - \Omega r}{v_r}\right)^2\right]. \tag{III.26}$$

All other quantities appearing in the equations of the system may be rewritten by means of components of the pulsar wind velocity: v_r and v_{φ}. For example, β, defined by (III.17), when $P_{\|} \gg P_{\perp}$, if we take into account (III.1), (III.12) and (III.26) may be reduced to the following form:

$$\beta = \left(\frac{4\pi\varepsilon f^2}{\Phi^3}\right)\left(\frac{r}{\gamma v_r}\right)^2\left[1 - \left(\frac{\Omega r}{c}\right)^2 + \left(\frac{v_{\varphi} - \Omega r}{v_r}\right)^2\right]^{-3/2}, \tag{III.27}$$

while (III.23) in an analogous way leads to:

$$\xi = \left(\frac{\varepsilon f}{c^2\Phi}\right)\frac{1}{\gamma v_r}\left[1 - \left(\frac{\Omega r}{c}\right)^2 + \left(\frac{v_{\varphi} - \Omega r}{v_r}\right)^2\right]^{-1/2}. \tag{III.28}$$

Instead of the pair (III.15–III.16) we can also write an equivalent pair of new equations, derived by plain algebraic manipulations from (III.15–III.16):

$$\mu - \frac{L\Omega}{c^2} = (1 + \delta)\xi\gamma\left(1 - \frac{r\Omega v_{\varphi}}{c^2}\right), \tag{III.29}$$

$$L - \mu r v_{\varphi} = -(1 - \beta)\frac{\Phi r B_{\varphi}}{4\pi f}\left(1 - \frac{r\Omega v_{\varphi}}{c^2}\right), \tag{III.30}$$

III.3 discussion

It is convenient to continue the analysis of the equations derived in the previous subsection if we introduce dimensionless notations, slightly different from ones used in Goldreich & Julian (1970):

$$r_0^2 = \frac{\Phi^2}{4\pi f c}, \quad \lambda = \frac{L}{\Omega r_0^2}, \quad \sigma = \left(\frac{\Omega r_0}{c}\right)^2, \quad R = \frac{\varepsilon f}{c^3\Phi}, \quad x = \frac{\Omega r}{c}, \quad u = \frac{v_r}{c}, \quad v = \frac{v_{\varphi}}{c}$$

All these notations are standard (see Goldreich and Julian (1970)) except for the dimensionless parameter R connected with equation of state (III.1a) and hence , attributed to the $P_{\|}$. This R parameter is a new constant of the flow and it appeared just from taking into account ultrarelativistic temperatures.

Equations which were derived in the previous section may be rewritten in these dimensionless notations. For instance, (III.27) and (III.28) reduce to the following expressions

$$\beta = \left(\frac{R}{\sigma}\right)\left(\frac{x}{\gamma u}\right)^2\left[1 - x^2 + \left(\frac{v-x}{u}\right)^2\right]^{-3/2}, \tag{III.31}$$

$$\xi = \left(\frac{R}{\gamma u}\right)\left[1 - x^2 + \left(\frac{v-x}{u}\right)^2\right]^{-1/2}. \tag{III.32}$$

At the same time from (III.29) taking into account (III.24) and (III.32) one finds that

$$\frac{(\mu - \sigma\lambda)}{2R} = \frac{(1-xv)}{\left[u^2(1-x^2) + (v-x)^2\right]^{1/2}} \tag{III.33}$$

and this equation allows us to rewrite (III.31) in a more simple form

$$\beta = \left[\frac{(\mu - \sigma\lambda)^3}{8R^2\sigma}\right]\frac{x^2 u}{\gamma^2(1-xv)^3}. \tag{III.34}$$

On the other hand, since $1/\gamma^2 = 1 - u^2 - v^2$, if we express u^2 from (III.33) and insert it into the definition we get

$$\gamma^2 = \frac{(1-x^2)}{(1-A)(1-xv)^2} \tag{III.35}$$

where we introduce one more auxiliary parameter

$$A \equiv \frac{4R^2}{(\mu - \sigma\lambda)^2}. \tag{III.36}$$

Using this definition and taking into account (III.35) we can rewrite (III.34) in the following form

$$\beta = \frac{(1-A)(\mu - \sigma\lambda)}{2A\sigma}\frac{x^2 u}{(1-x^2)(1-xv)}. \tag{III.37}$$

Bearing in mind the definitions of constants, from (III.30) we obtain:

$$\lambda\left(1 - \frac{\mu}{\sigma\lambda}xv\right) = (1-\beta)\frac{(xv-1)(v-x)}{ux}. \tag{III.38}$$

Note that (III.33), (III.37) and (III.38) constitute a closed set of nonlinear algebraic equations for three unknown functions: $u(x)$, $v(x)$ and $\beta(x)$. The complicated structure of these equations suggests that an overall, general solution of the system is quite a difficult problem.

However, quite surprisingly, by combining (III.32) with other equations one arrives at the rather simple, analytical expression for the function ξ :

$$\xi(x) = \sqrt{\left|\frac{4R^2 - (\mu - \sigma\lambda)^2}{4(x^2 - 1)}\right|}. \qquad \text{(III.39)}$$

Note that $c^2\xi(x)$ is the specific enthalpy or chemical potential, which is defined in an usual way $c^2\xi \equiv \left(e + P_{\|}\right)/\rho$.

This equation is quite informative. In particular, it implies that: (a) if $4R^2 < (\mu - \sigma\lambda)^2$ and the pulsar wind is ultrarelativistic near the pulsar surface ($\xi(x_0) \gg 1, x_0 \ll 1$) then it should remain ultrarelativistic everywhere up to the light cylinder ($x_0 \leq x \leq 1$); (b) if $4R^2 > (\mu - \sigma\lambda)^2$ and the pulsar wind appears to be ultrarelativistic above the light cylinder (at $x \geq 1$) then it should remain ultrarelativistic in the limited region of the wind volume ($1 < x < x_*$) where $\xi(x)$ is still much more than unity.

A careful and detailed solution of the obtained set of equations, which needs tedious analysis of the existing critical points and the relationships between "the free parameters" contained in these equations, is beyond the scope of the present consideration. However, we have obtained set of analytic solutions through the following simplifying assumptions:

(**A**) this assumption regards the β parameter which is defined by (III.17). From the theory of plasma physics there is known another β_* parameter which is defined as a ratio of thermal and magnetic pressures i. e. $\beta_* = P_{thermal}/P_{magnetic}$. This parameter is recognized as a natural measure of thermal pressure anisotropy for collisionless, anisotropic plasma medium contained in a magnetic field. Bearing in mind that noticeable anisotropy will be established only in strong magnetic fields (up to $10^{12}G$ in pulsar magnetospheres), then it is clear that $\beta_* \ll 1$ in such a medium. As regards to our β parameter from (III.17) (with neglected $P_{\perp}$ in respect to $P_{\|}$), it can be said that since $|h|^2$ is related with B^2 (see III.5) or roughly the magnetic energy, we may *assume* that $\beta \ll 1$.

(**B**) We consider such a kind of the wind, which remains *cool* up to the light cylinder, but after passing the critical point $x = 1$, it is heated up to ultrarelativistic temperatures by certain mechanisms (for instance, heating by MHD waves excited due to plasma instabilities). Developing this reasonings and bearing in mind that flow constants μ, σ and λ describe source features (e. g. σ parameterizes the ability of the field to sling the particles to the high proper velocities —Michel (1969) etc.) and they seem to be really constant along the bulk of the flow, we *suppose* that it would be permissible to use overall information about the constants obtained in Goldreich and Julian (1970) for cool stellar winds. This approach gives us the ability to get analytical expressions for the main physical variables outside the light cylinder. According to Goldreich and Julian (1970) in the extreme relativistic approximation $\sigma \gg 1$, $\lambda \approx 1$ and $\mu = 1 + \sigma\lambda$. Hence $\mu/\sigma\lambda \approx 1$. These assumptions lead to considerable simplifications. For example (III.38) is reduced to the following simple relation

between dimensionless velocity components:

$$ux \approx x - v \tag{III.40}$$

substituting this into (III.33) and taking into account that in the considered case $A^{1/2} \approx 2R$ we get another relation between the same unknown wind variables:

$$u \approx 2R(1 - xv). \tag{III.41}$$

The system (III.40—III.41) can be solved immediately and the result is the following :

$$v(x) = \frac{x(2R-1)}{2Rx^2 - 1} \tag{III.42}$$

$$u(x) = \frac{2R(x^2-1)}{2Rx^2 - 1} \tag{III.43}$$

while for $\gamma^2 \equiv (1 - u^2 - v^2)^{-1}$ we get:

$$\gamma(x) = \frac{2Rx^2 - 1}{[(2R-1)(x^2-1)]^{1/2}}. \tag{III.44}$$

After simple algebraic calculations we obtained the rest of the physical quantities. The final results, as a representative solution (when it is assumed that (**A**) and (**B**) are fulfilled) in the region $x > 1$ are given by the following expressions

$$\beta(x) = \frac{(4R^2-1)}{4R\sigma} \frac{x^2}{x^2-1} \tag{III.45}$$

$$B_\varphi(x) = \frac{\Phi\Omega^2}{c^2} \frac{1}{x} \tag{III.46}$$

$$B_r(x) = \frac{\Phi\Omega^2}{c^2} \frac{1}{x^2} \tag{III.47}$$

$$|h(x)| = B_r(x) \tag{III.48}$$

$$\rho(x) = \left(\frac{f\Omega^2}{c^3}\right)\left(\frac{4R^2-1}{4R^2}\right)^{1/2} \frac{1}{x^2(x^2-1)^{1/2}} \tag{III.49}$$

$$P_{\|}(x) = \left(\frac{f\Omega^2}{c}\right)\left(\frac{4R^2-1}{4R}\right) \frac{1}{x^2(x^2-1)} \tag{III.50}$$

Note that these solutions are valid only for $1 < x < x_*$, where x_* is a distance where $\xi \gg 1$ ceases to exist, i. e. the wind flow temperature remains to be ultrarelativistic. The point $x = 1$, where some of these solutions become singular, is also beyond the considered wind region, because, as it is evident from (III.45) that our assumption $\beta \ll 1$ (**A**) violates, when $x \to 1$.

Concluding this section we shall emphasize that the obtained results are based on a simplified model developed by us. The next step could be more detailed investigation of

the critical points existed in the flow and hence, more accurate determination of the flow constants (i.e. with out simplifying assumptions (**A**) and (**B**) employed in the above study).

IV Balls Composed by Massive, Degenerate Neutrinos in the Vicinity of Active Galactic Nuclei

IV.1 introduction

In this section employing standard theory of geometrically thin accretion disks we shall investigate what influence a ball composed by massive, degenerate neutrinos may have on the accretion process occurring in the vicinity of the active galactic nuclei (AGN). Basic physical properties of the neutrino balls along with some of their possible observational implications were outlined in series of papers Viollier, 1994; Viollier et al., 1993; Viollier et al., 1992. In this section we present yet one more feasible observational signature of the neutrino balls which is based on the results from (Tsiklauri and Viollier, 1996). Before we start formulation of the problem itself let us outline some basic introductory facts and discuss briefly existed literature in this field.

It is generally accepted that active galactic nuclei are powered by a central black hole. The most reasonable explanation of the observed radiation from AGN is that the emitted energy is generated due to viscous dissipation processes occurring in the matter accreting on the central black hole. Since the gas pressure is dominant, temperature is low enough in the bulk of the flow and presumably the accreting matter has nonzero angular momentum, the assumption that the accretion process occurs in the form of a geometrically thin accretion disk seems to be the most appropriate. A large fraction of the energy emitted from an AGN falls in the ultraviolet region, the so called 'Big Blue Bump' (BBB) of the spectrum.

Various models have been constructed to explain the spectrum emitted from AGN. The common characteristic feature of these models is that the BBB can be explained by thermal emission from the innermost regions of the accretion disk around the central black hole (Shields, 1978; Ulrich, 1981; Malkan 1983; Sun & Malkan, 1989). However, these models have certain difficulties: Firstly, the absence of an absorption edge in AGN spectra at the Lyman α limit; Secondly, the weak polarization of the blue light in the direction parallel to the radio axis; Thirdly, detailed studies of the response of emission lines of different ionization levels in the broad line region of AGN spectra do not show any time delays which are expected if the ionization continuum draws its origin from the accretion disk. Nevertheless, the approach seems to be correct in general. Other authors have taken into account more detailed effects such as coronal reprocessing (Collin-Souffrin, 1991), heat advection (Abramowicz, 1991;

Narayan & Yi, 1994; Narayan & Yi, 1995; Abramowicz et al., 1995), deviation from the Keplerian motion, which is important in the disk region adjacent to the black hole (Duschl, 1988; Krolik & Begelman, 1988), Comptonization of the spectrum emitted from AGN using analytic fitting formulae (Czerny & Elvis, 1987; Wandel & Petrosian, 1988) and incoherent Compton scattering (Ross et al., 1992; Lithchfield et al., 1989; Laor & Netzer, 1989).

Recently, some authors (Perry & Dyson, 1985; Perry & Williams, 1993) studied the influence of a stellar cluster surrounding the black hole on the physical processes occurring in an AGN. In particular, Perry & Williams, 1993 showed that the presence of a stellar cluster can significantly change the spectrum emitted by an AGN. In their model the 'IR bump' which exists in wide class of AGN (Malkan, 1989) was interpreted as a spectral signature of the stellar cluster.

As we mentioned above, in this section we study the influence of a possible dark matter neutrino ball on the accretion process in the AGN and we investigate observable signatures of such a ball which is supported by degeneracy pressure. The idea itself that massive neutrinos may form some stable, long-lived structures is not new. Based on the spontaneous parity and charge-conjugation breakdown in a left-right-symmetric theory Holdom (Holdom, 1987 & 1993) proposed the existence of so-called right handed neutrino balls. According to this scenario, right-handed neutrinos can be confined in a region of space within which the local vacuum structure conveys upon them a light Majorana mass. Outside the trapped region the right-handed neutrinos have a large Majorana mass. Prior to a phase transition in the early universe, the spontaneous breaking of parity leads to the formation of domain walls which separate the left and right vacuums. Because of the difference in the neutrino masses on both sides of the wall, neutrino transport across the wall is forbidden. Further, the infinite domain walls will disappear, leading to the formation of stable spherically symmetric right handed neutrino balls. Inside the neutrino ball, the right-handed neutrinos interact via weak interaction producing electron-positron pairs through annihilation. These electron-positron pairs then drift outside the neutrino ball. Due to the cooling process and the decreasing of average energy inside the ball, electron-positron pair creation through annihilation of neutrinos is more and more difficult and finally the neutrinos slowly approach their degenerate state. As regards astrophysical implications of the trapped neutrino balls, Holdom & Malaney (1994) recently proposed a mechanism involving right handed neutrino balls to explain the origin of the gamma-ray bursts. Dolgov and Markin (1991) also developed a model which implies that the cosmic balls of trapped right-handed neutrinos may mimic the properties we observe in quasars.

In the recent past, an alternative approach for the description of heavy neutrino matter supported by degeneracy pressure against self-gravity was developed (Viollier, 1994; Viollier et al., 1993; Viollier et al., 1992). In this study we focus our attention on the role of such a dark matter ball in the vicinity of AGN. The keystone of our approach will be the standard

model of a stationary, geometrically thin accretion disk around a central black hole. In addition, we consider a dark matter ball which is formed by degenerate heavy neutrino matter. We assume that spherically distributed dark matter supported by degeneracy pressure extends to ~ 0.05 pc in the vicinity of the supermassive black hole. Since we consider balls with masses $\sim 10^9 M_\odot$, it is clear that presence of such objects will change the gravitational potential of the system significantly.

It is obvious that the spectrum emitted by the AGN accretion disk depends on the gravitational potential within which it resides. The presence of the ball will exert additional shear between adjacent layers of the disk through changing the gravitational potential. Viscous dissipation processes due to the extra shear will lead to additional heat production in the disk. Hence, if we assume that the opacity is high enough and the disk radiates away the released gravitational binding energy locally, with a black body spectrum, the shape of the emitted spectrum from the disk will be changed noticeably.

It is worthwhile to note that the assumption of high opacity in the bulk of the disk (and hence the description of the disk in terms of an effective temperature) and the adoption of the black body law of emission is, of course, an oversimplification. Strictly speaking, these assumptions are valid only in the innermost region of the disk, where the temperature is the order of $\sim 10^4$ K and accreting matter is fully ionized. However, at larger distances from the black hole the hydrogen recombines due to the cooling, causing a noticeable decrease of the opacity. Going up on the scale of distance from the black hole, the opacity will perhaps increase once more due to the existing dust when the temperature decreases below 2000K. Further, the disk becomes optically thin because the dust will be destroyed by incident X-rays. All these specific features are taken into account by more detailed models of the accretion disks in AGN (Collin-Souffrin & Dumont, 1990; Cannizzo & Reiff, 1992). However, here we neglect all these effects assuming that the opacity is high in the bulk of the disk and that the disk may be described by an effective temperature.

We also would like to remark that as far as the accretion disk spectrum is a tracer of the gravitational potential within which it resides, basically, it is irrelevant whether modification of the gravitational potential is due to a stellar cluster or a massive ball composed by degenerate neutrinos. Therefore, basing on the idea proposed by Perry & Williams, 1993, we demonstrate that if a ball of heavy neutrinos, supported by degeneracy pressure, does exist in the vicinity of an AGN, it will cause a bump in IR region of the emitted spectrum which is observed for several AGN (Malkan, 1989). We also find that if the bump at $\sim$1000K in the typical radio loud quasar 3C 273 spectrum is due to a neutrino ball, then our model implies mass of the black hole $10^8 M_\odot$, a ball mass of $4 \times 10^9 M_\odot$ and in turn, a neutrino mass of ~ 3 keV$/c^2$.

IV.2 the model

In the standard theory of steady and geometrically thin accretion disk the power liberated in the disk per unit area is given by

$$D(R) = \frac{\dot{M}\Omega\Omega' R}{4\pi}\left[1 - \left(\frac{R_i}{R}\right)^2\left(\frac{\Omega_i}{\Omega}\right)^2\right], \tag{IV.1}$$

where $\dot{M}$ is the accretion rate, Ω is the angular velocity of the accreting matter, R_i is inner edge of the disk which is normally taken as $3R_G$ (the last stable orbit for a Schwarzschild black hole), Ω_i denotes $\Omega(R_i)$ (the value of the angular velocity where its derivative attains zero due to deviation from the Keplerian law of rotation) and finally prime denotes the derivative with respect to R.

The mass of the spherical ball of heavy neutrinos within a sphere of radius R is given by

$$M_<(R) = \int_0^R \rho(r) 4\pi r^2 dr, \tag{IV.2}$$

where ρ stands for the density of the dark matter. Since the motion of the accreting matter in the bulk part of the disk (excluding the very innermost region) is Keplerian, we assume that the rotational law is given by

$$\Omega(R) = \sqrt{\frac{G(M_h + M_<(R))}{R^3}}, \tag{IV.3}$$

where M_h denotes the mass of the black hole. It is worthwhile to note that, even if the ball did start at R_i, its effect on the accretion process would be negligible. Thus we can safely substitute $\sqrt{GM_hR_i}$ instead of $R_i^2\Omega_i$ in the Eq.(IV.1). We assume, further, that the opacity is high enough throughout the disk so that we can describe it with an effective temperature $T_{\rm eff}$. Assuming that the gravitational binding energy released is radiated immediately away locally according to the black body emission law, we arrive at Stefan-Boltzmann's law

$$\sigma T_{\rm eff}^4(R) = D(R), \tag{IV.4}$$

where σ denotes Stefan-Boltzmann's constant. Substituting the explicit form of the rotational law (IV.3) into the Eq.(IV.4), we obtain

$$\sigma T_{\rm eff}^4(R) = \left[\frac{3G\dot{M}M_h}{8\pi R^3} - \frac{G\dot{M}R}{8\pi}\frac{d}{dR}\left(\frac{M_<(R)}{R^3}\right)\right] \times \left[1 - \sqrt{\frac{M_hR_i}{(M_h + M_<(R))\,R}}\right]. \tag{IV.5}$$

Following Perry & Willams (1993), we introduce a useful auxiliary parameter $M_R = (4\pi/3)\cdot\rho(R)R^3$. We may rewrite, further, Eq.(IV.5) to get

$$\sigma T_{\rm eff}^4(R) = \frac{3G\dot{M}M_h}{8\pi R^3}\left[1 + \frac{M_<(R)}{M_h} - \frac{M_R}{M_h}\right] \times \left[1 - \sqrt{\frac{M_hR_i}{(M_h + M_<(R))\,R}}\right]. \tag{IV.6}$$

Now, it is necessary to specify the spatial distribution $\rho(R)$ of the dark matter. Degenerate self-gravitating heavy neutrino matter can be described using the statistical method due to Thomas and Fermi, in which the local Fermi energy is set equal to the local gravitational binding energy (Viollier, 1994; Viollier et al., 1993; Viollier et al., 1992)

$$\frac{\hbar^2}{2m_\nu}\left(6\pi^2 n_\nu/g\right)^{2/3} = m_\nu(\Phi - \Phi_0), \tag{IV.7}$$

where m_ν and n_ν are the neutrino mass and number density, respectively, g is the spin degeneracy factor and Φ is the gravitational potential of the neutrino matter. One also has to adopt Poisson's equation for the gravitational potential

$$\Delta\Phi = -8\pi G m_\nu n_\nu. \tag{IV.8}$$

In the latter equation, we assumed that number densities of neutrinos n_ν and antineutrions $n_{\bar{\nu}}$ are equal. It is worthwhile to note that self-gravitating heavy neutrino matter can be alternatively described by the hydrostatic equations likewise a polytropic star. In particular, we have the equation of hydrostatic equilibrium

$$\frac{1}{r^2}\frac{d}{dr}\left(\frac{r^2}{\rho_\nu}\frac{dP_\nu}{dr}\right) = -8\pi G\rho_\nu \tag{IV.9}$$

and polytropic equation of state

$$P_\nu = K{\rho_\nu}^{\frac{n+1}{n}} \tag{IV.10}$$

were $\rho_\nu = m_\nu n_\nu$ is density of the neutrino matter. However, we should note that Eqs(IV.9–IV.10) must be consistent with Eqs.(IV.7–IV.8). This requirement specifies the polytropic index $n = 3/2$ and polytropic constant

$$K = \left(\frac{6}{g}\right)^{2/3}\frac{\pi^{4/3}\hbar^2}{5{m_\nu}^{8/3}}. \tag{IV.11}$$

Following the standard theory of polytropic stars (Cox & Giuli, 1968), we define a dimensionless function θ by writing

$$\rho = \rho_c\theta^n. \tag{IV.12}$$

We now, also, introduce another dimensionless variable (Cox & Giuli, 1968), ξ, defined by the relation

$$r = r_n\xi, \tag{IV.13}$$

where r_n is defined by

$$r_n = \sqrt{\frac{(n+1)K}{8\pi G}}{\rho_c}^{\frac{1-n}{2n}}.$$

Doing so, we finally arrive at well-known Lane-Emden equation

$$\frac{1}{\xi^2}\frac{d}{d\xi}\left(\xi^2\frac{d\theta}{d\xi}\right) = -\theta^n \tag{IV.14}$$

with polytropic index n=3/2. It is worthwhile to note that the spatial density distribution in our approach is governed in a self-consistent way by the Lane-Emden equation, whereas Perry & Willams (1993) had to assume a matter distribution for their stellar cluster. Hence, our model is more restrictive in this context.

IV.3 numerical results

Having specified the spatial density distribution in our model, we now turn back to the temperature distribution which in the general case is is given by Eq.(IV.6). It is clear that even in the absence of the gravitational effect of the dark matter ball, this expression implies the presence of at least one maximum which is, in turn, responsible for the BBB in the emitted spectrum. However, one can see that the Eq.(IV.6) implies also the presence of a second maximum (due to the interplay of the terms $M_<(R)/M_h$ and M_R/M_h) which, as we will show below, will produce a bump in the IR region of the spectrum for a certain choice of physical parameters. It is evident that for a constant density distribution in the ball, its presence will not change the temperature distribution and the emitted spectrum at all, because when $\rho = const$ then $M_<(R) = M_R$ (Perry and Williams, 1993). The influence of the ball is the stronger the more rapidly the density decreases. The latter fact is clearly demonstrated in Figs. IV.1 and IV.2, where we plot the behaviour of the quantity $M_<(R)/M_h - M_R/M_h$ from Eq.(IV.6) for two different choices of neutrino mass. These figures also demonstrate how strongly the mass of the ball itself depends on the mass of the neutrinos (since the last term M_R/M_h is directly proportional to the density which, of course, vanishes at the radius of the ball and finally we have only the ratio $M_<(R)/M_h$).

Perry and Williams (1993) assume that the stellar cluster consists of a core with constant density and beyond the core the density decreases with constant slope. For such a *discontinuous* density profile the secondary maxima in the temperature distribution occurs just beyond the core radius. Further, the authors suggest that in the case of *smooth* behaviour of the density the temperature might increase with increase of radius, which is consistent with our results.

In Fig. IV.3 we plot the numerical solution of the Lane-Emden equation with boundary conditions conditions $\theta = 1$ and $d\theta/d\xi = 0$ at $\xi = R_i/pc$. One can clearly see from the graph that the slope drastically increases as one tends close to the radius of the ball and it is almost zero for the all distances which are less than this radius. Thus it is obvious that one should expect that the maximal effect of presence of the ball will appear (recall Figs. IV.1 & IV.2) at the distances *close* to the radius to which the ball extends.

In Fig. IV.4 the solid curve represents the effective temperature of the disk versus the distance from the central black hole in the case without ball. From observational data it is

known that for several AGN there exists a IR bump which in terms of effective temperature should occur around ~1000K. If we want to explain this bump by the presence of the dark matter ball supported by degeneracy pressure then, bearing in mind that maximal effect of a ball occurs near its radius, the ball radius should be about ~0.05pc (or in logarithmic scale $\log(0.05/pc) \approx -1.3$). One can see from fig.4 that just around the latter distance, the value of the effective temperature of an isolated black hole (solid curve) is of the same order (~1000K). Otherwise, if we assume that the radius of the ball is larger, then to cause the same effect (bump up to the ~1000K), we need to claim the presence of the much more massive ball which would be in contradiction with the Chandrasekhar mass limit (Viollier, 1994).

We find that, in order to be self-consistent with the observational data, we must assume that the conventional heavy neutrino has a mass of 3 keV/c^2 which, in turn, yields a reasonable mass of the ball itself — $4 \times 10^9 M_\odot$. In Fig. IV.4 the dotted curve corresponds just to the latter set of parameters (we also assumed a typical accretion rate of $\dot{M} = 100\, M_\odot yr^{-1}$ for the object under study). It is obvious from Fig. IV.4 that the secondary maximum due to presence of the ball occurs just about ~1000K, which is consistent with observational data. The dashed curve on the same figure represents $T_{\rm eff}$ for a neutrino mass of 4 keV/c^2, which then yields a ball mass $4 \times 10^8 M_\odot$. We see from this graph that in this case, the maximum occurs at a lower temperature which is not acceptable. As we have already mentioned, we assume that the opacity is large enough throughout the disk and that the disk radiates away the released gravitational binding energy locally with a black body spectrum.

Then with the black body assumption, we can write for the flux at frequency ν

$$F_\nu = \frac{2\hbar \cos i \nu^3}{c^2 D^2} \int_{R_i}^{R_{out}} \frac{RdR}{\exp\left[h\nu/kT_{\rm eff}(R)\right] - 1}, \qquad \text{(IV.15)}$$

where D is the distance to the object and the i is the angle of inclination of the disk. Following Perry & Williams (1993), we neglect disk inclination effects assuming $2\cos i = 1$. Using Eq.(IV.15) we can work out numerically the disk spectrum. The results are presented in the Fig. IV.5. For the distance to the object under study, we use $948/h_{50}$ Mpc which is consistent with the distance to the well known 3C 273 (Perry et al., 1987). One can learn from the Fig. IV.5 that there is no secondary bump (in IR region) in the case without ball (solid curve), while, for the ball with the mass $4 \times 10^9 M_\odot$ (dotted curve), the bump in IR region can be clearly seen exactly at the same location where it is observed for several AGN (Malkan, 1989). Also, we see that with the decrease of mass of the ball the effect becomes less and less pronounced (see dashed curve representing the case when mass of the ball is $4 \times 10^8 M_\odot$) as it should be. Since the maximum in the effective temperature distribution is fixed at ~1000K, based on the observational data, we find that the most appropriate parameters of the heavy neutrino ball supported by degeneracy pressure in the vicinity of 3C 273 (of course if we imply that the bump in IR region is due to the presence of the ball)

should be radius of — 0.06pc and a mass of — $4 \times 10^9 M_\odot$.

VI.4 conclusions

We have demonstrated that the dark matter balls formed by degenerate heavy neutrinos would have a significant effect on the accretion process in AGN, since they will drastically change the gravitational potential of the system. We conclude that a possible signature of heavy neutrino balls will be the thermal bump in the IR region of the spectrum emitted from AGN. Applying our model to the typical quasar 3C 273 and assuming that the IR bump is due to a heavy neutrino ball, we determine the main physical parameters of such a ball. The results are consistent with those obtained in Perry & Williams, 1993 and Perry et.al, 1987. Our model is based on a rather simple model of a steady and optically thick accretion disk around the black hole. As we have already mentioned, many other more realistic models of AGN have been constructed. However, our aim was to outline possible observational signatures of the dark matter balls and to demonstrate clearly their influence on the physical processes in the vicinity of AGN.

Concluding this section we would like to say a few words about the mass of heavy neutrino, since it still remains a tantalizing issue. One may question, if the mass of neutrino used in this study is consistent with bounds set by existing knowledge (Big Bang Nucleosynthesis, supernova explosion etc.). In fact, stringent limits on the mass of neutrinos can be obtained from the fact that the primordial helium abundance is sensitive to massive neutrinos (Rothstein, 1995). The present laboratory bound on the tau neutrino (ALEPH collaboration, 1995) is 24 MeV, which is based on looking for missing energy in the decay $\tau \rightarrow 5\pi^{\pm}(\pi^0)$. And this bound is just in the range where primordial nucleosynthesis feels the effects of the neutrino mass. The nucleosynthesis bounds rule out neutrino masses from the lab upper limit down to a few hundred keV (Rothstein, 1995). Using the Boltzmann kinetic equation to calculate the Helium abundance, it is found (Dolgov & Rothstein, 1993) that for Majorana masses the forbidden mass range is $0.5\,\mathrm{MeV} < m_M < 35\,\mathrm{MeV}$ and for Dirac neutrinos the forbidden mass range is $0.3\,\mathrm{MeV} < m_D < 35\,\mathrm{MeV}$. A more stringent bound of 15 keV for a Dirac mass of the tau neutrino comes from supernova SN 1987A (Burrows et al., 1992). We can see from the above consideration that our 3 keV tau neutrino matches all existing astrophysical and laboratory bounds.

V Compressible Hydromagnetic Shear Flows: Non-modal Study of Waves and Instabilities

V.1 introduction

In this section we shall study physical processes in the sheared hydromagnetic flows. Significance of the shear flows in the astrophysics or in a laboratory plasma devices can not be underestimated. It is reasonable to state that a velocity field of almost all real astrophysical or laboratory hydrodynamic and hydromagnetic flows is commonly spatially inhomogeneous. When various adjacent layers of the flow move with different velocities (differential motion), the flow is said to be sheared. Feasible examples of astrophysical shear flows are differentially rotating fluid systems: planetary rings, stars and protostellar nebulae, accretion disks and spiral galaxies (Narayan, Goldreich and Goodman, 1987). The complicated kind of three-dimensional shear motion is present in active galactic nuclei outflows (jets), stellar and pulsar winds. We do not restrict ourselves by investigation of any concrete astrophysical object since it would be related with loss of generality of this notion. At the same time we may well state that the basic results of this study are applicable to the variety of space objects or laboratory plasma devices. Below we shall review previous contributions to this field of study and then switch to presentation of our original results which are chiefly based on the papers (Chagelishvili, Rogava and Tsiklauri (1996a) and Chagelishvili, Rogava and Tsiklauri (1996b)).

A variety of different types of waves and instabilities occurring in the hydrodynamic and hydromagnetic shear flows have been studied in the past and the recent past. Goldreich and Lyndenn-Bell (1965) invented the "shearing sheet model", in order to discard purely geometrical complications, arising in flows with untrivial geometrical symmetry, while retaining dynamical effects of the shear (differential rotation) (Drury, 1980). In the framework of the model the linear equations for perturbations can be rewritten in comoving shearing reference frame, where they become temporaly inhomogeneous just alike to the non-modal approach. In these coordinates, performing *spatial* Fourier expansion, the problem is reduced to the analysis of ordinary differential equations with time dependent coefficients. In the framework of the "shearing sheet model" there was investigated evolution of the galactic density waves (Toomre, 1969; Goldreich & Tremaine, 1978); there was undertaken analytical study of shear instability in the Keplerian accretion discs (Lominadze, Chagelishvili & Chanishvili, 1988); there were found rapidly growing non-axisymmetric, inviscid disturbances in the convectively unstable accretion discs (Ryu and Goodman, 1992); and there was investigated interplay of Parker and shear instabilities in the accretion discs (Foglizzo and Tagger, 1995). Recent discovery of powerful, local shear instability in weakly magnetized (high-β) accretion

discs by Balbus & Hawley (firstly, originated from (Velikhov, 1959) and (Chandrasekhar, 1960)) initiated new interest in this field of study. Among their series of papers we would like to mention Balbus & Hawley (1992) where they applied shearing sheet formalism to the study of non-axisymmetric modes in the disc. Besides, it was shown (Tagger, Pellat & Coroniti, 1992) that non-axisymmetric (spiral) waves are subject to similar but physically different instability occurring in low-β discs. Resuming aforesaid, the model proved itself as a good and convenient technique for solving the wide class of analogous problems, although its relation to the more usual and standard normal modes approach seems to be problematic.

As regards laboratory shear flows, it is worthwhile to note that importance of the non-modal solutions of the magnetohydrodynamic (MHD) equations governing the Tokamak devices was also revealed in previous contributions (Cooper, 1988), in particular, the author considered the ballooning instabilities in Tokamak devices with sheared toroidal flow. Basing on the covering space concept (Dewar and Glasser, 1983), which, in fact, does not constrain any unstable solution to evolve as $\exp(i\omega t)$, it was shown that adequate description of the ballooning mode can be performed considering the non-modal solutions of the equations. Basically, the ballooning-mode eikonal representation used by the author is similar to the "Kelvin formalizm" but its mathematical formulation is different since it is applied to the physical system with axial symmetry.

However, it should be noted, that nowadays a change in the overall paradigm is taking place in the field of hydrodynamic stability (Trefethen et al., 1993). See major monoghraps (Lin, 1955; Betchov & Criminale, 1967; Drazin & Reid, 1987) in the field of the flow stability for the discussion. The traditional paradigm (normal modes approach) is eigenvalue analysis, which proceeds in two stages: (i) linearize about the regular (laminar) solution and afterwards (ii) look for unstable eigenvalues of the linearized problem (Trefethen et al., 1993; Trefethen, Trefethen and Reddy, 1992). According to the standard theory the unstable eigenvalue (i.e. that one from the complex upper half-plane) corresponds to the exponentially growing eigenmode of the linearized problem. The necessary condition for the flow to behave unstably is thought to be the existence of such eigenmodes. For some flows (e.g. thermally driven instabilities in Rayleigh-Benard convection flow, or centrifugally driven instabilities in rotating Couette (Taylor-Couette) flow) this conclusion is in good agreement with experimental results. At the same time for the other kind of hydrodynamic flows, especially those driven predominantly by shear forces, the predictions of the normal modes approach fail to match most experiments (Trefethen et al., 1993). For Couette flow, for instance, instabilities are observed to "switch on" for Reynolds numbers as low as $Re{\approx}350$, while the common eigenvalue analysis predicts stability for all Re-s. Traditionally, this anomaly was recognized as a failure of linearization and was attributed to non-linear effects. Recently, it was argued, however, that the failure of the normal modes analysis should be attributed to step (ii) (Trefethen et al., 1993; Trefethen, Trefethen and Reddy, 1992; Butler

and Farrell, 1992; Reddy and Henningson, 1993). As it is stated in (Trefethen et al., 1993) "It is a fact of linear algebra that even if all of the eigenvalues of a linear system are distinct and lie well inside the lower half-plane, inputs to that system may be amplified by arbitrarily large factors if the eigenfunctions are not orthogonal to one other." According to the definition, a matrix or operator whose eigenfunctions are orthogonal is said to be "normal" (Kato, 1976), and while the operators arising in the Rayleigh-Benard and Taylor-Couette problems fall in this category, the operators that arise in Poiseuille and Couette flow are not normal (Reddy, Schmidt & Henningson, 1993). That is why small perturbations to these flows may be amplified by factors of thousands, even when all the eigenvalues are in the lower half-plane (Trefethen et al., 1993; Butler and Farrell, 1992; Reddy and Henningson, 1993). Historically, this fact firstly was outlined by A. Sommerfeld who recognized that difference between self-adjoint and non self-adjoint differential operators is responsible for quite unusual, power-low rather then exponential *transient* behaviour (*transient* growth) of the perturbations even if the flow is asymptotically stable.

Turning now, again, attention to the non-modal approach, it should be noted that its application to the study of the hydrodynamic instabilities in shear flows, originated from Lord Kelvin (Lord Kelvin, 1887), recently became well established and extensively used (Trefethen et al.,1993; Trefethen, Trefethen and Reddy, 1992; Butler and Farrell, 1992; Reddy and Henningson, 1993; Reddy, Schmidt and Henningson, 1993; Chagelishvili et al., 1992,1993; Chagelishvili, Rogava and Segal, 1994; Chagelishvili, Rogava and Tsiklauri, 1996a, 1996b; Criminale, Jackson and Lasseigne, 1995; Criminale and Drazin, 1990). In the framework of this formalism one considers temporal evolution of *spatial Fourier harmonics* ("Kelvin modes" (Marcus and Press, 1977)) of the perturbations without any spectral expansion in time. The wave number of each spatial Fourier harmonic (SFH) along the mean flow shear varies in time: in the linear approximation there exists a "drift" of the SFH in the plane of wave numbers ($\vec{k}$-space) (Chagelishvili et al., 1992,1993; Chagelishvili, Rogava and Segal, 1994; Chagelishvili et al., 1996; Rogava, Mahajan and Berezhiani, 1996; Chagelishvili, Rogava and Tsiklauri, 1996a, 1996b). The method establishes itself as an effective and convenient tool in the study of the wide range of physical processes taking place in shear hydrodynamic (Marcus and Press, 1977; Chagelishvili et al., 1992; Chagelishvili, Rogava and Segal, 1994) and hydromagnetic (Chagelishvili et al., 1993, 1996; Rogava, Mahajan and Berezhiani, 1996; Chagelishvili Rogava and Tsiklauri, 1996a, 1996b) flows, including anomalous processes of energy exchange between the mean flow and the perturbations—the shear energy drawing by SFH in these flows.

Until now, the non-modal approach was predominantly applied to the study of incompressible (Marcus and Press, 1977; Chagelishvili et al., 1992) and compressible (Chagelishvili, Rogava and Segal, 1994) hydrodynamic shear flows, or incompressible magnetohydrodynamic (MHD) shear flows (Chagelishvili et al., 1993). In particular, authors of

Chagelishvili et al., 1992 demonstrated the "transient growth" of SFH in the incompressible two-dimensional (2D) Couette flow. In (Chagelishvili et al., 1993), consideration of the magnetized (MHD) analogue of the same flow, revealed existence of the anomalous amplification of the SFH, corresponding to slow magnetosonic mode. In (Chagelishvili, Rogava and Segal, 1994) the evolution of 2D SFH in a compressible, plane Couette flow was studied. The new mechanism of the energy exchange between the mean flow and sound-type perturbations was found, leading to the non-exponential, monotonous growth of the SFH energy.

Recently, in the framework of non-modal approach authors of (Chagelishvili et al., 1996) investigated processes of energy exchange of Alfven, slow and fast magnetosonic waves with three dimensional, magnetized, isotropic Couette flow and also considered mutual transformations of these waves. The same kind of processes but in electron-positron MHD plasma were studied in (Rogava, Mahajan and Berezhiani, 1996).

In the present study we apply the non-modal approach to the consideration of compressible, magnetized free shear flow with anisotropic thermal pressure. For the sake of generality, we shall adopt the most general equations of state for a MHD medium (Tan and Abraham, 1972; Tsikarishvili et al., 1992). Some important and preliminary results of this study concerning the effect of coupling and linear transformation of hydromagnetic waves in shear flows, are represented, in part, in (Chagelishvili Rogava and Tsiklauri, 1996a). In the present study after deriving the general set of linearized equations for perturbations we shall investigate the case of strongly magnetized non-relativistic collisionless plasma flow. The pressure of the medium will be taken as anisotropic. However, in one of the subsections we also present results for the isotropic thermal pressure case which was initially investigated in Chagelishvili Rogava and Tsiklauri, 1996a. The physical influence of the shear on the MHD waves, as well as its interaction with plasma instabilities (firehose and mirror instabilities) in the flow will be considered. Section V.2 contains derivation of main equations governing the physical system under consideration in the framework of the non-modal approach. In the section V.3 we focus our attention on the 2D case. Whereas, in subsections we separately demonstrate cases of single and double transformations; and study novel effects due to the firehose and mirror instabilities. In the concluding section we discuss the physical importance of obtained results and their applicability to the above mentioned kinds of realistic shear flows.

V.2 Main Consideration

The basic system of equations, governing the physics of the magnetized plasma flow with anisotropic thermal pressure can be written in the following way:

$$\partial_t \rho + \mathrm{div}(\rho \vec{v}) = 0, \tag{V.1}$$

$$\partial_t\vec{v} + (\vec{v},\nabla)\vec{v} = -\frac{1}{\rho}\mathrm{grad}\left(P_\perp + \frac{B^2}{8\pi}\right) - \frac{1}{\rho}(\vec{B},\nabla)\left[\left(-\frac{1}{4\pi} + \frac{P_\parallel - P_\perp}{B^2}\right)\vec{B}\right], \tag{V.2}$$

$$\mathrm{div}\vec{B} = 0, \tag{V.3}$$

$$\partial_t\vec{B} = (\vec{B}\nabla)\vec{v} - (\vec{v}\nabla)\vec{B} - \vec{B}\mathrm{div}\vec{v}. \tag{V.4}$$

The latter equation—magnetic field induction equation may be written also in the form of so called *Walen equation* (Walen, 1946), which will be useful below

$$(\partial_t + (\vec{v},\nabla))\left(\frac{\vec{B}}{\rho}\right) = \left(\frac{\vec{B}}{\rho},\nabla\right)\vec{v}. \tag{V.5}$$

The equations of state in the most general form may be represented by the following pair of expressions (Tan and Abraham, 1972; Tsikarishvili et al., 1992):

$$P_\perp = c_\perp \rho B^\delta, \tag{V.6a}$$

$$P_\parallel = c_\parallel \rho\left(\frac{\rho}{B}\right)^{2\alpha}. \tag{V.6b}$$

Note that in (V.6) $c_\parallel$ and $c_\perp$ are some dimensional constants. When $P_\parallel = P_\perp$ and $\alpha = \delta = 0$ the equations of state reduce to conventional equation of state for isothermal ideal gas $P\sim\rho$. For anisotropic pressure case, when $P_\perp \neq P_\parallel$ and $\alpha = \delta = 1$ (which, actually, will be used in all numerical work) they represent usual Chew-Goldberger-Low equations of state (Chew, Goldberger and Low, 1956), while when $\alpha = \delta = 1/2$ we get equations of state for collisionless, strongly magnetized plasma with ultrarelativistic temperature (Tsikarishvili et al., 1992).

Let us consider the 3D compressible shearing sheet flow with the regular magnetic field $\vec{B}_0\|\vec{U}_0$ and mean velocity $\vec{U}_0 = (U_{0x} = Ay;\ 0;\ 0)$ (the X axis is directed along the regular velocity vector, the Y axis is directed along a gradient of the shear), where the constant A (without loss of generality, we adopt $A > 0$) parameterizes the regular velocity shear.

The basic system of linearized equations describing the evolution of the small-scale, 3D perturbations in this flow is:

$$(\partial_t + Ay\partial_x)d + \partial_x u_x + \partial_y u_y + \partial_z u_z = 0, \tag{V.7}$$

$$(\partial_t + Ay\partial_x)u_x + Au_y = -C_\parallel^2\partial_x S_\parallel + \left(C_\parallel^2 - C_\perp^2\right)\partial_x b_x, \tag{V.8}$$

$$(\partial_t + Ay\partial_x)u_y = -C_\perp^2\partial_y S_\perp + C_A^2[\partial_x b_y - \partial_y b_x] - \left(C_\parallel^2 - C_\perp^2\right)\partial_x b_y, \tag{V.9}$$

$$(\partial_t + Ay\partial_x)u_z = -C_\perp^2\partial_z S_\perp + C_A^2[\partial_x b_z - \partial_z b_x] - \left(C_\parallel^2 - C_\perp^2\right)\partial_x b_z, \tag{V.10}$$

$$(\partial_t + Ay\partial_x)b_y = \partial_x u_y, \tag{V.11}$$

$$(\partial_t + Ay\partial_x)b_z = \partial_x u_z, \tag{V.12}$$

$$\partial_x b_x + \partial_y b_y + \partial_z b_z = 0, \tag{V.13}$$

where $d \equiv \rho'/\rho_0$ (ρ_0 = const), $\vec{b} \equiv \vec{B}'/|\vec{B}_0|$ ($|\vec{B}_0|$ = const), $C_{||}^2 \equiv P_{||}/\rho_0$, $C_\perp^2 \equiv P_\perp/\rho_0$, and C_A is an Alfven velocity. As regards the quantities $S_{||} \equiv P_{||}'/P_{||}$ and $S_\perp \equiv P_\perp'/P_\perp$ they may be expressed through perturbations of density and magnetic field with a help of the equations of state:

$$S_\perp \equiv d + \delta b_y, \tag{V.14a}$$

$$S_{||} \equiv (2\alpha + 1)d - 2\alpha b_y. \tag{V.14b}$$

The non-modal analysis implies the following substitution of variables (Chagelishvili et al., 1992, 1993 Chagelishvili, Rogava and Segal, 1994; Chagelishvili et al., 1996; Rogava, Mahajan and Berezhiani, 1996; Chagelishvili, Rogava and Tsiklauri, 1996a, 1996b): $x_1 = x - Ayt$; $y_1 = y$; $z_1 = z$; $t_1 = t$. Doing so we can rewrite the equations (V.7–V.12) in the following form:

$$\partial_{t_1} d + \partial_{x_1} u_x + (\partial_{y_1} - At_1\partial_{x_1})u_y + \partial_{z_1} u_z = 0, \tag{V.15}$$

$$\partial_{t_1} u_x + Au_y = -C_{||}^2 \partial_{x_1} S_{||} + \left(C_{||}^2 - C_\perp^2\right)\partial_{x_1} b_x, \tag{V.16}$$

$$\partial_{t_1} u_y = -C_\perp^2(\partial_{y_1} - At_1\partial_{x_1})S_\perp - C_A^2(\partial_{y_1} - At_1\partial_{x_1})b_x + \left(C_A^2 - C_{||}^2 + C_\perp^2\right)\partial_{x_1} b_y, \tag{V.17}$$

$$\partial_{t_1} u_z = -C_\perp^2 \partial_{z_1} S_\perp - C_A^2 \partial_{z_1} b_x + \left(C_A^2 - C_{||}^2 + C_\perp^2\right)\partial_{x_1} b_z, \tag{V.18}$$

$$\partial_{t_1} b_y = \partial_{x_1} u_y, \tag{V.19}$$

$$\partial_{t_1} b_z = \partial_{x_1 1} u_z, \tag{V.20}$$

Let us perform the Fourier analysis of (V.15–V.20), expanding unknown functions denoted below, altogether, by F with respect to *only* spatial variables x_1, y_1, and z_1.

$$F = \int dk_{x1} dk_{y_1} dk_{z1} \hat{F}(k_{x1}, k_{y_1}, k_{z1} t_1) \exp[i(k_{x1}x_1 + k_{y_1}y_1 + k_{z1}z_1)], \tag{V.21}$$

where under F we imply all unknown functions appearing in (V.15–V.20). Further, using Eq.(V.14) and the Fourier transform of Eq.(V.13) (prewritten in variables x_1, y_1, and z_1) we can get:

$$D^{(1)} = v_x + \beta(\tau)v_y + \gamma v_z, \tag{V.22}$$

$$v_x^{(1)} = -Rv_y - (2\alpha + 1)D - \left[(2\alpha + 1) - \varepsilon^2\right](\beta(\tau)b + \gamma b_*), \tag{V.23}$$

$$v_y^{(1)} = -\varepsilon^2\beta(\tau)D + \left[(\varepsilon^2 + \sigma^2 - 1) + (\delta\varepsilon^2 + \sigma^2)\beta^2(\tau)\right]b + \left(\delta\varepsilon^2 + \sigma^2\right)\gamma\beta(\tau)b_*, \tag{V.24}$$

$$v_z^{(1)} = -\varepsilon^2\gamma D + \left[(\varepsilon^2 + \sigma^2 - 1) + (\delta\varepsilon^2 + \sigma^2)\gamma^2\right]b_* + \left(\delta\varepsilon^2 + \sigma^2\right)\gamma\beta(\tau)b, \tag{V.25}$$

$$b^{(1)} = -v_y, \tag{V.26}$$

$$b_*{}^{(1)} = -v_z, \tag{V.27}$$

where hereafter $F^{(n)}$ will denote the n-th order time derivative of F and $D{\equiv}i\hat{d}$, $b{\equiv}i\hat{b}_y$, $b_*{\equiv}i\hat{b}_z$, $R{\equiv}A/(C_{\|}k_{x_1})$, $\sigma^2{\equiv}(C_A/C_{\|})^2$, $\varepsilon^2{\equiv}(C_{\perp}/C_{\|})^2$, $\tau{\equiv}C_{\|}k_{x_1}t_1$, $\beta(\tau){\equiv}k_{y_1}/k_{x_1}-R\tau{\equiv}\beta_0-R\tau$, $\gamma{\equiv}k_{z_1}/k_{x_1}$, $v_i{\equiv}\hat{u}_i/C_{\|}$, $(i=x,y,z)$.

Note that the wave number of a SFH along the flow shear $[k_y(\tau){\equiv}k_{y_1}-Rk_{x_1}\tau]$ varies in time. This process of the linear drift of SFH in the $\vec{k}$-space below will be referred as "the linear drift." It brings qualitative novelty in the evolution of perturbations in the shear flow [discussed in details in (Chagelishvili et al., 1992, 1993)].

If we introduce a new variable: $\psi{\equiv}D+\beta(\tau)b+\gamma b_*$ we can reduce the system (V.22–V.27) to three intercoupled ordinary differential equations of the second order:

$$\psi^{(2)}+{\omega_1}^2\psi=\chi_1(\tau)b+\chi_2 b_*, \tag{V.28}$$

$$b^{(2)}+{\omega_2}^2 b=\chi_1(\tau)\psi+\chi_3(\tau)b_*, \tag{V.29}$$

$$b_*{}^{(2)}+{\omega_3}^2 b_*=\chi_2\psi+\chi_3(\tau)b. \tag{V.30}$$

where we introduce the following auxiliary notations:

$$\omega_1{\equiv}\sqrt{2\alpha+1}, \tag{V.31}$$

$$\omega_2(\tau){\equiv}\sqrt{(\varepsilon^2+\sigma^2-1)+((1+\delta)\varepsilon^2+\sigma^2)\beta(\tau)^2}, \tag{V.32}$$

$$\omega_3{\equiv}\sqrt{(\varepsilon^2+\sigma^2-1)+((1+\delta)\varepsilon^2+\sigma^2)\gamma^2}, \tag{V.33}$$

$$\chi_1(\tau){\equiv}\varepsilon^2\beta(\tau), \tag{V.34}$$

$$\chi_2{\equiv}\varepsilon^2\gamma, \tag{V.35}$$

$$\chi_3(\tau){\equiv}-\left[(1+\delta)\varepsilon^2+\sigma^2\right]\gamma\beta(\tau). \tag{V.36}$$

Note that the quantity ψ is, actually, the x-th component of a perturbation of the "Walen vector" (Walen, 1946) $\vec{B}/\rho$ and the first order differential equation: $\psi^{(1)}=-Rb+v_x$ is directly derived through the x-th component of the Walen equation (V.5).

The further consideration becomes much common, since the equations of this type are well-known in the general theory of oscillations (Magnus, 1976; Kotkin & Serbo, 1971). They describe coupled oscillations with three degrees of freedom. Uncoupled eigenfrequencies and coupling coefficients appearing in (V.31–V.36) are ω_i and χ_i $(i=1,2,3)$ respectively. The presence of shear in the flow ($R{\neq}0$) ensures temporal variability of some of these quantities. However, their dependence on time may be considered as adiabatic when $R{\ll}1$ (Chagelishvili, Rogava and Segal, 1994). Generally speaking, theory of coupled oscillations is applicable to a quite wide class of different physical systems. For instance, mechanical systems with $n>1$ degrees of freedom consisting of coupled oscillators; various kinds of molecules consisting of several atoms; oscillatory circuits with capacitive or inductive coupling and etc. (Magnus, 1976; Kotkin & Serbo, 1971). It is widely acknowledged that existence of the

coupling leads under certain circumstances to the energy exchange between the oscillators and transformation of fundamental oscillations into each other.

Hydrodynamic and other type of plasma flows constitute a such kind of oscillatory systems, where coupling, as a rule, is associated with non-linear processes — wave decay processes (Davidson, 1972), which ensures the mutual transformation of different wave modes. In plasma physics a linear coupling phenomena is also known: mutual transformation of different kind of plasma waves arising due to a *spatial inhomogeneity* of a medium. For example, existence of the density inhomogeneity induces coupling between MHD oscillations (Moiseev & Smiliansky, 1965); or, the transformation of compressional-type waves into electromagnetic-type waves propagating across a density discontinuity (Kritz & Mintzer, 1960), etc. However, we must emphasize that the nature of the wave transformation effect, discussed in this study, qualitatively differs from the already known *linear* transformation mechanisms (Moiseev & Smiliansky, 1965; Kritz & Mintzer, 1960). Density inhomogeneity induced mode transformation occurs permanently in the limited spatial area (across the density inhomogeneity), while in our case transformation of the linear waves occurs in the whole volume, filled by the flow, in the limited time interval (see below).

V.3 Two dimensional Shearing Sheet

Hereafter we shall consider plane $(X0Y)$ "shearing sheet". Evidently, the system (V.22–V.27) reduces, in this case, to the following set of four first order differential equations:

$$D^{(1)} = v_x + \beta(\tau)v_y, \tag{V.37}$$

$$v_x^{(1)} = -Rv_y - (2\alpha+1)D - \Big[(2\alpha+1) - \varepsilon^2\Big]\beta(\tau)b, \tag{V.38}$$

$$v_y^{(1)} = -\varepsilon^2\beta(\tau)D + \Big[(\varepsilon^2+\sigma^2-1) + (\delta\varepsilon^2+\sigma^2)\beta^2(\tau)\Big]b, \tag{V.39}$$

$$b^{(1)} = -v_y, \tag{V.40}$$

while the corresponding set of coupled second order ordinary differential equations takes the following form:

$$\psi^{(2)} + {\omega_1}^2\psi = \chi_1(\tau)b, \tag{V.41}$$

$$b^{(2)} + {\omega_2}^2 b = \chi_1(\tau)\psi. \tag{V.42}$$

where ω_1 and ω_2 are the same as in (V.31) and (V.32) but with $\gamma = 0$. Fundamental frequencies of corresponding coupled (normal) oscillations are (Magnus, 1976; Kotkin & Serbo, 1971):

$${\Omega^2}_{1,2} = \frac{1}{2}\Big[\omega_1^2 + \omega_2^2(\tau) \mp \sqrt{(\omega_1^2 - \omega_2^2(\tau))^2 + 4{\chi_1}^2(\tau)}\Big]. \tag{V.43}$$

Note that in our case Ω_1 and Ω_2 correspond to slow and fast magnetosonic waves (SMW and FMW) respectively. Since the oscillatory system, described by (V.41–V.42) has, two degrees of freedom, its behavior may be determined by two functions $\psi(\tau)$ and $b(\tau)$. Note that all physical quantities from (V.37–V.40) may be expressed through ψ, b and their first derivatives.

As regards the total energy density of a particular SFH , we start its derivation from the standard expression for the energy density in the physical space:

$$\epsilon_{\rm tot} = \left(\rho_0 \frac{u_x^2 + u_y^2}{2}\right) + \left(p'_\perp + \frac{p'_\parallel}{2}\right) + \left(\frac{B^2}{8\pi}\right) \qquad \text{(V.44)}$$

where the first term r.h.s. stands for the kinetic part of the total energy and the second and the third ones for the internal (compressional) and magnetic contributions to the total energy respectively.

Further, using equations of state and retaining only perturbational terms of the second order we can obtain the following expression for total energy of the perturbations in the physical space:

$$e_{\rm tot} = \rho_0 \frac{u_x^2 + u_y^2}{2} + p_\perp^0 \left[\frac{b_y^2}{2} + \left(\frac{\rho'}{\rho_0}\right) b_x\right] + p_\parallel^0 \left[\frac{3}{2}\left(\frac{\rho'}{\rho_0}\right)^2 + \frac{3b_x^2}{2} - \frac{b_y^2}{2} - 3\left(\frac{\rho'}{\rho_0}\right) b_x\right] + \frac{B_0^2}{8\pi}\left[b_x^2 + b_y^2\right] \qquad \text{(V.45)}$$

Finally, normalizing $e_{\rm tot}$ by $\rho_0 C_\parallel^2$, writing it for Fourier transforms of physical quantities and rearranging the terms we arrive at energy density of a particular SFH in the $\vec{k}$-space:

$$E_{\rm tot}(\tau) = \frac{|v|_x^2 + |v|_y^2}{2} + \frac{3|D|^2}{2} - (\varepsilon^2 - 3)\beta(\tau) D b + (\varepsilon^2 + \sigma^2 - 1)\frac{|b|^2}{2} + (3 + \sigma^2)\frac{\beta^2(\tau)|b|^2}{2} \qquad \text{(V.46}a\text{)}$$

Here, we must emphasize the following: Eq.(V.46a) represents the total energy density of a *particular* SFH, in other words the single harmonic of the Fourier expansion (V.21). However, realistic wave packet may be composed by a *number* (even infinite amount) of the SFH. Below, for brevity we shall use term "wave" instead of the "SFH of a wave" but simultaneously keeping this remark in our mind.

Note, that strictly speaking, $E_{\rm tot}(\tau)$ is not positively defined physical quantity, for instance in the case when the condition for firehose instability ($\varepsilon^2 + \sigma^2 < 1$, see below) is satisfied, then the second term from the end in Eq.(V.46a) is negative and also mirror instability requires large values of ε^2 (see below) which presumably can make the third term negative. We will turn back to this point when we will discuss our numerical results concerning these instabilities.

Besides the mathematically strict derivation of $E_{\rm tot}(\tau)$, our confidence in correctness of its form is backed by the fact that in all our numerical results (see below) the $E_{\rm tot}(\tau)$ curve is fairly smooth although all contributing physical quantities are rather oscillatory (see, for instance, Fig. V.23 and corresponding energy curve Fig. V.24).

Since the basis of this study of the shear flows with anisotropic thermal pressure (Chagelishvili, Rogava & Tsiklauri 1996b) is the novel transformation mechanism found firstly for the the isotropic pressure case (Chagelishvili, Rogava & Tsiklauri 1996a), it is also useful to present here some basic results of the latter study. As we said above reduction of the equations from the anisotropic case to the isotropic one is straightforward, namely in all equations we must set $\varepsilon = 1$ and $\alpha = \delta = 0$. As regards the total energy in the isotropic case it can be easily shown that it is given by the following expression (Chagelishvili, Rogava & Tsiklauri, 1996a):

$$E_{tot}(\tau) = (|v_x|^2 + |v_y|^2)/2 + |D|^2/2 + \sigma^2(|b_x|^2 + |b_y|^2)/2 \qquad (V.46b)$$

V.3.1 Stable Oscillatory Modes

In this subsection we consider only stable oscillatory modes exited in the flow understudy. We demonstrate here single and double transformations of magnetosonic waves due to the linear mechanism found by us. Firstly, let us focus our attention on those necessary conditions which are to be satisfied in order to make the mutual transformation of the fundamental oscillatory modes $\Omega_1(\tau)$ and $\Omega_2(\tau)$ possible. In fact, these conditions, but for *isotropic*, compressible magnetized shear flows were firstly outlined in (Chagelishvili, Rogava & Tsiklauri, 1996a). Basically, the transformation conditions remain the same for the *anisotropic* shear flow case as well, but the latter case is much more fertile, since it involves new phenomena like firehose and mirror instabilities which may be of an importance, for instance, for the fusion devices or MHD generators when it comes to the laboratory, or say, radiation mechanisms from various cosmic objects, etc. For completeness we present here the conditions (Chagelishvili, Rogava & Tsiklauri, 1996a; Kotkin & Serbo, 1971) fulfillment of which ensures mutual transformation of SMW and FMW:

- (A) There should exist a so called "degeneration region" (DR) where $|\omega_1^2 - \omega_2^2| \leq |\chi_1(\tau)|$; *
- (B) the DR should be "passed" slowly – in time interval sufficiently exceeding the beating period $\chi_1(\tau)$: $|\omega_2^{(1)}(\tau)| \ll |\chi_1(\tau)|$.

---

*in other words, this condition, which is relevant in the case of weak coupling, implies that $\omega_1 \approx \omega_2$. The latter, in turn, implies that the maximum energy exchange between the pendulums (see below) occurs when they have approximately the same length.

The exact mechanical analogy of the oscillatory system, governed by the same kind of equations, is the following: Let us consider two coupled pendulums: the first one with constant uncoupled eigenfrequency

$$\omega_1 = \sqrt{2\alpha + 1} = \begin{cases} \sqrt{3}, & \text{in the case of anisotropic thermal pressure;} \\ 1, & \text{in the case of isotropic thermal pressure;} \end{cases}$$

and the second one whose uncoupled eigenfrequency $\omega_2(\tau)$ is slowly (adiabatically) varied by some external means (e.g., a variable length). The interpendulum coupling coefficient $\chi_1(\tau)$ is also time-dependent. As regards the condition (A), it is important to note following: Bearing in mind that the mechanical analogy will partially loose its clarity when it will come to consideration of unstable oscillatory modes (firehose and mirror instabilities), it is worthwhile to outline what a graphical representation the condition (A) has while considering the dispersion curves $\Omega_1(\tau)$ and $\Omega_2(\tau)$ (We use here the term dispersion curve since τ is related to $\beta(\tau)$, which itself is related with angle θ between $\vec{B}_0$ and wave vector $\vec{k}$ by simple relation $\beta(\tau) = \tan\theta$). Again involving the mechanical analogy, it is reasonable to state that in the case of weak coupling the maximum energy exchange (i.e. transformation) between the pendulums with fundamental eigenfrequencies $\Omega_1(\tau)$ and $\Omega_2(\tau)$ occurs when they have the same length. In other words when $\omega_2(\tau) \to \omega_1$ and if the coupling between the pendulums is week then this implies that $\Omega_2(\tau) \to \Omega_1(\tau)$ (or i.e. the root in the Eq.(V.43) becomes negligible). *Finally, we conclude that in the case of weak coupling the transformation of the oscillatory modes occurs when their corresponding fundamental eigenfrequencies* $\Omega_1(\tau)$ *and* $\Omega_2(\tau)$ *are coming close to each other therefore forming the DR and indeed, in addition, the condition* (B) *also must be satisfied.* However, as we will see below on the example of mirror instability, the latter graphical criterion, or it is better to say hint, is not generally true in the case of strong coupling.

V.3.1.1 case of single transformation

Since we study two dimensional, compressible and magnetized flow, it is clear that in such a medium there can exist two oscillatory modes (fast and slow magnetosonic waves FMW and SMW), whose dispersion relation is given by (V.43). Basing on the method developed in (Magnus, 1976) it is possible to set such initial conditions for the Eqs.(V.37–V.40) that to excite a distinct wave mode. Further, due to the presence of shear, as we mentioned above, this distinct mode namely $\Omega_1(\tau)$ or $\Omega_2(\tau)$ will evolve in time and if the transformation conditions are satisfied these two wave modes can undergo reciprocal transformations. We performed numerical calculations both for isotropic and anisotropic thermal pressure cases. Results for isotropic case are given on Fig.V.1 whereas the anisotropic pressure case is

represented on the Figs. V.3–V.7 were we plot numerical solution of the Eqs.(37-40). In both cases we set initial conditions in such a way that initially was exited SMW i.e. $\Omega_1(\tau)$. All these graphs unambiguously show that the SMW has been transformed into the fast magnetosonic wave (FMW). The effect of transformation of SMW into FMW is rather pronounced in Figs V.1, V.3, V.5 and V.6 where we see that initially oscillations have low frequency and their amplitude is almost constant, as it should be, since $\Omega_1(\tau)$ far from DR is significantly smaller than $\Omega_2(\tau)$ and remains almost constant (see Figs. V.2 and V.8). However, after passing the DR frequency of the oscillation increases drastically and amplitude starts to increase. Especially the transformation can be clearly seen from the Figs. V.2 and V.8. (isotropic and anisotropic pressure cases respectively) where we plotted following quantities $E_{\rm tot}(\tau)/E_{\rm tot}(0)$, $\Omega_1(\tau)/\Omega_1(0)$ and $(\Omega_2(\tau)/\Omega_2(100)) \times (\Omega_1(100)/\Omega_1(0))$. The latter quantity is rescaled as to reveal the true dispersion of the SMW and FMW. It can be gathered from the graph that initially $E_{\rm tot}(\tau) \sim \Omega_1(\tau)$ but after passing the point $\tau = \tau_* \equiv \beta_0/R = 100$ (midpoint of DR) where actually the $\Omega_1(\tau)$ and $\Omega_2(\tau)$ come close to each other the SMW is transformed into the FMW but there still remains small admixture of SMW which explains not exact proportionality of $E_{\rm tot}(\tau)$ with $\Omega_2(\tau)$. Such a behavior of energy when the waves evolve so that $E_{\rm tot}(\tau) \sim \Omega_{1,2}(\tau)$ can by easily explained by the fact that all physical quantities of the oscillatory system vary in time adiabatically because $R \ll 1$. Since the parameters of the oscillatory system (adiabatically) vary in time, this means that the system is not a closed physical system. In turn, after transformation as energy of FMW is quasilinearly increasing with time, this implies that the growth of the wave occurs on expense of shear energy of the mean flow. It is worthwhile to note that we on purpose choose demonstration of transformation of SMW into FMW. Indeed, reverse process could take place if initially we would excite FMW which certainly would transform into SMW as both conditions (A) and (B) are well satisfied for the set of parameters considered in this example. But, it is important to mention that energy of FMW is quasilinearly increasing in time, so, certainly at some stage non-linear effects will switch on leading to the turbulization of the flow. Therefore, this new transformation mechanism could be helpful for understanding of the stability of the laboratory flows. Although, one should bear in mind rather idealized picture studied here. Say, in realistic physical situation, for instance in Tokamaks, the flows have much more complicated geometry and velocity shear can not be simply described in the framework of mere model of plane Couette flow. However, on small scales every flow with non-linear shear profile can be effectively represented by superposition of thin layers with linear shear so this example gains certain relevance to the stability analysis of the realistic physical flows.

V.3.1.2 case of double transformation

Another interesting feature of the linear transformation mechanism found by us is double transformation. Namely, in the case of anisotropic thermal pressure, for certain choice of parameters ε^2 and σ^2 looking at the dispersion curves Figs. V.14 or V.20, we gather that there are two degeneration regions where $\Omega_1(\tau)$ and $\Omega_2(\tau)$ are coming close to each other. In Fig. sets V.9–V.13 and V.15–V.19 we present numerical solutions of Eqs.(V.37-V.40) for different sets of physical parameters. It can be seen from the graphs that in both cases there is an energy exchange between oscillatory modes $\Omega_1(\tau)$ and $\Omega_2(\tau)$ in the DR-s where these two dispersion curves are coming close to each other. This exchange can be unambiguously seen from the Figs.V.9–V.13 and V.15–V.19, remarking drastical changes in amplitudes of the oscillations of the physical quantities during their presence in the both DR-s. However, these two cases differ significantly as each of them represents physical situation when after coming through the second degeneracy region the final oscillatory mode remains to be SMW (Fig. V.14) and in the second case the final oscillatory mode is FMW (Fig. V.20). Although we stress that in both cases initially there was precisely exited only SMW mode. Explanation of this novel effect can be given by the following reasonings: After passing the first DR, in the flow there will be present a mixture of SMW and FMW. In (Chagelishvili et al., 1993) it was demonstrated that the outcome of the amplification process of the slow magnetosonic wave in incompressible, magnetized Couette flow with isotropic thermal pressure significantly depends on the phase with which the wave enters the amplification region. The physical system under present consideration differs from the one studied in (Chagelishvili et al., 1993) (as in our case we have two oscillatory modes). But, presumably, the outcome of the process of energy exchange between SMW and FMW depends on the phase difference between these oscillatory modes at time moment when the mixture leaves the second DR. The latter depends on duration of presence of the mixture in the second DR (which, in turn, is determined by R parameter — smaller R is longer time the mixture remains in the DR) and on physical parameters ε^2 and σ^2. So far, for different set of physical parameters (i.e. for opposite phase difference at instance when the mixture leaves the second DR) we can end up either with SMW or FMW.

Besides, it is worthwhile to give some comments for behavior of $E_{\rm tot}$ in the latter two cases (Figs V.14 and V.20) where we plotted quantities $E_{\rm tot}(\tau)/E_{\rm tot}(0)$, $\Omega_1(\tau)/\Omega_1(0)$ and $[\Omega_2(\tau)/\Omega_2(\text{midpoint of the first DR}) \times \Omega_1(\text{midpoint of the first DR})/\Omega_1(0)]$. Again the latter quantity is rescaled as to reveal the true dispersion of the SMW and FMW. On the both graphs we see that initially $E_{\rm tot}(\tau) \sim \Omega_1(\tau)$ as it should be, since we exited SMW but this lasts until the oscillatory mode is far from the first DR (about $\tau = 70.66$ in one case and $\tau = 71.71$ in the other). However, we clearly see that after passing the first DR $E_{\rm tot}$ deviates from the SMW dispersion curve (dashed curve), which apparently shows that there was an energy exchange between the SMW and FMW. Further, (from the first DR until the second DR) there is a mixture of $\Omega_1(\tau)$ and $\Omega_2(\tau)$ propagating. But in one case (Fig.V.14) after

leaving the second DR we have again SMW, whereas in another case (Fig.V.20) finally we have FMW.

V.3.2 Unstable Oscillatory Modes

In this subsection we study unstable oscillatory modes which appear in the flow with anisotropic thermal pressure, namely, firehose and mirror instabilities and their interplay with effect of presence of the shear. Firstly, let us derive stability criteria in the flow under study. Eq.(V.43) implies that the oscillatory mode becomes unstable when $\omega_1^2\omega_2^2 < \chi_1^2(\tau) = \varepsilon^4\beta^2(\tau)$. Further, using expressions for ω_1 and ω_2 and also straightforward equalities: $\cos^2\theta = 1/(1+\beta^2(\tau))$ and $\sin^2\theta = \beta^2(\tau)/(1+\beta^2(\tau))$ we arrive to the condition

$$\sin^2\theta \cdot \varepsilon^4 - 3(1+\sin^2\theta)\cdot\varepsilon^2 + 3(\cos^2\theta - \sigma^2) > 0 \qquad \text{(V.47)}$$

and its fulfillment ensures unstable behavior of the anisotropic flow. We can get traditional criterion (Krall & Trivelpiece, 1973) (adopted for our notations, of course) for firehose instability simply putting $\theta = 0$ in the latter formula, which yields: $\varepsilon^2 + \sigma^2 < 1$. Doing the same but with $\theta = \pi/2$ we can obtain criterion for mirror instability: $\sigma^2 + 2\varepsilon^2 < \varepsilon^4/3$.

There are variety of physically interesting cases which arise in this consideration. But, we restrict ourselves by two examples with firehose instability and one example with mirror instability which in our opinion are the most interesting from the point of view possible experimental implications.

Before starting consideration of the numerical results, we would like to emphasize a very important difference which arises due to presence of the shear in the flow. If we look at the dispersion curves Figs.V.22 and V.24 we can mention that the unstable region for firehose instability is located in the middle of the graphs i.e. around $\tau \simeq 100$ where the real part of the $\Omega_1(\tau)$ (curve with circles), on which actually this instability occurs, remains to be zero while it has non-zero imaginary part there, which of course is not drawn on the graphs. Now if there would be no shear, in the flow under consideration there could propagate either SMW or FMW with *fixed* frequency given by any point which belongs to the $\Omega_1(\tau)$ or $\Omega_2(\tau)$, or their linear superposition. But, the point is, that with presence of the shear there does exist a linear drift in the $\vec{k}$-space, which basically means that if we excite a wave, say, SMW with initial frequency $\Omega_1(0)$ (Figs. V.22 or V.24) it will evolve changing its frequency following the $\Omega_1(\tau)$ curve and certainly at moment of time when it will reach the unstable region the firehose instability will switch on leading to the growth of the wave. Whereas in the case without shear we would have a stable wave propagating with its initial fundamental frequency $\Omega_1(0)$. So, we conclude that in the shear flow occurrence of firehose instability on the SMW branch of dispersion is unavoidable (if the appropriate condition $\varepsilon^2 + \sigma^2 < 1$ is

fulfilled, of course). Basically, the same conclusions apply to the mirror instability as well (see Fig.V.26). But in differ from the firehose instability which has finite instability region, mirror instability has two infinite unstable regions $(-\infty; -\tau_{\text{inst}}]$ and $[\tau_{\text{inst}}; +\infty)$. Where

$$\tau_{\text{inst}} = \frac{1}{R}\left[\beta(0) - \sqrt{\frac{\varepsilon^2 + \sigma^2 - 1}{(\varepsilon^4/3) - 2\varepsilon^2 - \sigma^2}}\right].$$

V.3.2.1 case of firehose instability

Now, turning back to the firehose instability, we can make much more far reaching conclusions. Suppose, we exited FMW wave which is apparently stable in what is called "standard MHD theory" (since $\Omega_2^2(\tau)$ itself never becomes negative). But, in the case when we have got a shear in the flow and *there is possibility of transformation or i.e. energy exchange between SMW and FMW*, FMW can gain significant part of energy from the unstable SMW branch. Further, of course at some stage non-linear effects will switch on and in the end flow will loose stability i.e. become turbulized. Now we discuss concrete examples of our numerical work. On the Figs.V.21 and V.23 we present numerical solutions of the Eqs.(V.37-V.40) for different sets of physical parameters. In both cases initially was exited FMW. looking at the corresponding dispersion curves Figs. V.22 and V.24 we see that in both cases there is an unstable region on the SMW. To avoid any doubt we choose physical parameters in such a way that the growth rates (i.e. imaginary part in $\Omega_1(\tau)$) of firehose instability is the *same* in both cases (in other words in the midpoint of instability region ($\beta = 0$) the quantity $\varepsilon^2 + \sigma^2 - 1$ is the same) and also R parameter is the same, thus ensuring the same duration of presence of FMW in the region where $\Omega_1(\tau)$ and $\Omega_2(\tau)$ come close to each other. But in the first case we see that the FMW gained significant amount of energy from the unstable SMW, while in the second case there is no amplification of FMW at all. Explanation of this fact is lucid: from the dispersion curves (Figs.V.22 and V.24) we gather that in first case dispersion curves $\Omega_1(\tau)$ and $\Omega_2(\tau)$ (curves with circles) are coming rather close to each other and thus creating two DR-s, while in the second case the curves pass by at a significant distance and hence avoiding formation of the DR. We clearly see from the Fig. V.22 that although initially there was exited FMW after passing the first DR total energy of the wave increased significantly since it gained energy from the firehose-unstable SMW finally reaching values two orders of magnitude more than its initial value. On the Fig.V.24 we see that there is no exchange of energy between FMW and SMW since we see that the during the hole considered time interval E_{tot} is strictly proportional to the $\Omega_2(\tau)$ which actually was exited right from the beginning. We would like to mention that this interesting effect can occur because of existence of shear in the flow and its revealing

became possible due to the non-modal approach. While it was not perceived under the more traditional normal modes paradigm.

V.3.2.2 case of mirror instability

We also studied the case when the mirror instability can occur in the flow. Our numerical results are presented on the Figs.V.25 and V.26 where we plot numerical solutions of the Eqs.(V.37-V.40), corresponding dispersion curves and the total energy. As an illustrative example we again choose the case when initially was exited FMW (since it is rather novel and unusual when we have amplification of "classically stable" FMW wave). We see that although the dispersion curves of $\Omega_1(\tau)$ and $\Omega_2(\tau)$ do not come close come to each other, we still see amplification of the FMW i.e. energy exchange between FMW and SMW still occurs. This also has its explanation which can be seized if we recall what is a definition (Eq.(V.34)) of coupling constant in this case. In fact, the latter one is proportional to the ε^2. To get mirror instability condition satisfied we need to require large values of ε^2 which in considered case is 10. This means that in this case coupling between SMW and FMW is so strong that in spite of the fact that the dispersion curves do not come close enough to each other the energy exchange between the oscillatory modes still occurs, thus leading to the amplification of FMW. Therefore, we conclude, that if the condition for occurrence of the mirror instability is satisfied the amplification of the FMW seems to be unavoidable.

As we can see from the Fig.V.26 total energy of the FMW goes to large negative values. One should not be surprised by this fact as firstly, strictly speaking the the total energy as we mentioned above is not positively defined quantity, since it contains negative terms, but this is ad hoc explanation; secondly, normally in plasma physics there is a possibility to have waves with negative energies (Davidson, 1972; Bekefi, 1966; Briggs, 1964; Coppi, 1969; Cairns, 1979) which basically means, that to excite such a wave no net energy is necessary to be input into the medium, just contrary to that, energetically is more gainable when the wave gives away its energy to the medium. In other words it can be said that the medium is non-equilibrium. In the case of firehose instability (Fig. 22) the E_{tot} also falls down to negative values while being in the unstable region (however, this is obscured in the graph). Basically, FMW after passing first DR gets admixture of SMW which has obviously negative energy (since it is unstable). But instability region has finite width and the SMW further becomes stable, which therefore ensures that energy becomes again positive with much more increased magnitudes. In the case of mirror instability the FMW gained admixture of SMW which remains unstable in infinite time interval $[\tau_{\text{inst}}; +\infty)$ with permanently increasing growth rate of instability. Thus the total energy of the wave will be negative all the time.

V.4 conclusion

We have observed from the above study that the pressure anisotropy brought significant novelty to the consideration through the two key aspects. First one, possibility of creation of the two degeneration regions which, in turn, yields in a novel phenomenon which we have called the double transformation. Including, interesting alternative in the final outcome of the transformation process when there is a possibility to end up with either SMW or the FMW. Second, possibility of occurrence of the firehose and mirror instabilities and their interplay with the effect of presence of the shear in the flow. Including, possibility of remarkable amplification of the FMW caused by the energy exchange with firehose-unstable SMW (when appropriate conditions are fulfilled); or unavoidable amplification of the FMW (due to the strong coupling) caused by the energy exchange with mirror-unstable SMW. Besides, it must be stressed that all novel effects are caused purely by presence of the shear in the flow (through the time dependence of the fundamental frequencies, which, in turn, is a consequence of the linear drift in $\vec{k}$-space). And, of course, obtaining of the new results became possible thanks to the relevant description of a physical system such as shear flow is — i.e. in the framework of the non-modal approach.

Although, examples considered in this study are rather idealistic they still may be useful for understanding of the stability of plasma in realistic laboratory devices such as Tokamaks or MHD generators are (we made more detailed remarks concerning this point in relevant places of the text). Besides, usually, plasma instabilities also play an important role in the formulation of radiation mechanisms from various space objects (for instance, in pulsar winds the shear effect may have importance after the co-rotation radius and in addition, bearing in mind a condition $\varepsilon^2 \equiv (C_\perp/C_\parallel)^2 = P_\perp^2/P_\parallel^2 \ll 1$, relevant for this outflow, one should not exclude a possibility of fulfillment of criterion of the firehose instability ($\varepsilon^2 + \sigma^2 < 1$) which finally will, perhaps, result in the interplay of these phenomena similar to that of considered in this study). Thus, presumably, some of the effects studied here may suffice to the understanding of some of the astrophysical problems as well. Primarily, the aim of this study was to investigate these effects theoretically, in a rather simplified framework. However, if one should desire to be more precise and rigid in the statements when it comes to realistic physical or astrophysical situations, then more complicated flow geometries and symmetries should be taken into consideration. But in our opinion this contribution can serve as a basic starting point for this task.

VI On the Effect of Conical Refraction of Hydromagnetic Waves in Plasma With Anisotropic Thermal Pressure

VI.1 introduction

Like in previous sections we shall again employ magnetohydrodynamic description of the plasma. However, we should emphasize that in this study motion of the plasma as a whole is not essential. Basically, the effect discussed in this section presumably can occur in several space plasma magnetohydrodynamical flows, e.g. solar wind — where physical conditions are quite similar to ones considered in this study. The only requirement of applicability of the latter statement is that the flow should have uniform mean velocity field. In other words, it must be possible to choose global reference frame moving with the flow. Essentially results of this section are based on the recent papers Tsiklauri 1996a and 1996b. Below we make some introductory remarks and then switch to presentation of the results.

A phenomenon of the conical refraction — a peculiar kind of light refraction in biaxial crystals taking place when a direction of a light beam coincides with some of the optical axes (binormals) of the crystal, was predicted theoretically by W.R. Hamilton as early as in 1832. He discovered this phenomenon basing on the Huygens–Fresnel principle (formulated 17 years earlier) applied for the biaxial crystals. In 1833 H. Lloyd proved experimentally existence of the phenomenon. For instance, in the biaxial crystals observation of the optical conical refraction is possible if the parallel, narrow beam of natural (non-polarized) light falls along the optical axis (binormal) of wave normals on a plate cut so that its two parallel faces are perpendicular to the binormal. While propagating through the crystal the beam will form an empty cone with permanently changing linear polarization. Thus, producing a circle on the photographic plate placed after the crystal.

Further, the phenomenon of the conical refraction was discovered for the elastic waves propagating along the acoustical axis of the crystal. For example, the inner conical refraction may take place when purely shearing waves propagate through the crystal along the third order symmetry axis (principal axis of symmetry [001] in triagonal crystals; direction [111] along the diagonal of a cube in the cubical crystals). In certain cases phenomenon of the acoustical conical refraction may be rather pronounced. The angle of the conical refraction (i.e., angle of deflection of the beam from the acoustical axis of the crystal) may have significant magnitude, for instance, in calcit $CaCO_3 \approx 30°$, in quartz $\approx 17°$ etc.

Resuming aforesaid, the phenomenon of the conical refraction in the crystals (optical and acoustical) is known for quite a long time and hence is completely studied. However, further display of the phenomenon is rather surprising: in (Sivukhin, 1966) there was theoretically discovered the phenomenon analogous to the inner conical refraction for *magnetosonic* waves

propagating in the isotropic plasma which is considered as a perfectly conducting fluid with adiabatical perturbations in it (see for brief description of the effect more accessible (Akhiezer & Akhiezer, 1973)). In particular (Sivukhin, 1966), if the Alfven velocity coincides with the speed of sound then in the case of propagating of a quasiplane magnetosonic wave along the uniform magnetic field the beams corresponding to the wave will form an empty cone with the opening angle 53°08′, i. e. the angle of conical refraction for the magnetosonic waves in isotropic plasma was predicted to be 26°34′.

In the present study, while considering adiabatical disturbances in collisionless plasma contained in a uniform external magnetic field and hence described by the theory of Chew, Goldberger and Low (Chew, Goldberger & Low, 1956; Krall & Trivelpiece, 1973; Cap, 1976), is discovered phenomenon analogous to the inner conical refraction. Initially it was found (Tsiklauri, 1996a) that angle of the conical refraction for the magnetohydrodynamical (MHD) waves in the plasma with anisotropic thermal pressure should be 18°26′. However, further, more general consideration showed (Tsiklauri, 1996b) that the angle of the conical refraction depends on the ratio of the Alfven speed and sound speed measured in perpendicular direction in respect to the external magnetic field.

VI.2 main consideration

Let us consider the most general form of the dispersion relation for the MHD waves in magnetized plasma with anisotropic thermal pressure:

$$\omega^2 = \frac{k^2}{2\rho_0}\left[\frac{B_0^2}{4\pi} + p_\perp(1+\delta\sin^2\theta) + 2\alpha p_{||}\cos^2\theta \right.$$

$$\left. \pm\sqrt{\left(\frac{B_0^2}{4\pi} + p_\perp(1+\delta\sin^2\theta) - 2(\alpha+1)p_{||}\cos^2\theta\right)^2 + 4p_\perp^2\sin^2\theta\cos^2\theta}\right]. \qquad \text{(VI.1)}$$

The latter equation can be derived from the dispersion relation obtained in (Tsikarishvili & Rogava, 1994) while considering its nonrelativistic limit (i.e. neglecting displacement current and ultrarelativistic temperature effects), but retaining a freedom in choice of the polytropic indexes δ and α. Note, that in the derivation of Eq.(VI.1) there were used equations of state given by Eq.(V.6a) and (V.6b). Of course, taking into due account the limiting cases $\alpha = \delta = 0$ and $\alpha = \delta = 1$ in Eq.(VI.1) results in the correct expressions for the dispersion relations for the linear MHD waves in isotropic and anisotropic pressure plasmas accordingly, which can be found in any textbook of plasma physics.

For the sake of convenience we use further following notations (Tsiklauri, 1996a):

$$a = \frac{B_0}{\sqrt{4\pi\rho_0}},\quad c_\perp = \sqrt{\frac{p_\perp}{\rho_0}},\quad c_{||} = \sqrt{\frac{p_{||}}{\rho_0}}$$

where a stands for the Alfven velocity, $c_\perp$ and $c_\parallel$ are the sound speeds measured in perpendicular and parallel directions in respect to the uniform, external magnetic field $\vec{B}_0$.

Now we can rewrite Eq.(VI.1) in the following form:

$$V^2 = \frac{1}{2}\Big[a^2 + c_\perp^2(1+\delta\sin^2\theta) + 2\alpha c_\parallel^2\cos^2\theta$$

$$\pm\sqrt{\left(a^2 + c_\perp^2(1+\delta\sin^2\theta) - 2(\alpha+1)c_\parallel^2\cos^2\theta\right)^2 + 4c_\perp^4\sin^2\theta\cos^2\theta}\Big] \qquad \text{(VI.2)}$$

where $V = \omega/k$ denotes the phase velocity of the waves.

In (Tsiklauri, 1996a) after this step, in order get desired result (theoretical demonstration of the existence of the conical refraction) author required fulfillment of the following relation between $c_\parallel$ and $c_\perp$: $c_\perp = \sqrt{2}c_\parallel$. Furthermore, according to (Tsiklauri, 1996a) final necessary condition for occurrence of the effect was obtained as: $a = c_\perp = \sqrt{2}c_\parallel$. However, now let us restrict ourselves with much more weak condition (Tsiklauri, 1996b):

$$a^2 + c_\perp^2 - 2(\alpha+1)c_\parallel^2 = 0, \quad \text{or} \quad c_\parallel^2 = \frac{a^2 + c_\perp^2}{2(\alpha+1)}. \qquad \text{(VI.3)}$$

Substituting in Eq.(VI.2) the latter expression for $c_\parallel^2$ and introducing χ and ψ as

$$\chi^2 = a^2 + (1+\delta)c_\perp^2 \text{ and } \psi^2 = \frac{\alpha a^2 - [\delta(\alpha+1)-\alpha]c_\perp^2}{\alpha+1}$$

we can obtain:

$$V^2 = \frac{1}{2}\Big[\chi^2 + \psi^2\cos^2\theta \pm \sqrt{\chi^4 + 2(2c_\perp^4 - \chi^4)\cos^2\theta + (\chi^4 - 4c_\perp^4)\cos^4\theta}\Big] \qquad \text{(VI.4)}$$

Possessing the formula for the phase velocity of the wave it is easy to derive expression for the group velocity $\vec{u}$ via straightforward, but time consuming calculations:

$$\vec{u} = \frac{\partial\omega}{\partial\vec{k}} = \vec{N}V + k\frac{\partial V}{\partial\vec{k}} =$$

$$V\Bigg[\frac{[\cos\theta/2V^4]\,(\psi^2 T(\theta) + (2c_\perp^4 - \chi^4) + (\chi^4 - 4c_\perp^4)\cos^2\theta)}{1 - C/V^4}\vec{A} +$$

$$\frac{[1/2V^4]\,((2V^2 - \psi^2\cos^2\theta)T(\theta) - (2c_\perp^4 - \chi^4)\cos^2\theta - (\chi^4 - 4c_\perp^4)\cos^4\theta)}{1 - C/V^4}\vec{N}\Bigg] \qquad \text{(VI.5)}$$

where we introduced following notations: unit vectors $\vec{N} = \vec{k}/|\vec{k}|$ and $\vec{A} = \vec{B}_0/|\vec{B}_0|$; $T(\theta) \equiv 2V^2 - (\chi^2 + \psi^2\cos^2\theta)$ and

$$C \equiv (2\alpha+1)[a^2 + c_\perp^2(1+\delta\sin^2\theta)]\left(\frac{a^2 + c_\perp^2}{2(\alpha+1)}\right)\cos^2\theta$$

$$-(2\alpha+1)\left(\frac{a^2+c_\perp^2}{2(\alpha+1)}\right)^2\cos^4\theta - c_\perp^4\sin^2\theta\cos^2\theta.$$

Here we must note that in Eq.(VI.5) we used biquadratic equation

$$V^4 - (\chi^2+\psi^2\cos^2\theta)V^2 + C = 0,$$

solution of which dispersion relation (VI.4) actually is.

To realize the physical picture geometrically it is worthwhile to state here following reasonings (Sivukhin, 1966): let multiply scalarly Eq.(VI.5) formula by $\vec{N}$:

$$(\vec{u}\vec{N}) = V \qquad \text{(VI.6)}$$

i.e. projection of group velocity on the direction of wave normal is equal to the phase velocity in the same direction. Multiplying eq.(VI.6) by k one can get: $(\vec{u}\vec{k}) = \omega$. Hence, for the infinitesimal changes of $\vec{u}$, $\vec{k}$ and ω the following relation is valid: $(\vec{u}\delta\vec{k}) + (\vec{k}\delta\vec{u}) = \delta\omega$. According to the definition of group velocity $(\vec{u}\delta\vec{k}) = \delta\omega$. Therefore, $(\vec{k}\delta\vec{u}) = 0$, or in other terms

$$(\vec{N}\delta\vec{u}) = 0 \qquad \text{(VI.7)}$$

The vector $\delta\vec{u}$ is located in the plane tangential to the surface (so called beam surface (Sivukhin, 1966)) formed by the ends of vectors of the group velocities drawn away from the arbitrary point O. Therefore, Eq.(VI.7) implies that the plane, tangential to the beam surface, is perpendicular to the corresponding wave normal. i.e. the beam surface is the envelope for the plane wave fronts, which were propagated from reference point O in every directions per unit time. The latter statement in combination with Eq.(VI.6) completely determines geometrical relationship between surface of phase velocities with the beam surface. However, it should be stressed that this geometrical relationship is valid only for the waves whose phase velocities depend only on the direction and not on the length of the wave vector $\vec{k}$. It is enough to show that in such case Eq.(VI.6) is valid. Let V (phase velocity) be arbitrary function of wave vector $\vec{k}$. Then $\omega = kV(\vec{k})$ and hence, $\vec{u} = \partial\omega/\partial\vec{k} = V(\vec{k})\vec{k}/k + k\partial V/\partial\vec{k}$. It is necessary and sufficient for condition (VI.6) to be hold that the V must satisfy the following requirement: $\vec{k}\partial V/\partial\vec{k} = 0$ or that is the same as $k_i\partial V/\partial k_i = 0$. Therefore, one can conclude that V must be homogeneous function of k_i components of the zeroth order. The latter statement is equivalent to the requirement that function V depends only on the direction of wave vector $\vec{k}$ and not on its length. As it can be seen clearly the dispersion relations (VI.1) and of course (VI.2) and (VI.4) satisfy this condition.

It is known (Sivukhin, 1966) that while possessing surface formed by phase velocities one can construct geometrically the beam surface (formed by the ends of vectors of the group velocities) and *vice versa*. But instead of doing this it more convenient to carry out analytical calculation.

Let us describe a direction of the group velocity $\vec{u}$ by an angle φ between $\vec{u}$ and $\vec{B}_0$ (i.e., between $\vec{u}$ and $\vec{A}$). One can determine the angle φ by the formula:

$$\tan\varphi = \frac{\vec{u}\times\vec{A}}{\vec{u}\cdot\vec{A}}$$

which with the aid of Eq.(VI.5) yields:

$$\tan\varphi = \frac{(2V^2-\psi^2\cos^2\theta)T(\theta)-(2c_\perp^4-\chi^4)\cos^2\theta-(\chi^4-4c_\perp^4)\cos^4\theta}{(2V^2+\psi^2\sin^2\theta)T(\theta)+(2c_\perp^4-\chi^4)\sin^2\theta+(\chi^4-4c_\perp^4)\cos^2\theta\sin^2\theta}\tan\theta. \quad \text{(VI.8)}$$

Note, that $T(\theta)\to 0$ when $\theta\to 0$.

The latter equation determines the direction of the group velocity $\vec{u}$ whereas its modulus can be calculated by expression:

$$|\vec{u}| = V/\cos(\varphi-\theta) \quad \text{(VI.9)}$$

It is worth of remarking that the Eq.(VI.9) is a consequence of the expression (VI.6).

Now, it can be easily shown that the expressions for group velocity and $\tan\varphi$ [Eqs. (VI.5) and (VI.8) correspondingly] exhibit uncertain behaviour as 0/0 when $\theta\to 0$. Removing of the uncertainty (for the sake of brevity we omit, here, several steps of this task) results in:

$$\tan\varphi(+0) = \lim_{\theta\to 0}\tan\varphi(\theta) = \pm\left(\frac{\alpha+1}{2\alpha+1}\right)\frac{1}{1+(a/c_\perp)^2} \equiv \pm\left(\frac{\alpha+1}{2\alpha+1}\right)\Gamma^2, \quad \text{(VI.10)}$$

$$|\vec{u}(+0)| = \sqrt{\left[1+\left(\frac{\alpha+1}{2\alpha+1}\right)^2\Gamma^4\right]\left(\frac{2\alpha+1}{\alpha+1}\right)}\sqrt{\frac{a^2+c_\perp^2}{2}}. \quad \text{(VI.11)}$$

In Eq.(10) sign "+" and "−" correspond to the slow and fast MHD waves. It is worthwhile to note that Eqs.(10) and (11) (obtained in Tsiklauri,1996b) are, of course, in agreement with previous results (Tsiklauri, 1996a; Sivukhin, 1966). If we consider the isotropic pressure limit ($p_\parallel = p_\perp = p$, $c_\parallel = c_\perp = c$, and $\alpha = \delta = 0$) and require $a^2 = c^2$ (Sivukhin, 1996) then Eqs.(10) and (11) reduce to the form:

$$\tan\varphi(+0) = \pm\frac{1}{2} \quad \text{and} \quad |\vec{u}(+0)| = \frac{\sqrt{5}}{2}c = \frac{\sqrt{5}}{2}a \quad \text{(VI.12)}$$

as it was actually obtained in (Sivukhin, 1966). Whereas, applying the condition imposed in (Tsiklauri, 1996a) $a = c_\perp = \sqrt{2}c_\parallel$ we arrive at

$$\tan\varphi(+0) = \pm\frac{1}{3} \quad \text{and} \quad |\vec{u}(+0)| = \sqrt{\frac{5}{3}}c_\perp = \sqrt{\frac{5}{3}}a. \quad \text{(VI.13)}$$

We must admit, here, that in the Eq.(9) for the modulus of the group velocity from the (Tsiklauri, 1996a) factor of $\sqrt{\frac{3}{2}}$ is missing. Apparently, substituting $V(\theta=0) = \sqrt{\frac{3}{2}}\cdot a = \sqrt{\frac{3}{2}}\cdot c_\perp$ and $\cos\varphi = \sqrt{10}/3$ in the Eq.(VI.9) results in Eq.(VI.13). This should not cause a confusion,

as it does not affect the main result of the (Tsiklauri, 1996a) — theoretical demonstration of possibility of the occurrence of the conical refraction in the anisotropic plasma plus calculation of the angle of the conical refraction, which is, actually, an experimentally observable physical quantity. We see that the results obtained in this consideration are consistent with previous contributions (Tsiklauri, 1996a; Sivukhin, 1966). However, it must emphasized that more general results given by Eqs.(VI.10) and (VI.11) obtained in (Tsiklauri, 1996b) bring more diversion in the predicted phenomenon (see below). Besides, from technical point of view it should be much easier to produce the plasma satisfying condition (VI.3) proposed in (Tsiklauri, 1996b), rather than condition $a = c_\perp = \sqrt{2}c_\parallel$ claimed in (Tsiklauri, 1996a).

VI.3 discussion

The above consideration shows that when the wave normal $\vec{N}$ tends to reach a direction parallel to $\vec{B}_0$ (i. e. when θ tends to zero), vector of group velocity $\vec{u}$ does not take the same direction, but its limiting position (when $\theta \to 0$) is the surface of an empty cone with opening angle $2\varphi(+0) \equiv 2\arctan[\varphi(+0)]$ given by Eq.(VI.10). When θ is zero exactly (which is quite unlikely from the experimental point of view as all waves produced in a laboratory may have only finite angle of aperture) then $\vec{u}$ is strictly parallel to $\vec{B}_0$. The discontinuous behavior exhibited by the vector $\vec{u}$ can be explained by means of existence of so called (Sivukhin, 1966; Tsiklauri, 1996a) angular point which in general case revealed to exist when $a^2 + c_\perp^2 - 2(\alpha+1)c_\parallel^2 = 0$ (Tsiklauri, 1996b). Thus, when $a^2 + c_\perp^2 - 2(\alpha+1)c_\parallel^2 = 0$ the angular point on the surfaces formed by the phase velocities (both fast and slow MHD waves) is located in the point of intersection of the ones with the direction of the magnetic field $\vec{B}_0$. Which, in turn leads to the discontinuous behaviour of $\vec{u}$ and causes the effect. In other words, as it was shown in (Tsiklauri, 1996a), the angular point exists when phase velocities of the slow and fast MHD waves do coincide. We observe form Eq.(VI.4) [again, which was obtained from general dispersion relation (VI.2) imposing condition (VI.3)] that when $\theta \to 0$ slow ("$-$") and fast ("$+$") branches of phase velocity equal to each other (viz., the square root vanishes), which results in an uncertain behavior of its derivative by $\vec{k}$ i.e. group velocity.

It is interesting to note that in differ to the result of (Tsiklauri, 1996a), now imposing less restrictive condition (VI.3) the angle of the conical refraction is not a *fixed* number but it depends [via Eq.(VI.10)] on the ratio $a^2/c_\perp^2$ (Tsiklauri, 1996b). Which, in turn, depends on the plasma medium physical parameters such as density and the magnitude of the exerted external magnetic field $\vec{B}_0$.

As regards a possible experimental corroboration of the effect, we may propose the following experiment: consider two collisionless plasma media contained in a uniform external

magnetic field $\vec{B}_0$. The media are separated by means of the insulating plane perpendicular to the $\vec{B}_0$. Let us choose physical parameters in the second medium as to satisfy the condition (VI.3). If we place a diaphragm between the first and second media then a narrow beam of MHD waves propagating from the first medium towards the second one, just after passing the diaphragm will deflect from the direction of $\vec{B}_0$ and form an empty cone with angle of opening $2\varphi(+0)$.

It is worthwhile to note that one of the possible applications of the effect of the conical refraction may be its usage in plasma diagnostics. The condition (VI.3) explicitly depends on the magnitude of external magnetic field $\vec{B}_0$. So, if in the above proposed experimental setup, in the second medium the condition (VI.3) is not satisfied a detector of MHD waves placed just opposite to the diaphragm (see Fig.VI.1) will fairly detect the waves. However, with variation of the magnitude of the exerted magnetic field we may achieve fulfillment of the condition (VI.3) which will result in a steep drop of the detector's indication, as due to the effect of the conical refraction the MHD waves will deflect from the $\theta = 0$ axis and form an empty cone with opening angle $2\varphi(+0)$, thus avoiding arrival of the waves into the detector (see Fig. VI.2). Since the condition VI.3 explicitly depends on the external magnetic field, in the event of occurrence of the phenomenon it must be possible to measure its magnitude if the thermodynamical parameters (pressure and density) of the plasma are known or vice versa. Therefore, we conclude that presumably this effect can be used in plasma diagnostics (Tsiklauri, 1996a, 1996b).

Besides, of a purely fundamental interest which experimental demonstration of the phenomenon might have, probably, this effect will find its applications in practice, since through variation of external parameters (viz., varying the ratio a^2/c_1^2) it is possible to regulate opening angle of the empty conical beam of the MHD waves. Which means, that, for instance, with simple from technical point of view variation of the magnitude of the external magnetic field it is possible to regulate a direction of propagation of the energy carried by the MHD waves. Because, it is known that the energy propagates along the direction of the wave's group velocity vector. Therefore, one should not exclude possible applications of this novel effect (revealed by the general consideration employed in Tsiklauri, 1996b) in the plasma devices such as MHD generators are.

Finally, we would like to emphasize on principal difference between the effect predicted in this study and the effect of the conical refraction occurring in the optically and acoustically biaxial crystals. First, the most evident difference is that the phenomenon can take place in media with qualitatively different physical properties (magnetized plasma with isotropic (Sivukhin, 1966) or anisotropic (Tsiklauri, 1996a) pressure on the one hand and the biaxial crystals on the other). Second, in the case of biaxial crystals, let us take for concreteness optical conical refraction, mathematical basis for theoretical formulation of the effect constitutes Maxwell's equations along with material equations and in addition *electrical* anisotropy

of the medium is assumed, i.e. such substances (crystals) are considered whose electrical excitations depend on the direction of the electric field (Born & Wolf, 1980). Whereas in our case anisotropy in the medium is brought by the external *magnetic* field and Euler's equation for the magnetized, perfectly conducting plasma is used. The only similarity of these two phenomena is that the equations which relate the phase velocity of the waves with their direction of propagation in respect to the anisotropy axis (optical axis in one case and the external magnetic field in the other) — Fresnel's equation of wave normals (Born & Wolf, 1980) and our dispersion relation (VI.4) (including its special subcases (Tsiklauri, 1996a) and (Sivukhin, 1966)) have the same mathematical structure. Thus, geometrical shape of the surface formed by the group velocity vectors when the phenomenon takes place is qualitatively the same — surface of the empty cone.

For the author is unknown whether the phenomenon analogous to the conical refraction for MHD waves in the anisotropic plasma was observed experimentally yet. However, one should take into account the difficulties in preparation of a plasma medium with permanently satisfied condition (VI.3) The aim of this study is to stimulate other authors, in spite of the technical difficulties, to prove the existence of the effect experimentally.

ACKNOWLEDGEMENTS

Research contributing to this study was supported in part by International Science Foundation (ISF, USA) long-term research grants RVO 000 and RVO 300; by South African Foundation of Research Development (FRD) through core bursary program and by Research Scholarship of the University of Cape Town.

It is my pleasure to express my deep gratitude to my supervisor Prof. Raoul D. Viollier for stimulating discussions and continuous interest to my research.

Appendix for section III

Here we outline some useful features of h^α four-vector. At first one can get from the definition of h^α (III.4) that:

$$h^t = \gamma(\vec{v}, \vec{B}) \tag{A.1}$$

$$\vec{h} = \frac{1}{\gamma}(\vec{B} + \gamma^2(\vec{v}, \vec{B})) \tag{A.2}$$

The latter formula leads to the following equality:

$$(\vec{v}, \vec{h}) = \gamma(\vec{v}, \vec{B}) \tag{A.3}$$

If we use (A.3) in φ-component of (III.7), we obtain that

$$r(v_r B_\varphi - v_\varphi B_r) = const \equiv K \equiv -r^2 B_r \Omega \tag{A.4}$$

Now we can calculate quantity $h_t h_r$:

$$h_t h_r = -\gamma^2 |h|^2 v_r + B_\varphi (v_r B_\varphi - v_\varphi B_r) \tag{A.5}$$

Inserting (A.4) in (A.5) finally we get:

$$h_t h_r = -\gamma^2 |h|^2 v_r + \frac{K B_\varphi}{r} \tag{A.6}$$

Now let us calculate quantity $h_\varphi h_r$. For this aim from (A.2), taking into account (III.5) we obtain

$$h_\varphi h_r = B_\varphi B_r (1/\gamma^2 + {v_r}^2 + v_\varphi^2) + v_r v_\varphi \gamma^2 |h|^2 \tag{A.7}$$

Than recalling the definition of γ results:

$$h_\varphi h_r = \gamma^2 |h|^2 v_\varphi v_r + B_\varphi B_r \tag{A.8}$$

REFERENCES

Abramowicz M.A., 1991, in *Variability of Active Galactic Nuclei*, eds., Duschl W.J., Wagner S.J., Camenzind M., Springer-Verlag, Berlin, p.255

Abramowicz M., Chen X., Kato S., Lasota J.P., and Regev O., 1995, Astrophys. J.,438, L37.

Akheizer A.I. and Akhiezer I.A., 1973, *Plasma Electrodynamics: Linear Theory*, Pergamon, London.

ALEPH collaboration CERN PPE/95-03

Asseo E. and Beauflis D., 1983, Astrophys. Space Sci., 89, 133.

Baggett J.S., Driscoll T.A., and Trefethen L.N., 1995, Phys. Fluids, 7, 833.

Balbus S.A. and Hawley J.F., 1992, Astrophys. J., 400, 610.

Bekefi G., 1966, *Radiation Processes in Plasmas*, Wiley.

Betchov R. and Criminale W.O., 1967,*Stability of Parallel Flows*, Academic Press, N.Y.

Briggs R.J., 1964, *Electron-Stream Interaction with Plasmas*, MIT press.

Born M. and Wolf E., 1980,*Principles of Optics*, Pergamon Press.

Burrows A., Ghandi R. and Turner M.S., 1992, Phys. Rev. Lett. 68, 3834.

Butler K.M. and Farrell B.F., 1992, Phys. Fluids (A), 4, 1637.

Cairns R.A., 1979, J. Fluid Mech., 92, 1.

Cannizzo J.K. and Reiff C.M., 1992, Astrophys. J., 385, 87.

Cap F.F., 1976, *Handbook of Plasma Instabilities*, Academic, New York.

Chagelishvili G.D., Chanishvili R.G., Lominadze J.G., and Segal I.N., 1992, in *Proceedings of the Fourth International Conference on Plasma Physics and Controlled Nuclear Fusion*, edited by T. D. Guenne, ESA, Noordwijk, p. 23

Chagelishvili G.D., Chanishvili R.G., Khristov T.S., and Lominadze J.G., 1993, Phys. Rev. (E), 47, 366.

Chagelishvili G.D., Chanishvili R.G., Lominadze J.G. and Tevzadze A.G., 1996, Submitted to Phys. Plasmas.

Chagelishvili G.D., Rogava A.D. and Segal I.N., 1994, Phys. Rev. (E), 50, R4283.

Chagelishvili G.D., Rogava A.D. and Tsiklauri D.G., 1996a, Phys. Rev. (E), 53, 6028.

Chagelishvili G.D., Rogava A.D. and Tsiklauri D.G., 1996b, Submitted to Phys. Plasmas.

Chandrasekhar S., 1960, Poc. Nat. Acad. Sci., 46, 253

Chew G., Goldberger M., and Low F., 1956, Proc. Roy. Soc. Ser. A 236, 112.

Collin-Souffrin S., 1991, Astron. Astrophys., 249, 344.

Collin-Souffrin S. and Dumont A.M., 1990, Astron. Astrophys., 229, 292.

Cooper W.A., 1988, Plasm. Phys. Contr. Fus., 30, 1805.

Coppi B., Rosenbluth M.N. and Sudan R.N., 1969, Ann. Phys., 55, 207.

Cox J.P. and Giuli R.T., 1968, *Principles of Stellar Structure*, vol.2, Godon and Beach, Sci. Publishers, New York.

Criminale W.O. and Drazin P.G., 1990, Stud. Appl. Math., 83, 123.

Criminale W.O., Jackson T.L. and Lasseigne D.G., 1995, J. Fluid Mech., 294, 283.

Czerny B. and Elvis M., 1987, Astrophys. J., 321, 305.

Davidson R.C., 1972,*Methods in Nonlinear Plasma Physics*, Academic Press, New-York.

Dewar R.L. and Glasser A.H., 1983, Phys. Fluids, 26, 3038.

Dolgov A.D. and Markin O.Yu., 1991, Prog. Theor. Phys., 85, 1091.

Dolgov A.D. and Rothstein I.Z., 1993, Phys. Rev. Lett., 71, 476.

Drazin P.G. and Reid W.H., 1987, *Hydrodynamic Stability*, Cambridge U. Press.

Duschl W.J., 1988, Astron. Astrophys., 194, 33.

Foglizzo T. and Tagger M., 1995, Astron. Astrophys., 301, 293.

Frank, King and Raine, 1992, *Accretion Power in Astrophysics*, Cambridge Univ. Press, Cambridge.

Friedman J.L., Ipser J.R. and Paker L., 1986, Astrophys. J, 304, 115.

Gedalin M.E., Lominadze J.G. and Tsikarishvili E.G., 1991, Astrophys. and Space Sci., 175, 291.

Goldreich, P. and Julian W. H., 1970, Astrophys. J., 160, 971.

Goldreich P. and Lyndenn-Bell D., 1965, Mon. Not. Roy. Astron. Soc., 130, 125.

Goldreich P. and Tremaine S., 1978, Astrophys. J., 222, 850.

Gordon P., 1996,Mon. Not. Roy. Astron. Soc., 279, 1071.

Hawley J.F. and Balbus S.A., 1995, Publ. Astron. Soc. Aust., 12, 159.

Holdom B., 1987, Phys. Rev. D, 36, 1000.

Holdom B., 1993, preprint (UTPT-93-18) hep-ph/9307359

Holdom B. and Malaney R.A., 1994, Astrophys. J., 420, L53.

Kato T., 1976, *Perturbation Theory for Linear Operators*, Springer-Verlag, New York.

Kennel C.F., Fujimura F.S. and Okamoto I., 1983, Geophys. Ap. Fluid Dynamics, 26, 147.

Kotkin G.L. and Serbo V.G., 1971, *Collection of Problems in Classical Mechanics*, Pergamon Press, New York.

Krall N.A. and Trivelpiece A.W., 1973, *Principles of Plasma Physics*, McGraw-Hill, New-York. Kritz A.H. and Mintzer D., 1960, Phys. Rev., 117, 382.

Krolik J.H. and Begelman M.C., 1988, Astrophys. J., 329, 702.

Laor A. and Netzer M., 1989, Mon. Not. Roy. Astron. Soc., 238, 897.

Lominadze J.G., Chagelishvili G.D. and Chanishvili R.A., 1988, Pis'ma Astron. Zh., 14, 856 [Sov. Astron. Lett., 14, 364 (1988)].

Lord Kelvin (W. Thomson), 1887, Phil. Mag., 24, Ser. 5, 188.

Lichnerowicz A., 1967, *Relativistic Hydrodynamics and Magnetohydrodynanics*, Benjamin, New York.

Lin C.C., 1955, *Hydrodynamic Stability*, Cambridge U. Press.

Lioure A. and Le Conte O., 1994, Astron. Astrophys., 285, 185.

Lithchfield S.J., King A.R. and Brooker J.R., 1989, Mon. Not. Roy. Astron. Soc., 237, 1067.

Lynden-Bell D. and Pringle J.E., 1974, Mon. Not. Roy. Astron. Soc., 168, 603.

Macdonald D. and Thorne K. S., 1982, Mon. Not. Roy. Astron. Soc., 198, 345.

Magnus K., 1976, *Schwingungen*, B. G. Teubner, Stuttgart.

Malkan M.A., 1983, Astrophys. J., 268, 582.

Malkan M.A., 1989, in *Theory of Accretion Disks*, eds. Meyer F., et.al, NATO ASI series vol.290, Kluwer Academic Publishers, Dordrecht.

Mestel L., 1968, Mon. Not. Roy. Astron. Soc., 138, 359.

Michel F.C., 1969, Astrophys. J., 158, 727.

Moiseev S.S. and Smiliansky V.R., 1965, Magnitnaya Gidrodinamika, 2, 23 (in Russian).

Narayan R., Goldreich P. and Goodman J., 1987, Mon. Not. Roy. Astron. Soc., 228, 1.

Narayan R. and Yi I., 1994, Astrophys. J., 428, L13.

Narayan R. and Yi I., 1995, Astrophys. J., in press.

Okamoto I., 1978, Mon. Not. Roy. Astron. Soc., 185, 69.

Papaloizou J.C.B. and Stanley G.Q.G., 1986, Mon. Not. Roy. Astron. Soc., 220, 593.

Parker E.N., 1963, *Interplanetary Dynamical Precesses*, Interscience, New York.

Perry J.J. and Dyson J.E., 1985, Mon. Not. Roy. Astron. Soc., 213, 665.

Perry J.J. and Ward M.J. and Jones M., 1987, Mon. Not. Roy. Astron. Soc., 228, 623.

Perry J.J. and Williams R., 1993, Mon. Not. Roy. Astron. Soc., 260, 437.

Popham R. and Narayan R., 1992, Astrophys. J., 394, 255.

Pringle J.E., 1977, Mon. Not. Roy. Astron. Soc., 178, 195.

Pringle J.E. and Savonije G.J., 1979, Mon. Not. Roy. Astron. Soc., 187, 777.

Pringle J.E., 1981, Ann. Rev. Astron. Astrophys., 19, 137.

Reddy S.C. and Henningson D.S., 1993, J. Fluid Mech., 252, 209.

Reddy S.C., Schmidt P.J., and Hennigson D.S., 1993, SIAM (Soc. Ind. Appl. Math) J. Appl. Math., 53, 15.

Rogava A. D., 1992, Gen. Rel. and Grav., 24, 617.

Rogava A.D., Mahajan S.M. and Berezhiani V.I., 1996, preprint-IC/IR/96/4, submitted to Phys. Plasmas.

Rogava A.D. and Tsiklauri D.G., 1993, Astrophys. and Space Sci., 204, 9.

Ross R.R., Fabian A.C. and Mineshige S., 1992, Mon. Not. Roy. Astron. Soc., 258, 189.

Rothstein I.Z., 1995, hep-ph/9506443.

Ryu D. and Goodman J., 1992, Astrophys. J. 388, 438.

Shields G.A., 1978, Nature, 272, 706.

Sivukhin D.V., 1966, Magnitnaya Gidrodinamica, 1, 35, (in Russian).

Shakura N.I. and Sunyaev R.A., 1973, Astron. Astrophys., 24, 337.

Shakura N.I. and Sunyaev R.A., 1988, Advanc. Space Res., 8(2), 135.

Stanley G.Q.G., 1988, Advanc. Space Res., 8(2), 113.

Straumann N., 1984, *General Relativity and Relativistic Astrophysics*, Springer-Verlag, Heidelberg.

Sun W.H. and Malkan M.A., 1989, Astrophys. J., 346, 68.

Tagger M., Pellat R.and Coroniti F.V., 1992, Astrophys. J., 393, 708.

Tan M. and Abraham B., 1972, Cosmic Electrodynamics, 3, 71.

Thorne M. and Macdonald K.S., 1982, Mon. Not. Roy. Astron. Soc., 198, 339.

Toomre A., 1969, Astrophys. J., 158, 899.

Trefethen L.N., Trefethen A.E., Reddy S.C., and Driscoll T.A., 1993, Science, 261, 578.

Trefethen L.N., Trefethen A.E., Reddy S.C., 1992, *Tech. Rep. TR 92-1291* (Department of Computer Science, Cornell University, Ithaca, NY)

Tsikarishvili E. G., Lominadze J. G., Rogava A. D. and Javakhishvili J. I. 1992, Phys. Rev. A, 46, 1078.

Tsikarishvili E.G. and Rogava A.D., 1994, Phys. Rev. E, 50, 3050.

Tsikarishvili E.G., Rogava A.D. and Tsiklauri D.G., 1995, Astrophys. J., 439, 822.

Tsiklauri D., 1996a, Phys. Plasmas, 3, 800.

Tsiklauri D., 1996b, Phys. Plasmas. 3, 3902.

Tsiklauri D. and Viollier R.D., 1996, Mon. Not. Roy. Astron. Soc., 282, 1299.

Ulrich M.H., 1981, Space Sci. Rev., 28, 89.

Velikhov E., 1959, Sov. Phys. JETP, 36, 1398.

Viollier R.D., 1994, Prog. Part. Nucl. Phys., 32, 51.

Viollier R.D., Trautmann D. and Tupper G.B., 1993, Phys. Lett., B306, 79.

Viollier R.D., Leimgruber F.R. and Trautmann D., 1992, Phys. Lett., B297, 132.

Walen C., 1946, Ark. Mat. Astr. Fys., 33A, 18.

Wandel A. and Petrosian V., 1988, Astrophys. J., 329, L11.

Weber E.I. and Davis L., 1967, Astrophys. J., 148, 217.

Figure captions

Fig. II.1 Angular velocity $\omega(x)$ against distance from the center of the star for different values of the stellar angular velocity $\omega_0^{(1)} = 0$, $\omega_0^{(2)} = 0.2$ and $\omega_0^{(3)} = 0.4$. The upper line represents Keplerian angular velocity. it looks like a straight line due to the narrowness of the BL.

Fig. II.2 Sound speed $c(x)$ against distance from the center of the star for different initial values $c_0^{(1)} = 0.0500$, $c_0^{(2)} = 0.0490$ and $c_0^{(3)} = 0.0458$.

Fig. II.3 Radial velocity $v(x)$ against distance from the center of the star for different initial values $v_0^{(1)} = 0.0047$, $v_0^{(2)} = 0.0048$ and $v_0^{(3)} = 0.0051$.

Fig. II.4 Radiation intensity $q^-(x)$ against distance from the center of the star for different values of the stellar angular velocity $\omega_0^{(1)} = 0$, $\omega_0^{(2)} = 0.2$ and $\omega_0^{(3)} = 0.4$.

Fig.IV.1 The behaviour of the quantity $M_<(R)/M_h - M_R/M_h$ from eq.(IV.6) for a neutrino of mass 4 keV/c^2 which then implies a mass of the ball of $4 \times 10^8 M_\odot$.

Fig.IV.2 The behaviour of the quantity $M_<(R)/M_h - M_R/M_h$ from eq.(IV.6) for a neutrino of mass 3 keV/c^2 which then implies mass of the ball of $4 \times 10^9 M_\odot$.

Fig.IV.3 Numerical solution of the Lane-Emden eqation (IV.14) for boundary conditions $\theta = 1$ and $d\theta/d\xi = 0$ at $\xi = R_i/pc$.

Fig. IV.4. Effective temperature of the disk versus the distance from the black hole. The solid curve repesents $T_{\rm eff}$ for an isolated black hole, whereas the dotted and dashed curves correspond to the case with the neutrino balls of masses $4 \times 10^9 M_\odot$ and $3 \times 10^8 M_\odot$ respectively.

Fig. IV.5. The spectral distribution of the emitted energy. The solid curve repesents νF_ν for an isolated black hole, whereas the dotted and dashed curves correspond to the case with the neutrino balls of masses $4 \times 10^9 M_\odot$ and $3 \times 10^8 M_\odot$ respectively.

Fig.V.1 Numerical solutions of the reduced for the isotropic pressure case Eqs.(V.37-V.40) for the set of following physical parameters: $\beta(0) = 5$, $R = 0.05$, $\sigma^2 = 1$ ($\varepsilon^2 = 1$). The solution was obtained with precise initial conditions $D(0) = .0050490243$, $v_x(0) = .010049510$ $v_y(0) = -.00099019514$ and $b(0) = .00099019514$ as to distinctly excite $\Omega_1(\tau)$ SMW mode. This set of Figs. represents single transformation of SMW into FMW (see details in the text). Such a high precision in the initial conditions is necessary to achieve exact separation of the wave modes, or in other words to excite exactly a particular wave mode.

Fig.V.2 $E_{\rm tot}(\tau)/E_{\rm tot}(0)$ (solid curve), $\Omega_1(\tau)/\Omega(0)$ (i.e. SMW) (dashed curve, which overlaps on $E_{\rm tot}(\tau)/E_{\rm tot}(0)$ in the time interval $0 < \tau < 100$) and $(\Omega_2(\tau)/\Omega_2(100)) \times (\Omega_1(100)/\Omega_1(0))$ (dotted curve) for the same set of physical parameters as in Fig. V.1. The graph unambiguously demonstrates transformation of SMW into FMW in the isotropic thermal pressure case.

Figs. set V.3–7. Numerical solutions of the Eqs.(V.37-V.40) for the set of following

physical parameters: $\beta(0) = 5$, $R = 0.05$, $\sigma^2 = 1$ and $\varepsilon^2 = 3$. The solution was obtained with precise initial conditions $D(0) = .057453183$, $v_x(0) = .10042547$ $v_y(0) = -.0085093635$ and $b(0) = .0085093635$ as to distinctly excite $\Omega_1(\tau)$ SMW mode. This set of Figs. represents single transformation of SMW into FMW (see details in the text).

Fig. V.8. $E_{\rm tot}(\tau)/E_{\rm tot}(0)$ (solid curve), $\Omega_1(\tau)/\Omega(0)$ (i.e. SMW) (dashed curve, which overlaps on $E_{\rm tot}(\tau)/E_{\rm tot}(0)$ in the time interval $0 < \tau < 100$) and $(\Omega_2(\tau)/\Omega_2(100)) \times (\Omega_1(100)/\Omega_1(0))$ (dash-dot curve) for the same set of physical parameters as in Figs. V.3–V.7. The graph unambiguously demonstrates transformation of SMW into FMW.

Figs. set V.9–V.13. Numerical solutions of the Eqs.(V.37-V.40) for the set of following physical parameters: $\beta(0) = 5$, $R = 0.05$, $\sigma^2 = 1$ and $\varepsilon^2 = 0.16$. The solution was obtained with precise initial conditions $D(0) = .086746719$, $v_x(0) = .10013253$ $v_y(0) = -.0026506562$ and $b(0) = .0026506562$ as to distinctly excite $\Omega_1(\tau)$ SMW mode. This set of Figs. represents the double transformation when initially exited SMW after passing two degeneracy regions remains be SMW. (see details in the text).

Fig. V.14. $E_{\rm tot}(\tau)/E_{\rm tot}(0)$ (solid curve), $\Omega_1(\tau)/\Omega(0)$ (i.e. SMW) (dashed curve, which overlaps on $E_{\rm tot}(\tau)/E_{\rm tot}(0)$ in the time interval $0 < \tau < 70.66$) and $(\Omega_2(\tau)/\Omega_2(70.66)) \times (\Omega_1(70.66)/\Omega_1(0))$ (dash-dot curve) for the same set of physical parameters as in Figs. V.9–V.13. $\tau = 70.66$ is a midpoint of the DR. After passing first DR $E_{\rm tot}$ deviates from SMW as it gets admixture of FMW and finally after the second DR it again almost exactly follows to SMW. In other words this graph represents the process SMW $\rightarrow$ mixture of SMW and FMW $\rightarrow$ SMW.

Figs. set V.15–V.19. Numerical solutions of the Eqs.(V.37-V.40) for the set of following physical parameters: $\beta(0) = 5$, $R = 0.05$, $\sigma^2 = 1$ and $\varepsilon^2 = 0.2$. The solution was obtained with precise initial conditions $D(0) = .084486997$, $v_x(0) = .10015513$ $v_y(0) = -.0031026006$ and $b(0) = .0031026006$ as to distinctly excite $\Omega_1(\tau)$ SMW mode. This set of Figs. represents the double transformation when initially exited SMW after passing two degeneracy regions finally almost completely transforms into FMW. (see details in the text).

Fig. V.20.$E_{\rm tot}(\tau)/E_{\rm tot}(0)$ (solid curve), $\Omega_1(\tau)/\Omega(0)$ (i.e. SMW) (dashed curve, which overlaps on $E_{\rm tot}(\tau)/E_{\rm tot}(0)$ in the time interval $0 < \tau < 71.71$) and $(\Omega_2(\tau)/\Omega_2(71.71)) \times (\Omega_1(71.71)/\Omega_1(0))$ (dash-dot curve) for the same set of physical parameters as in Figs. V.15–V.19. $\tau = 71.71$ is a midpoint of the DR. After passing first DR $E_{\rm tot}$ deviates from SMW as it gets admixture of FMW and finally after the second DR it almost exactly follows to FMW. In other words this graph represents the process SMW $\rightarrow$ mixture of SMW and FMW $\rightarrow$ FMW.

Fig. V.21. Numerical solutions of the Eqs.(V.37-V.40) for the set of following physical parameters: $\beta(0) = 5$, $R = 0.05$, $\sigma^2 = 0.9$ and $\varepsilon^2 = 0.01$. The solution was obtained with precise initial conditions $D(0) = .19920126$, $v_x(0) = -.00099101256$ $v_y(0) = .39820251$ and $b(0) = -.039820251$ as to distinctly excite $\Omega_2(\tau)$ FMW mode. This graph represents how

the FMW grows when it gets admixture firehose-unstable SMW after passing the first DR.

Fig. V.22. $E_{tot}(\tau)/E_{tot}(0)$ for the same set of physical parameters as in Fig. V.21. Notice, the more than two orders of magnitude grows of FMW's energy than is initial value. lower graph represents $\Omega_1(\tau)$ (curve with circles), $\Omega_2(\tau)$ (curve with asterisks), ω_1 (dashed curve), $\omega_2(\tau)$ (solid curve). Note that $\Omega_1(\tau)$ and $\Omega_2(\tau)$ are coming rather close to each other.

Fig. V.23. Numerical solutions of the Eqs.(V.37-V.40) for the set of following physical parameters: $\beta(0) = 5$, $R = 0.05$, $\sigma^2 = 0.01$ and $\varepsilon^2 = 0.9$. The solution was obtained with precise initial conditions $D(0) = .0048372180$, $v_x(0) = .00095262782$ $v_y(0) = .0094744361$ and $b(0) = -.00094744361$ as to distinctly excite $\Omega_2(\tau)$ FMW mode. This graph represents the evolution of the FMW in time. We see that there is no energy exchange between FMW and SMW.

Fig. V.24. $E_{tot}(\tau)/E_{tot}(0)$ for the same set of physical parameters as in Fig. V.23. Notice, that FMW's energy strictly follows $\Omega_2(\tau)$ curve which means that there is no energy exchange between FMW and firehose-unstable SMW. Lower graph represents $\Omega_1(\tau)$ (curve with circles), $\Omega_2(\tau)$ (curve with asterisks), ω_1 (dashed curve), $\omega_2(\tau)$ (solid curve). Note that $\Omega_1(\tau)$ and $\Omega_2(\tau)$ are not coming close to each other in this case.

Fig. V.25. Numerical solutions of the Eqs.(V.37-V.40) for the set of following physical parameters: $\beta(0) = 1$, $R = 0.05$, $\sigma^2 = 0.1$ and $\varepsilon^2 = 10$. The solution was obtained with precise initial conditions $D(0) = .00039580595$, $v_x(0) = .0099852097$ $v_y(0) = .029580595$ and $b(0) = -.00029580595$ as to distinctly excite $\Omega_2(\tau)$ FMW mode. This graph represents how the FMW grows as it permanently exchanges energy with mirror-unstable SMW.

Fig. V.26. $E_{tot}(\tau)/E_{tot}(0)$ for the same set of physical parameters as in Fig. V.25. This graph shows how FMW's energy grows as it experiences permanent energy exchange with mirror-unstable SMW. Lower graph represents $\Omega_1(\tau)$ (curve with circles), $\Omega_2(\tau)$ (curve with asterisks), ω_1 (dashed curve), $\omega_2(\tau)$ (solid curve). Note that $\Omega_1(\tau)$ and $\Omega_2(\tau)$ are not coming close to each other in this case. However, due to the strong coupling there still occurs energy exchange between FMW and SMW.

Fig.VI.1, Sketch of experimental set up, which may be used for demonstration of the effect of the conical refraction (see details in the text). The line with arrows represents the narrow, parallel beam of MHD waves. Note, that when in the medium II the condition $a^2 + c_\perp^2 - 2(\alpha + 1)c_\parallel^2 = 0$ is not satisfied the beam goes into detector without experiencing any changes while propagating through the second medium.

Fig.VI.2, the same as in Fig.VI.1. Note, that when in the medium II the condition $a^2 + c_\perp^2 - 2(\alpha + 1)c_\parallel^2 = 0$ is fulfilled, the beam due to the effect of the conical refraction deflects from its initial direction ($\theta = 0$) and forms an empty cone with opening angle $2\varphi(+0) \equiv 2\arctan[\varphi(+0)]$, thus avoiding arrival of the MHD waves into detector's receiver.

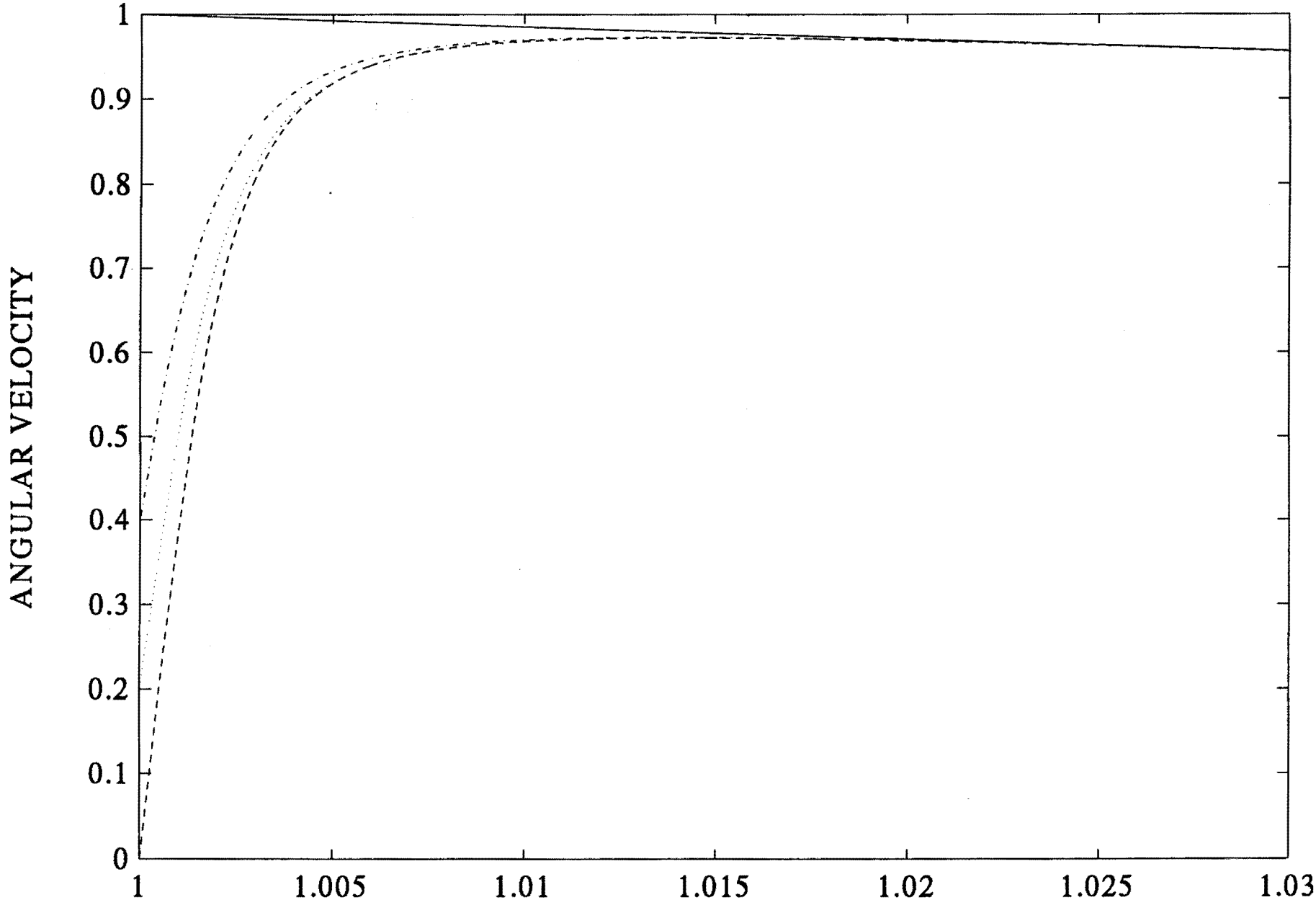
ANGULAR VELOCITY
1
0.9
0.8
0.7
0.6
0.5
0.4
0.3
0.2
0.1
0
1
1.005
1.01
1.015
1.02
1.025
1.03
DISTANCE FROM THE CENTER OF THE STAR

Fig. II.1

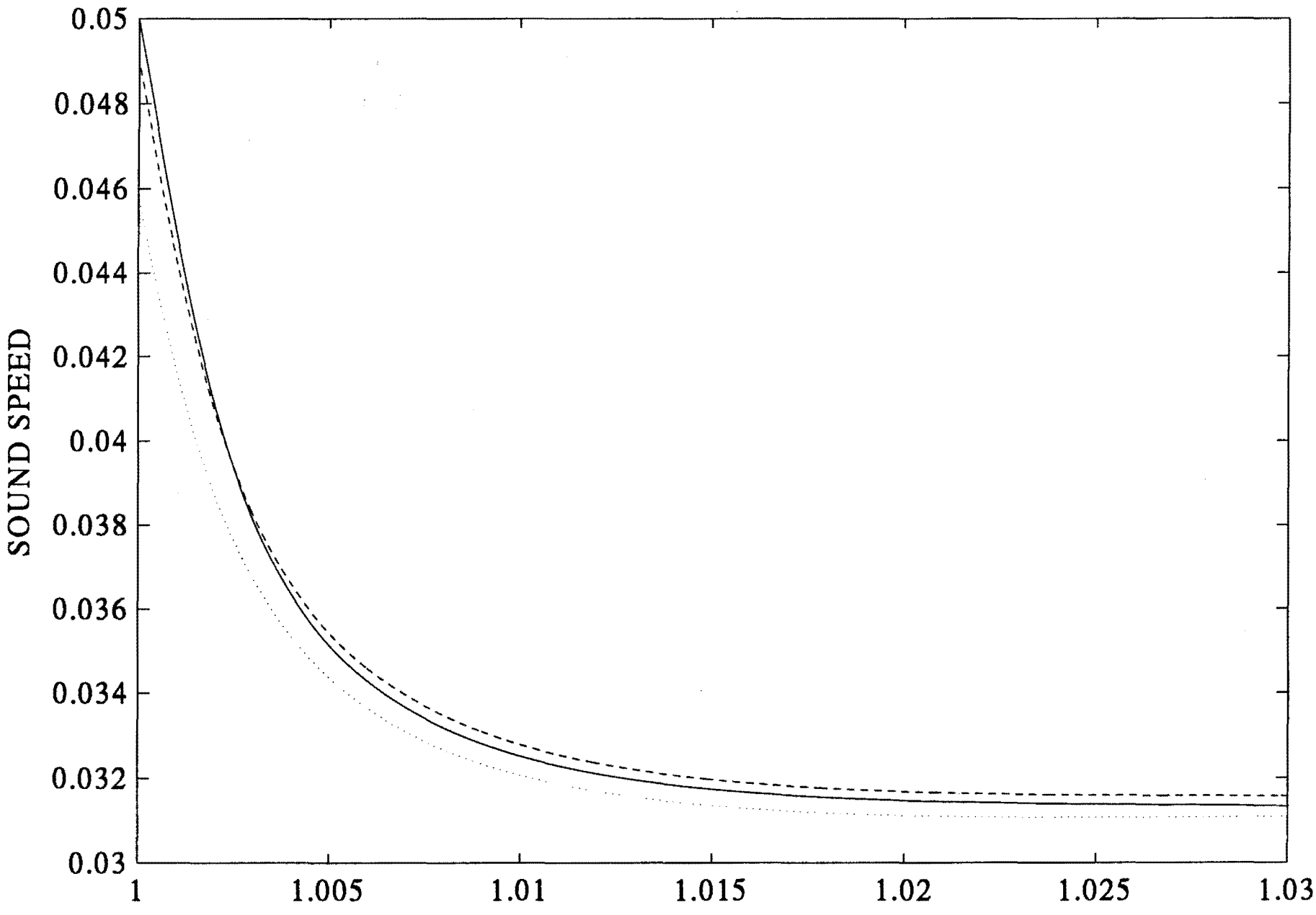
0.05
0.048
0.046
0.044
0.042
0.04
0.038
0.036
0.034
0.032
0.03
SOUND SPEED
1
1.005
1.01
1.015
1.02
1.025
1.03
DISTANCE FROM THE CENTER OF THE STAR

Fig 11.2

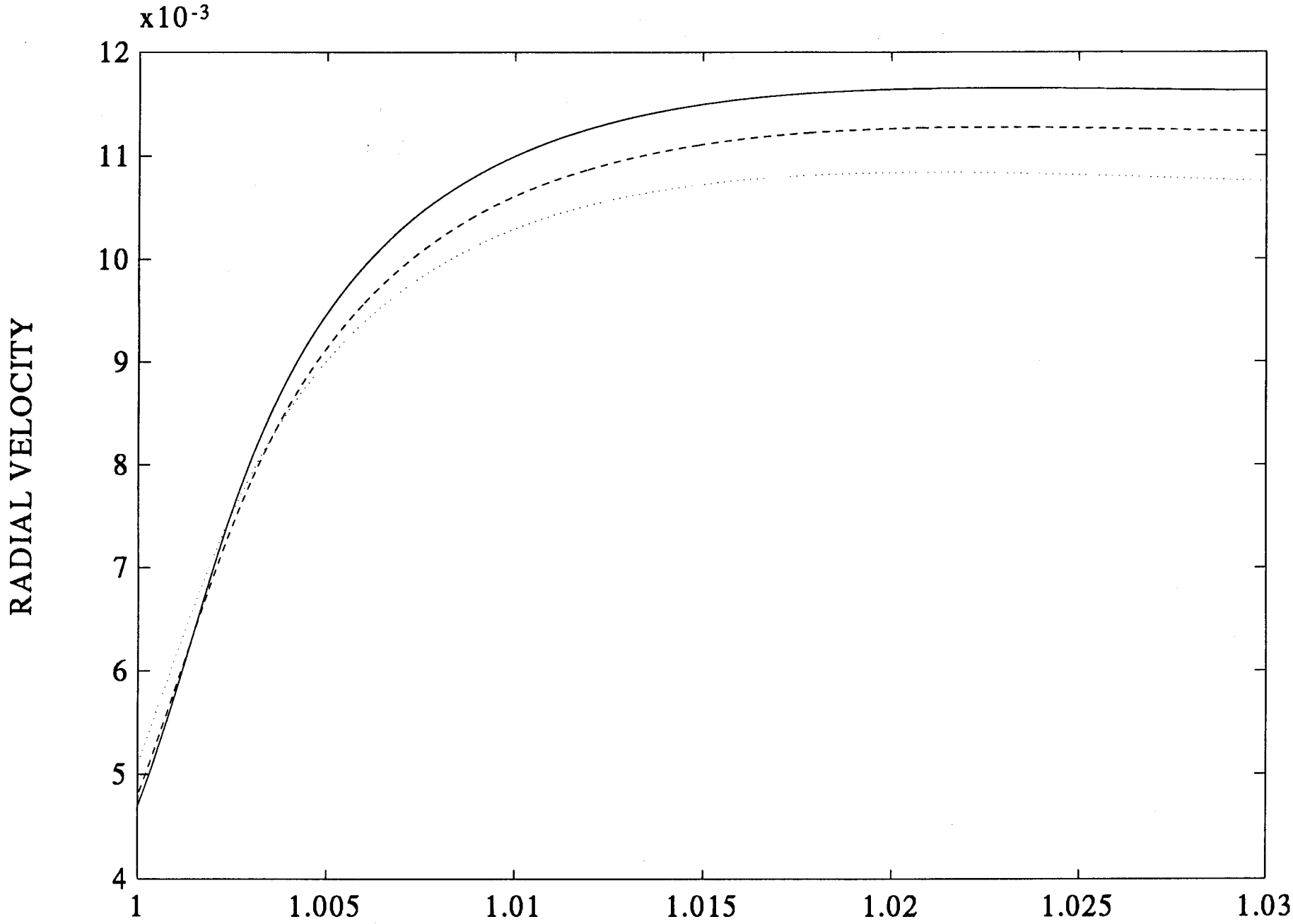
x10-3
12
11
10
9
8
7
6
5
4
RADIAL VELOCITY
1
1.005
1.01
1.015
1.02
1.025
1.03
DISTANCE FROM THE CENTER OF THE STAR

Fig. 11.3

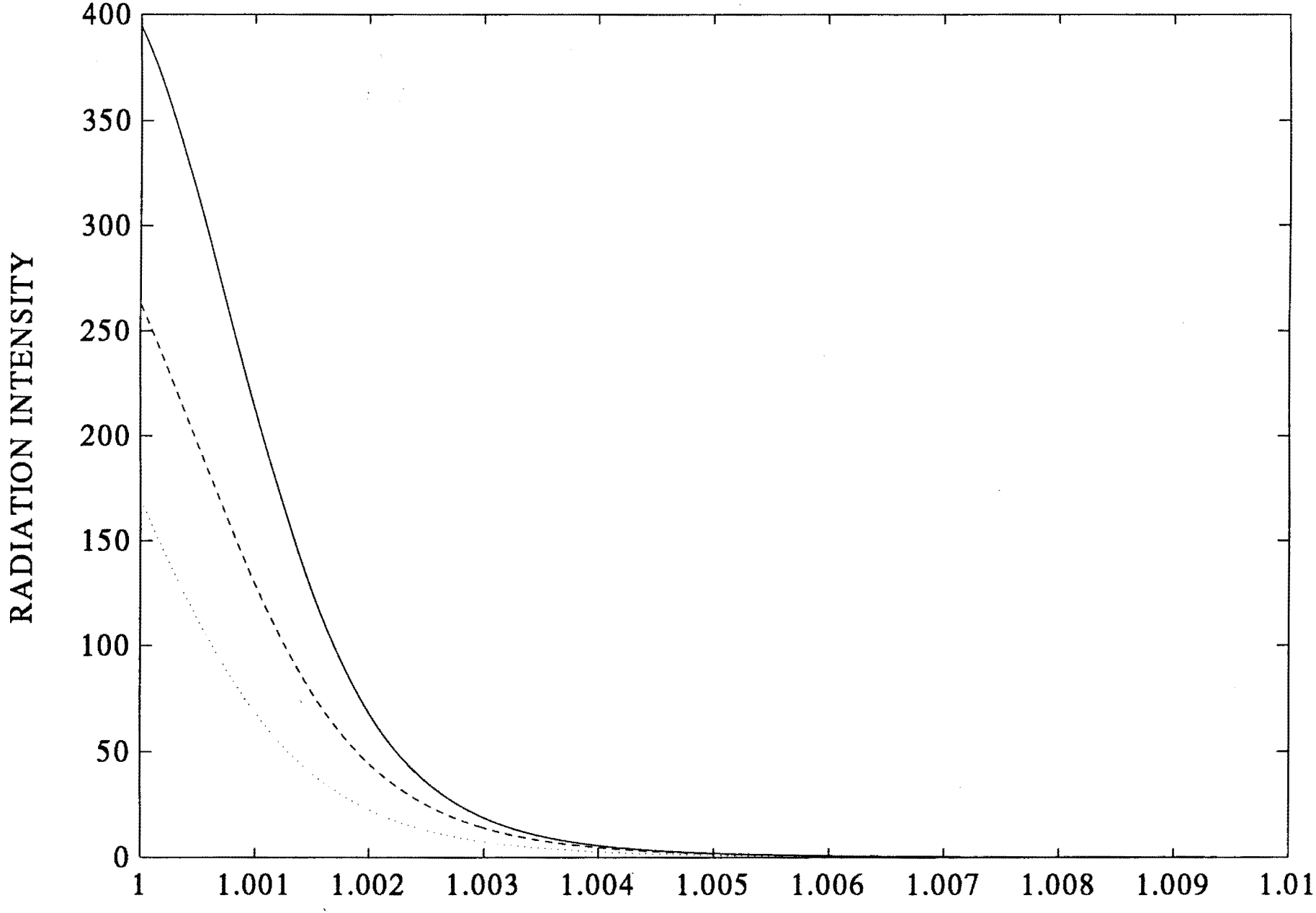
400
350
300
250
200
150
100
50
0
RADIATION INTENSITY
1
1.001
1.002
1.003
1.004
1.005
1.006
1.007
1.008
1.009
1.01
DISTANCE FROM THE CENTER OF THE STAR

Fig 1/4

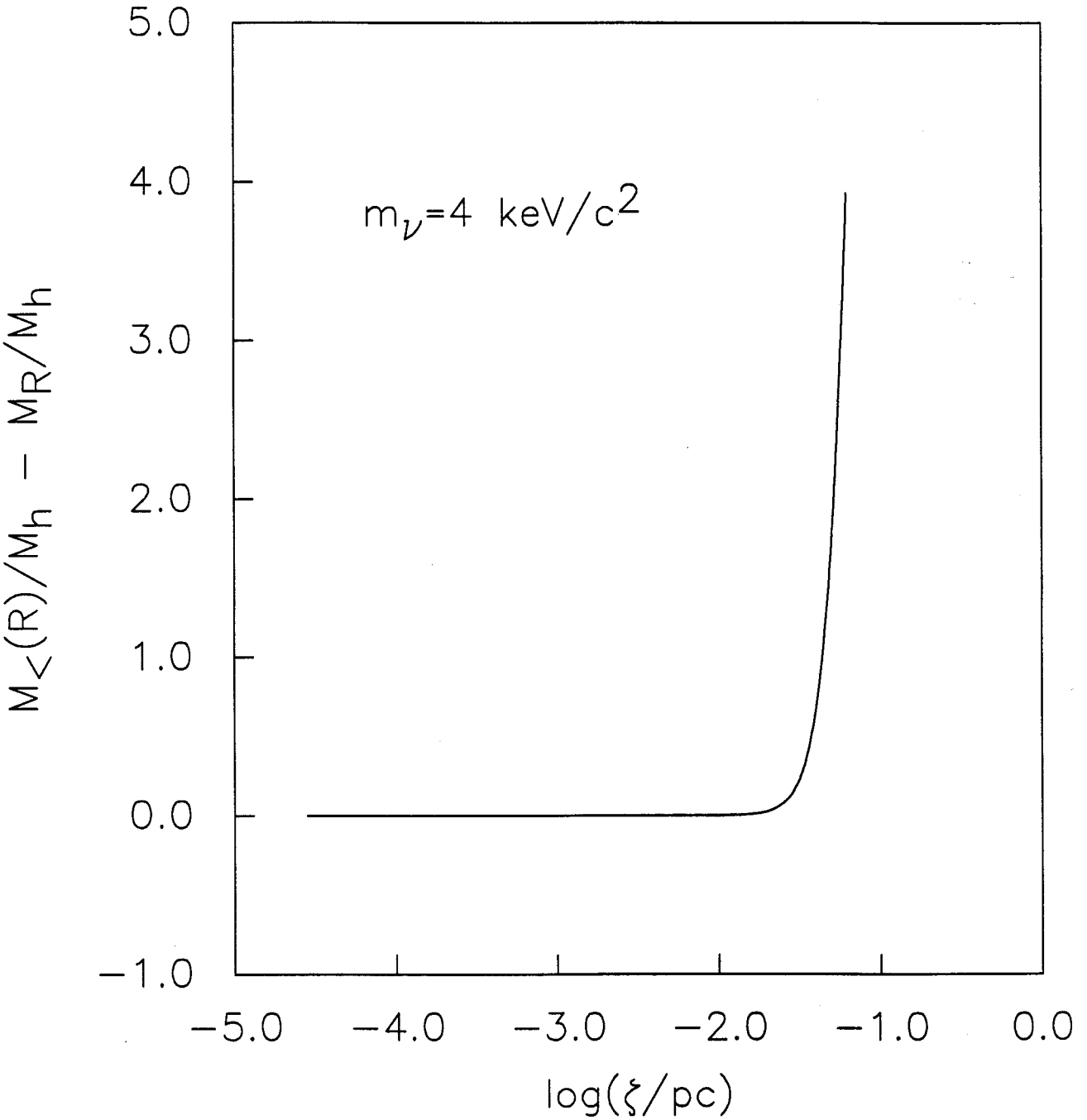

Fig. IV.1

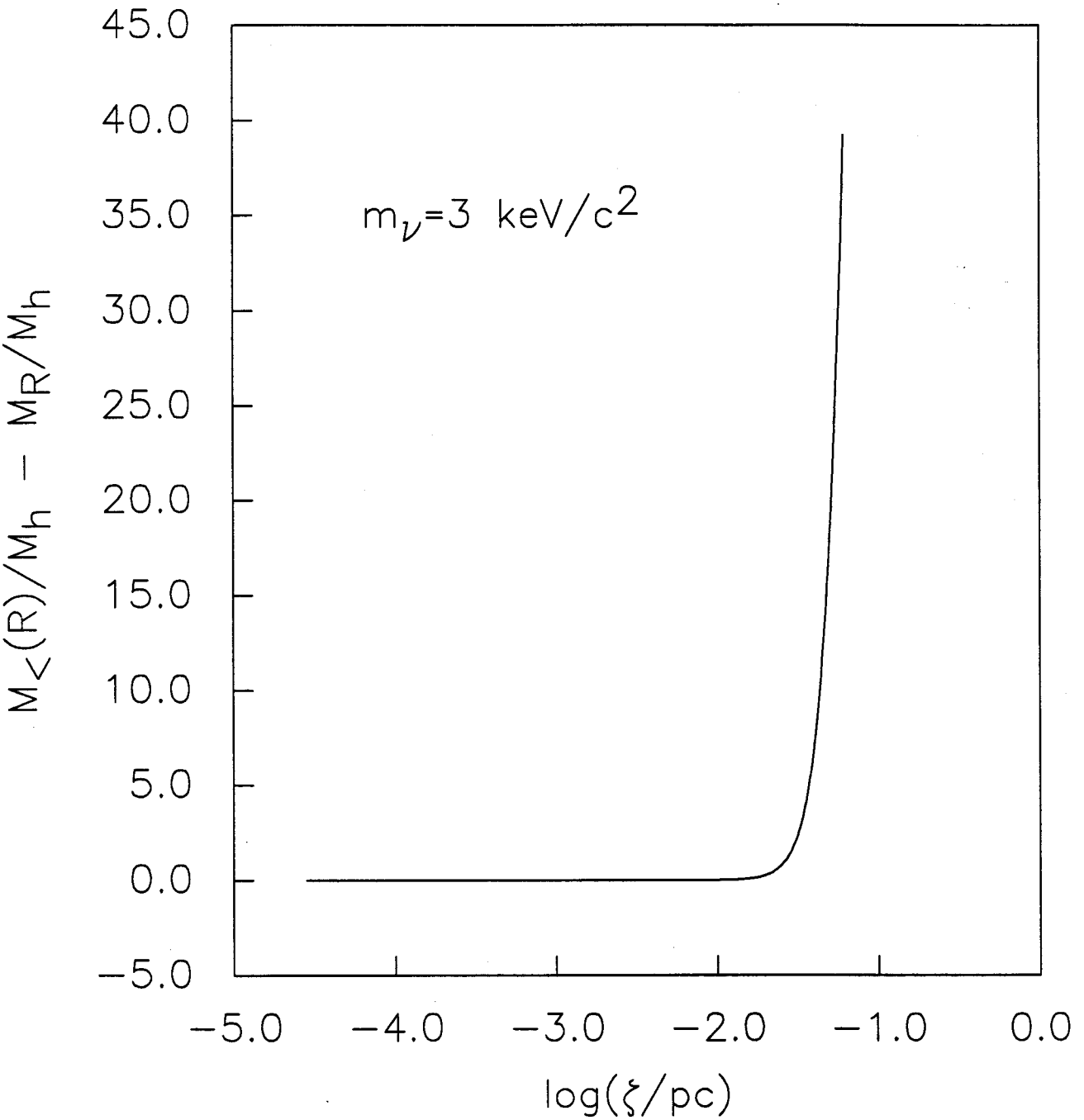
45.0
40.0
35.0
30.0
25.0
20.0
15.0
10.0
5.0
0.0
−5.0
m_ν=3 keV/c^2
$M_<(R)/M_h - M_R/M_h$
−5.0
−4.0
−3.0
−2.0
−1.0
0.0
log(ξ/pc)

Fig. IV.2

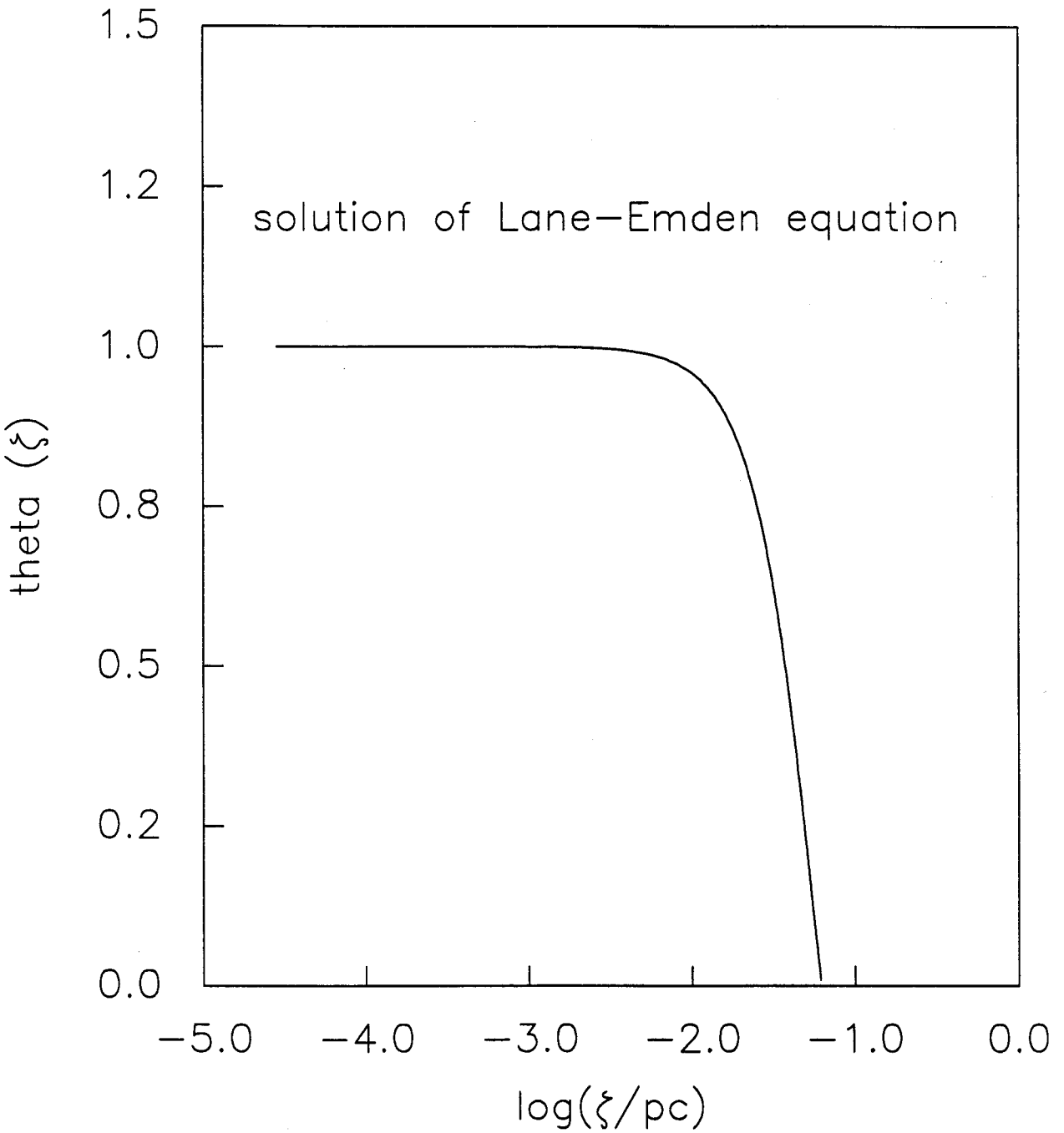
1.5
1.2
1.0
0.8
0.5
0.2
0.0
theta (ζ)
solution of Lane–Emden equation
−5.0
−4.0
−3.0
−2.0
−1.0
0.0
log(ξ/pc)

Fig. IV.3

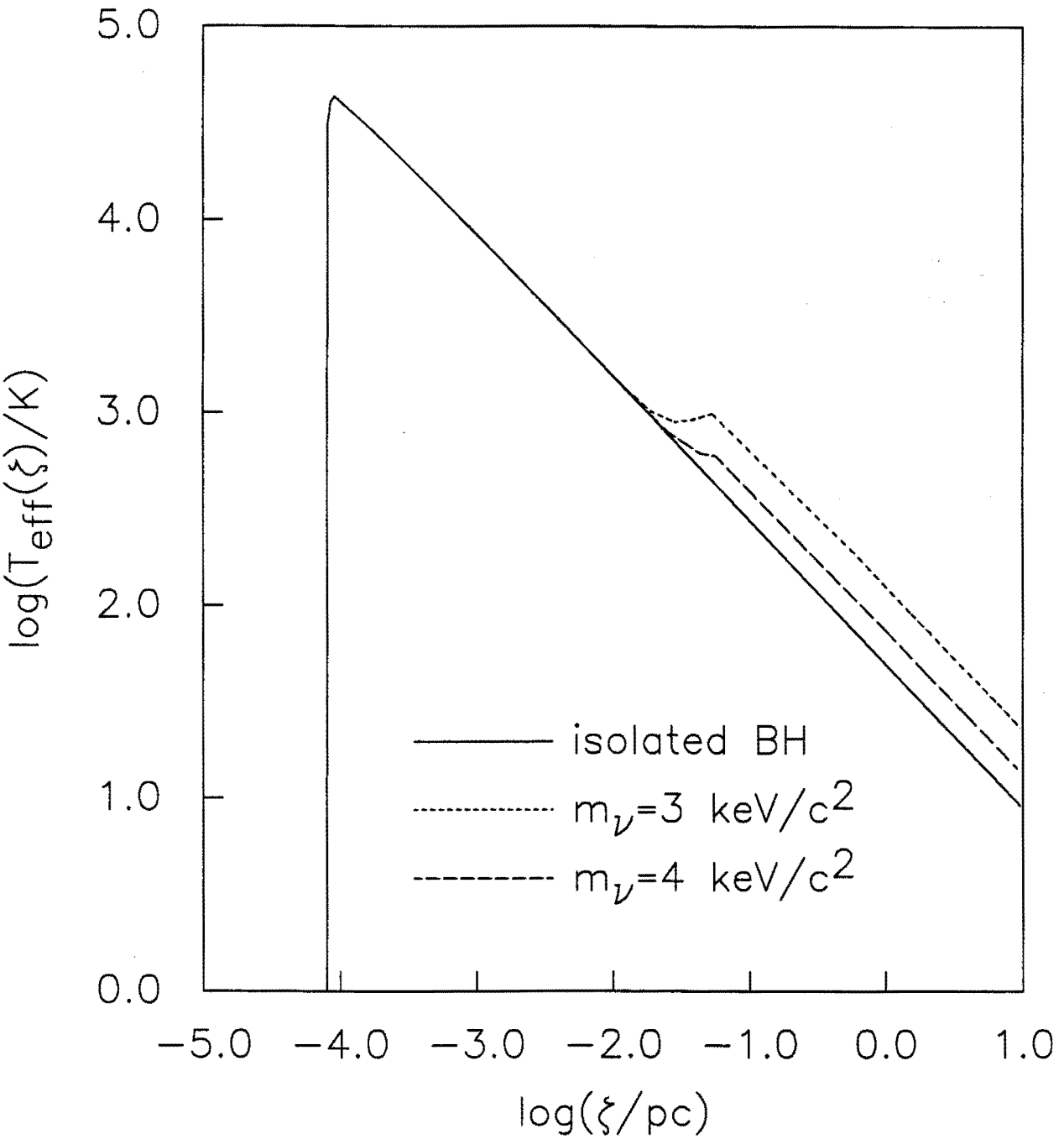
5.0
4.0
3.0
2.0
1.0
0.0
log(T_eff(ξ)/K)
isolated BH
m_ν=3 keV/c^2
m_ν=4 keV/c^2
−5.0
−4.0
−3.0
−2.0
−1.0
0.0
1.0
log(ξ/pc)

Fig IV.4

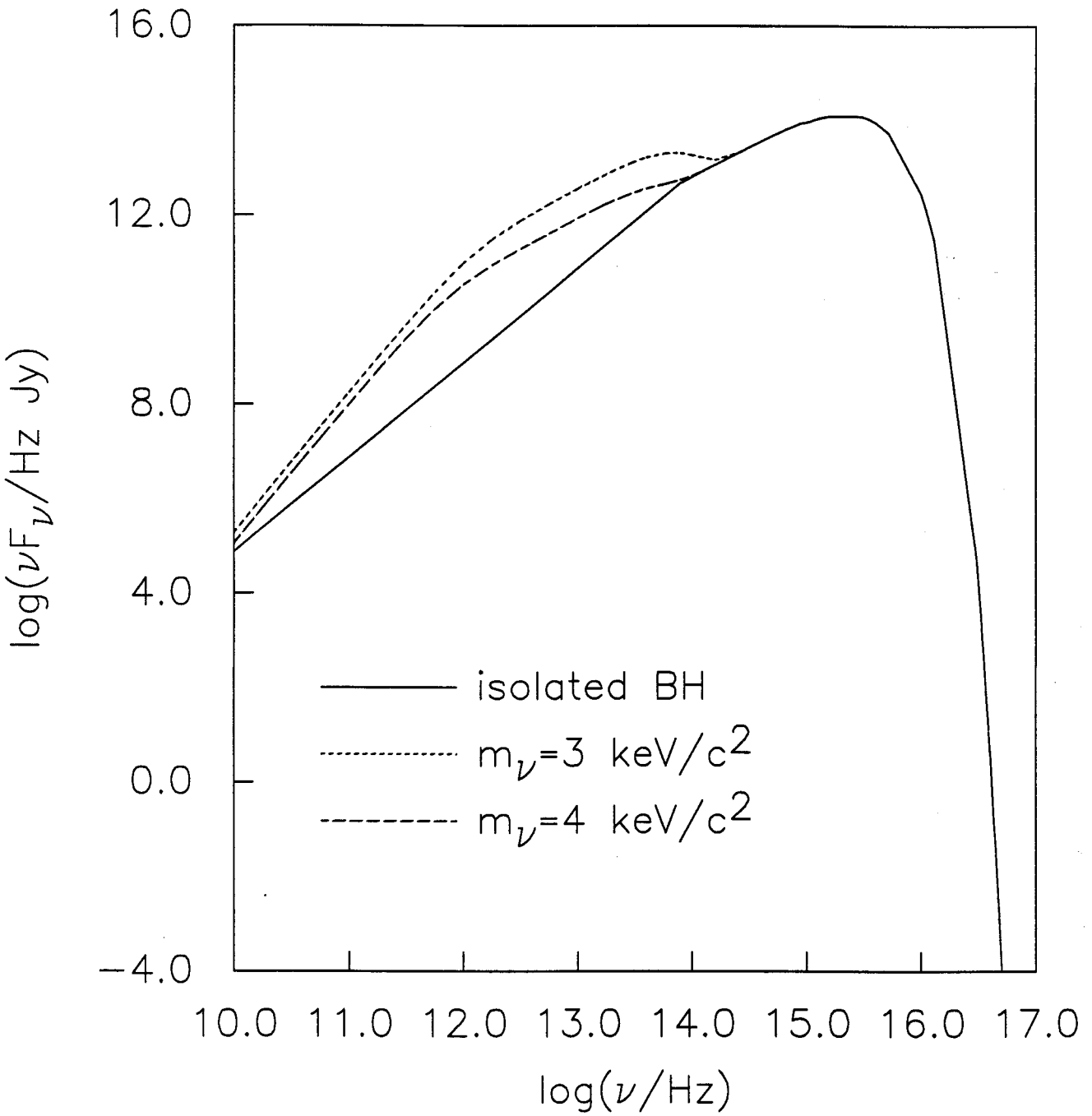
16.0
12.0
8.0
4.0
0.0
−4.0
log(νF_ν/Hz Jy)
isolated BH
m_ν=3 keV/c^2
m_ν=4 keV/c^2
10.0 11.0 12.0 13.0 14.0 15.0 16.0 17.0
log(ν/Hz)

Fig IV.5

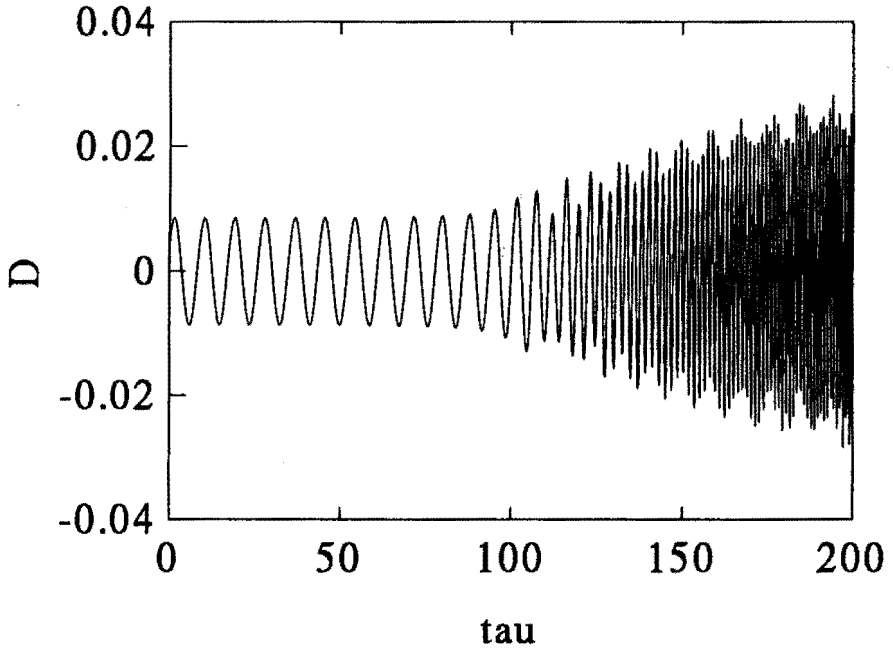
0.04
0.02
0
-0.02
-0.04
D
0
50
100
150
200
tau

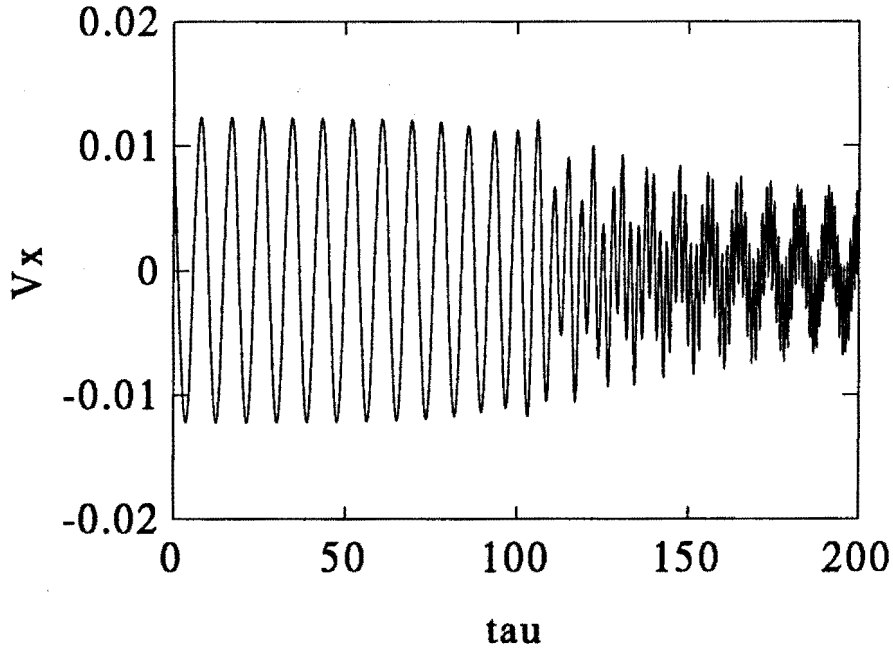
0.02
0.01
0
-0.01
-0.02
Vx
0
50
100
150
200
tau

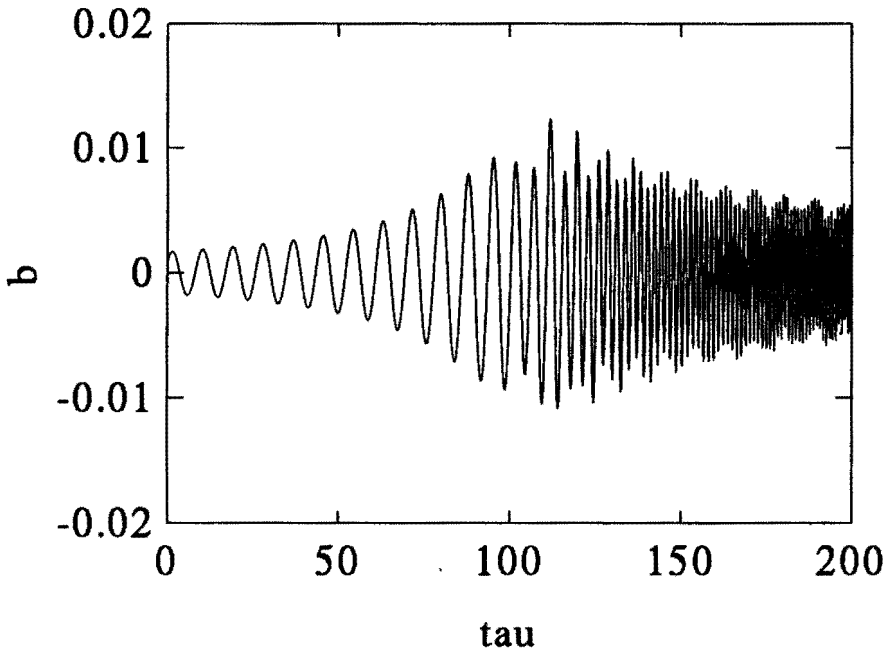
0.02
0.01
0
-0.01
-0.02
b
0
50
100
150
200
tau

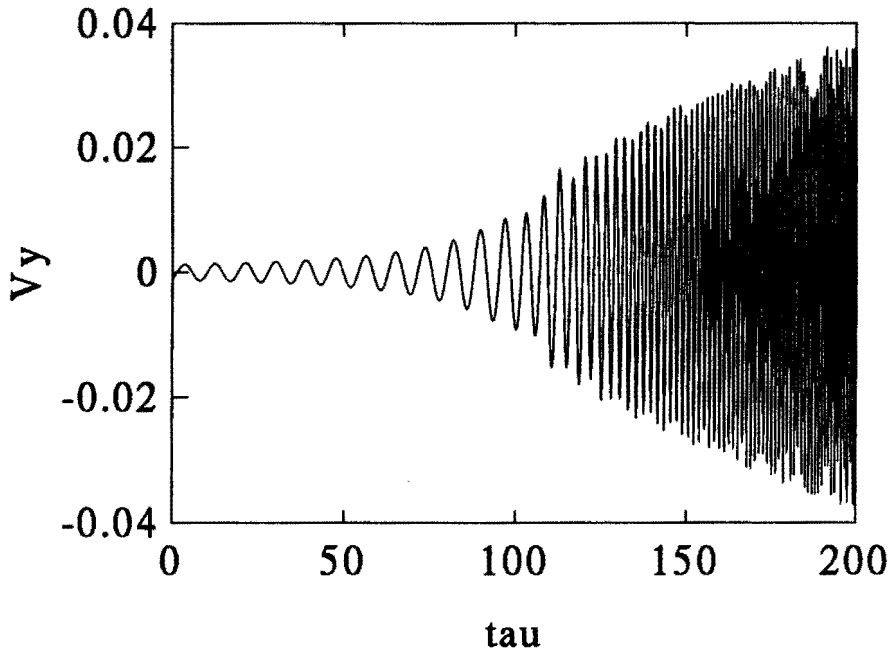
0.04
0.02
0
-0.02
-0.04
Vy
0
50
100
150
200
tau

Fig. V.1

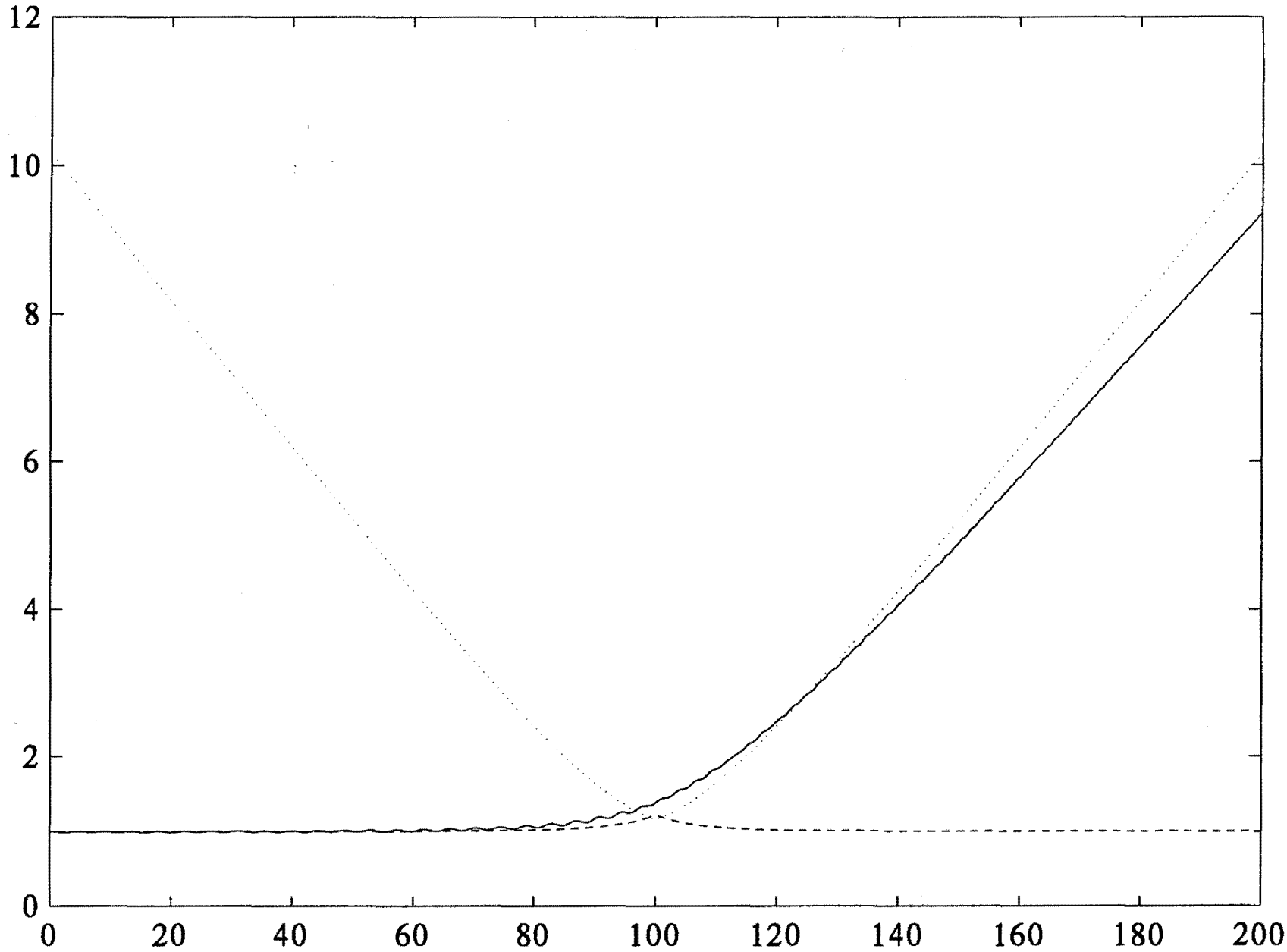
normilized energy and fast and slow fundamental frequencies
12
10
8
6
4
2
0
0
20
40
60
80
100
120
140
160
180
200
tau

Fig. V.2

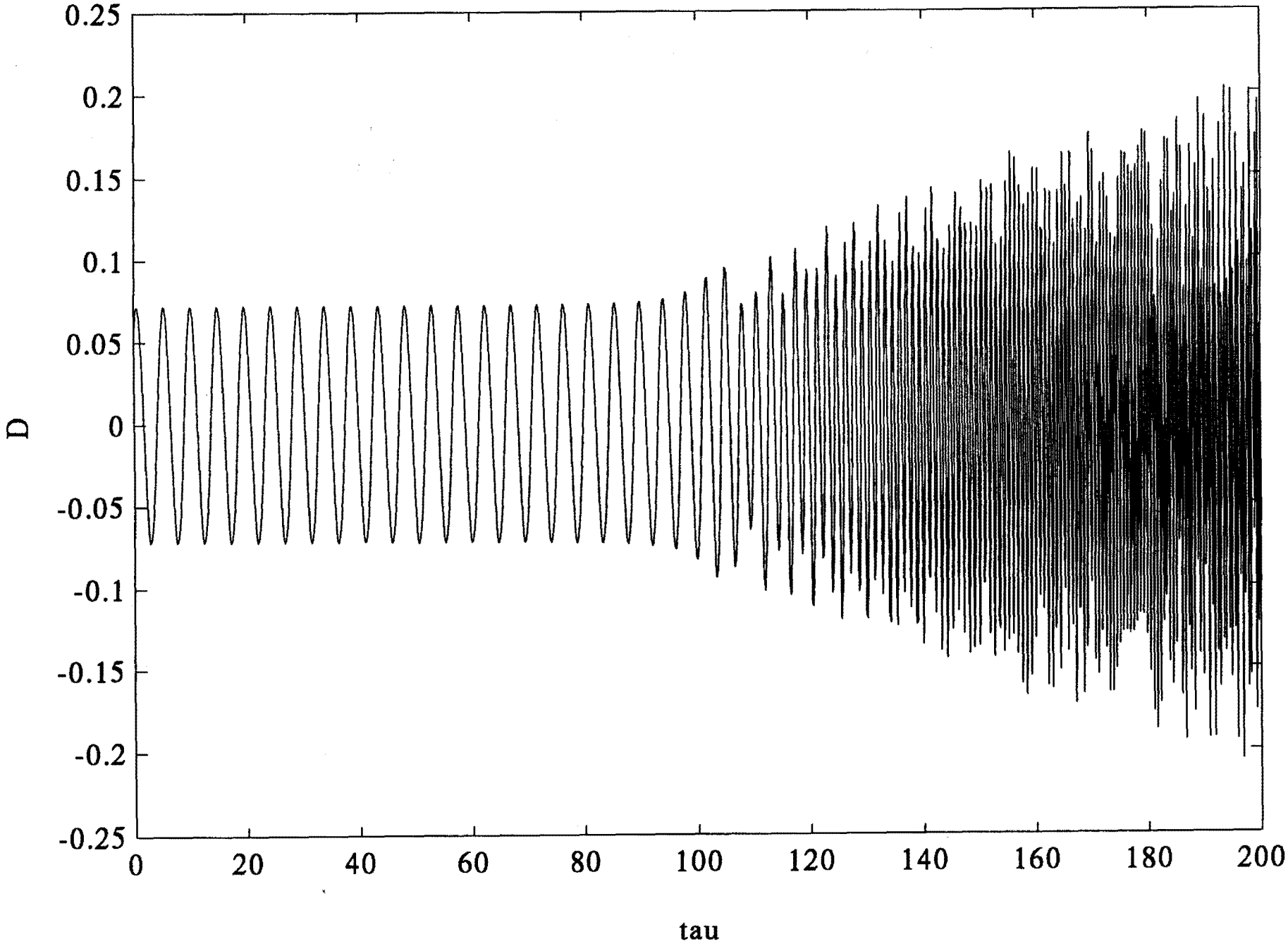
0.25
0.2
0.15
0.1
0.05
0
-0.05
-0.1
-0.15
-0.2
-0.25
D
0
20
40
60
80
100
120
140
160
180
200
tau

Fig. V.3

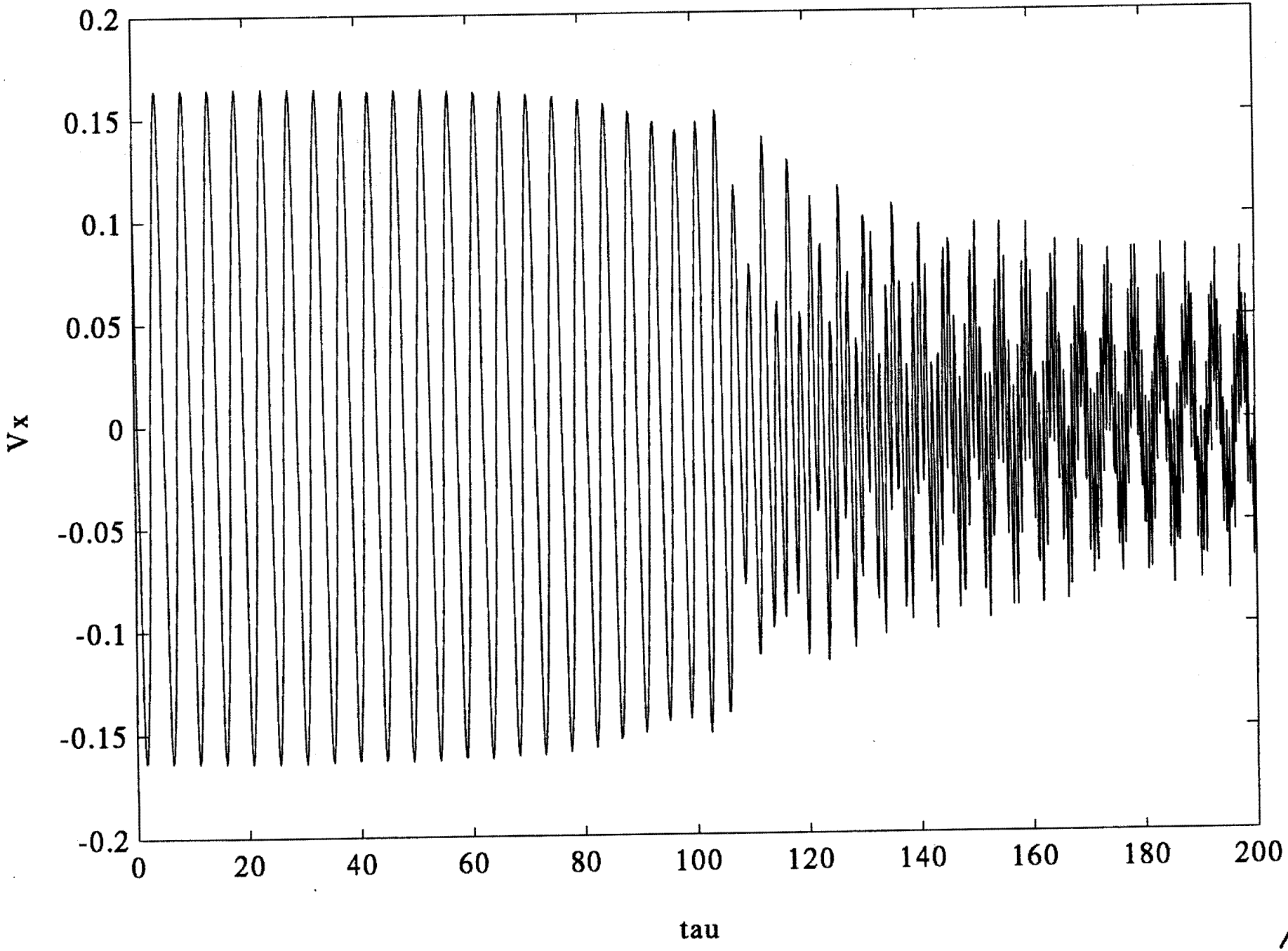
0.2
0.15
0.1
0.05
0
-0.05
-0.1
-0.15
-0.2
Vx
0
20
40
60
80
100
120
140
160
180
200
tau

Fig. V.4

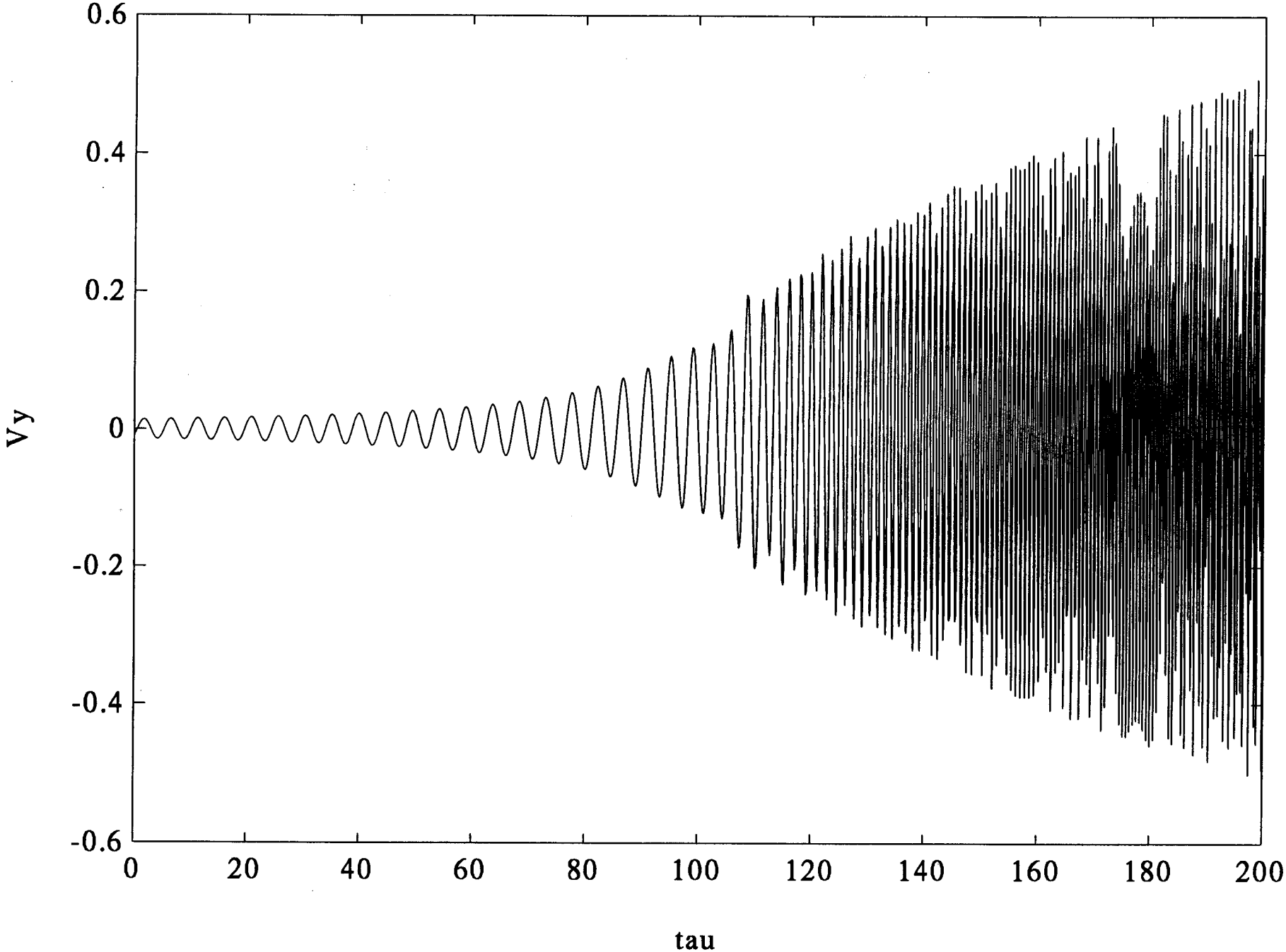

Fig. V.5

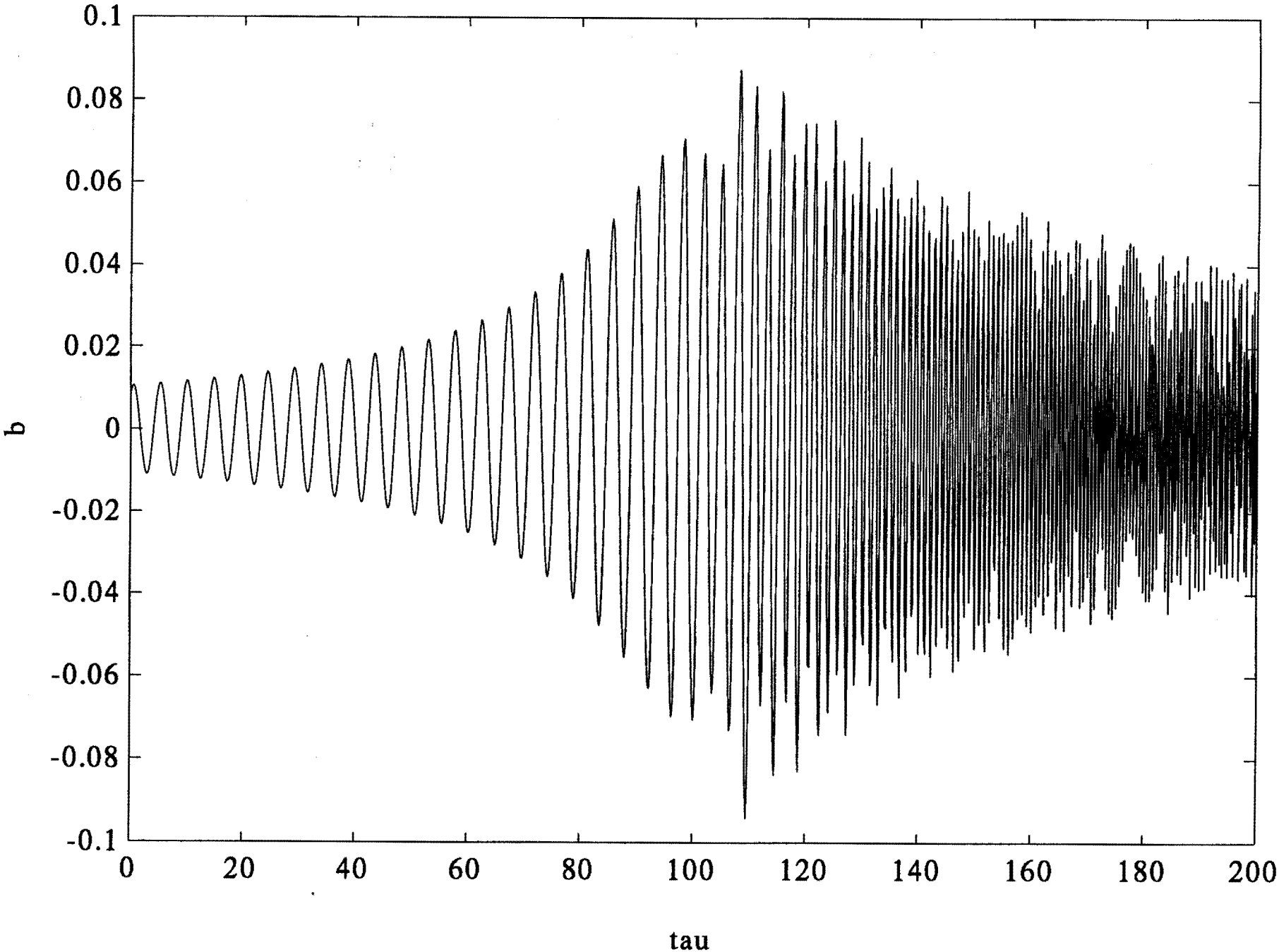
0.1
0.08
0.06
0.04
0.02
0
-0.02
-0.04
-0.06
-0.08
-0.1
b
0
20
40
60
80
100
120
140
160
180
200
tau

Fig. V.6

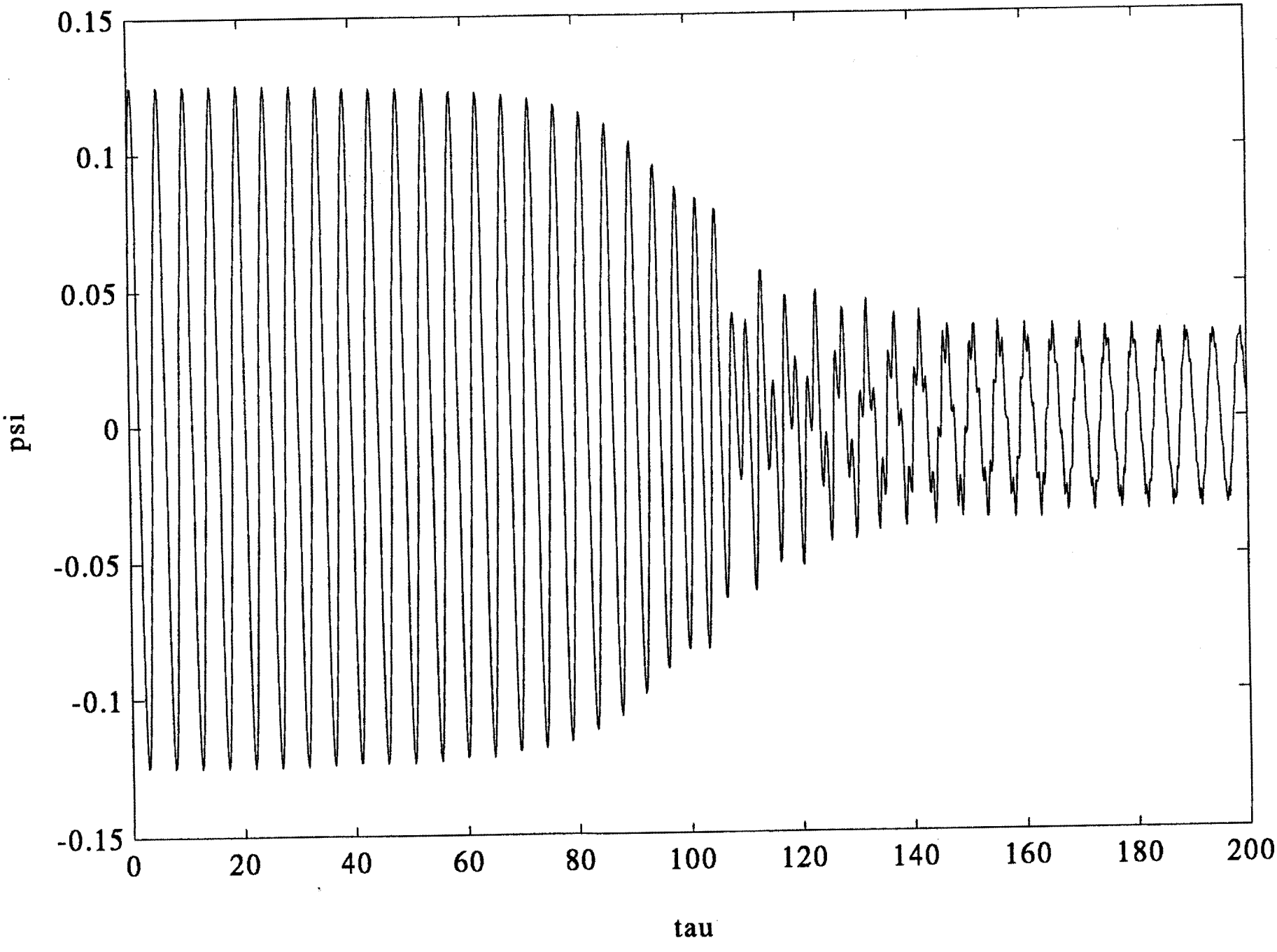
0.15
0.1
0.05
0
-0.05
-0.1
-0.15
psi
0
20
40
60
80
100
120
140
160
180
200
tau

Fig. V. 7

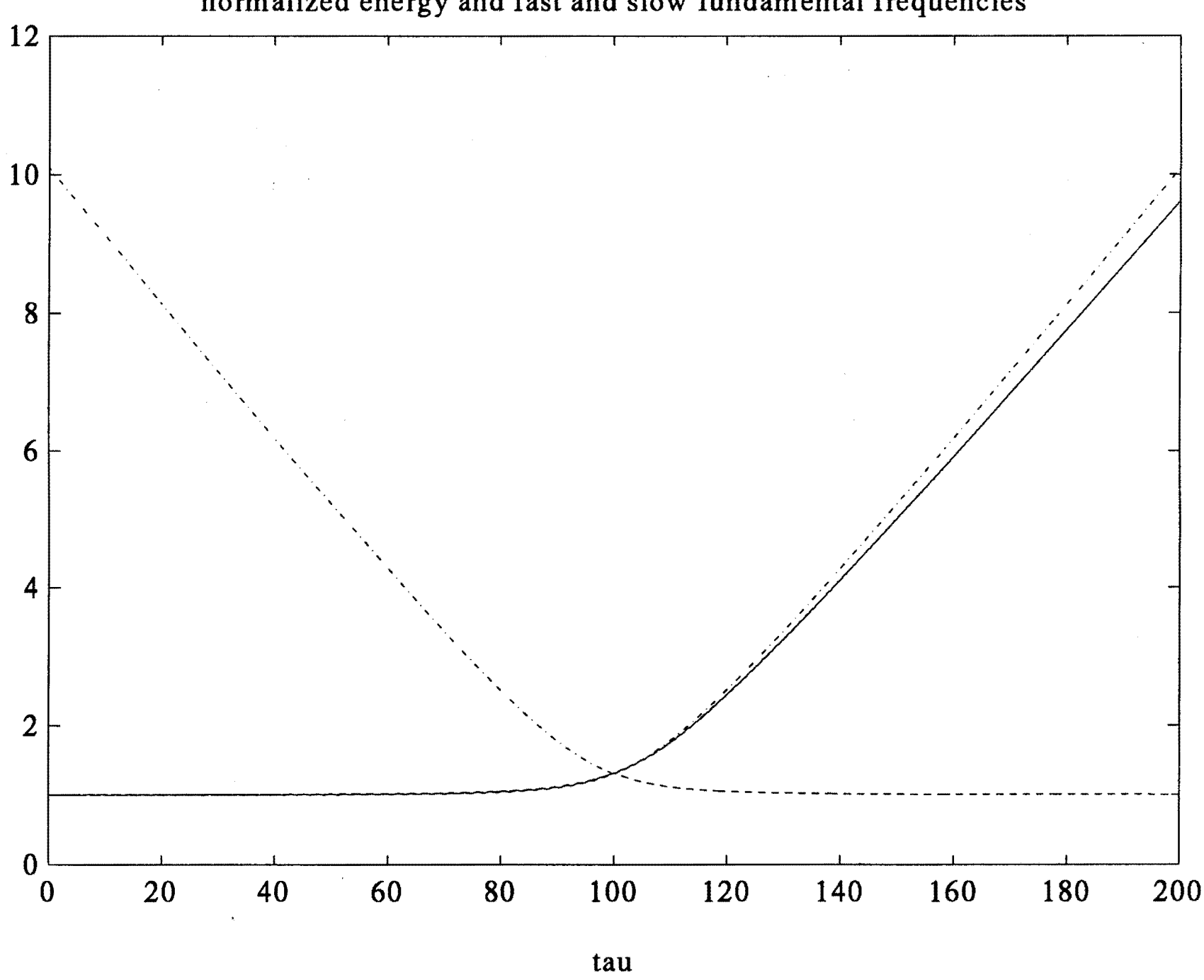
normalized energy and fast and slow fundamental frequencies
12
10
8
6
4
2
0
0
20
40
60
80
100
120
140
160
180
200
tau

Fig. V.8

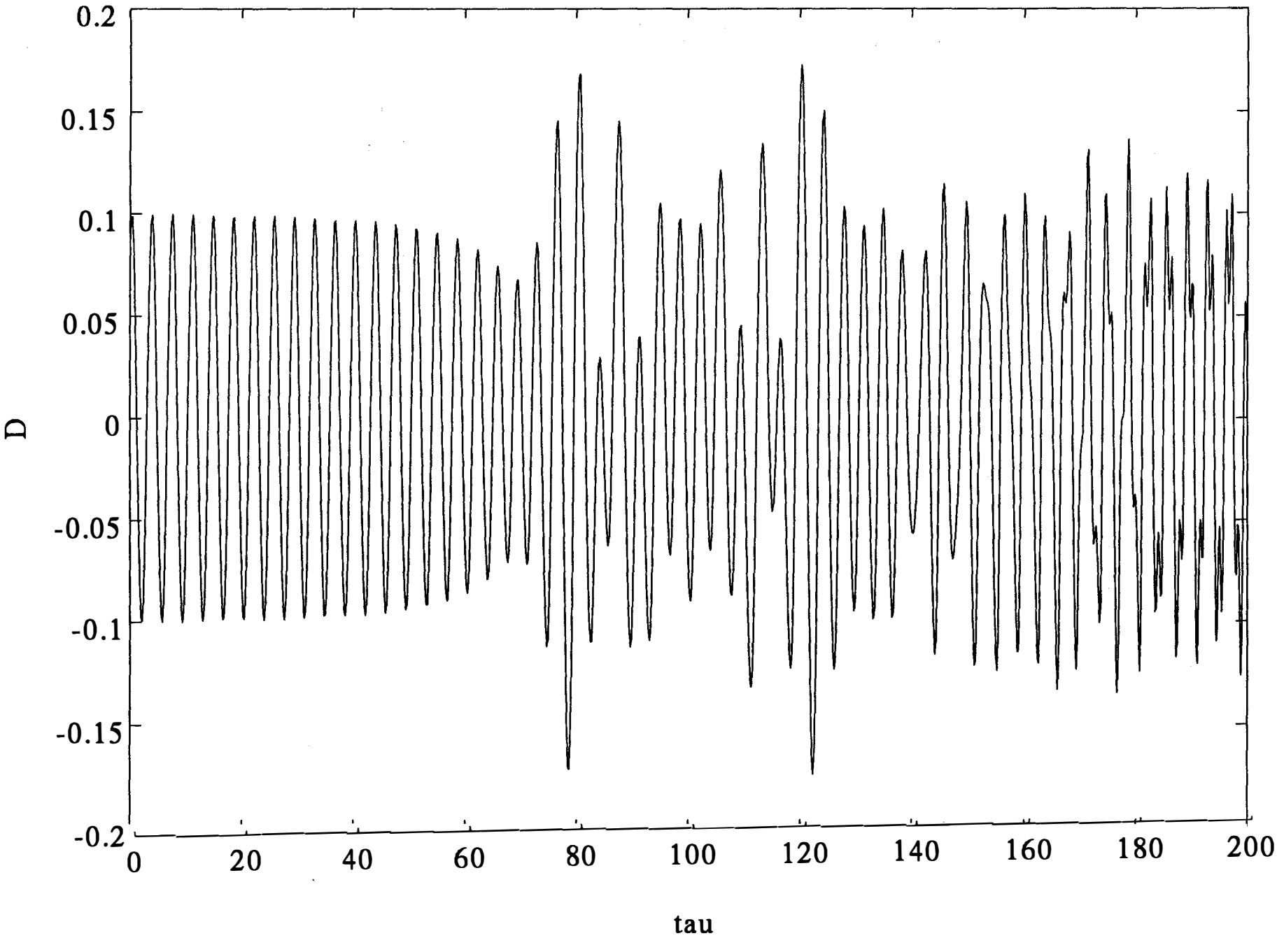
0.2
0.15
0.1
0.05
0
-0.05
-0.1
-0.15
-0.2
D
0
20
40
60
80
100
120
140
160
180
200
tau

Fig. V.9

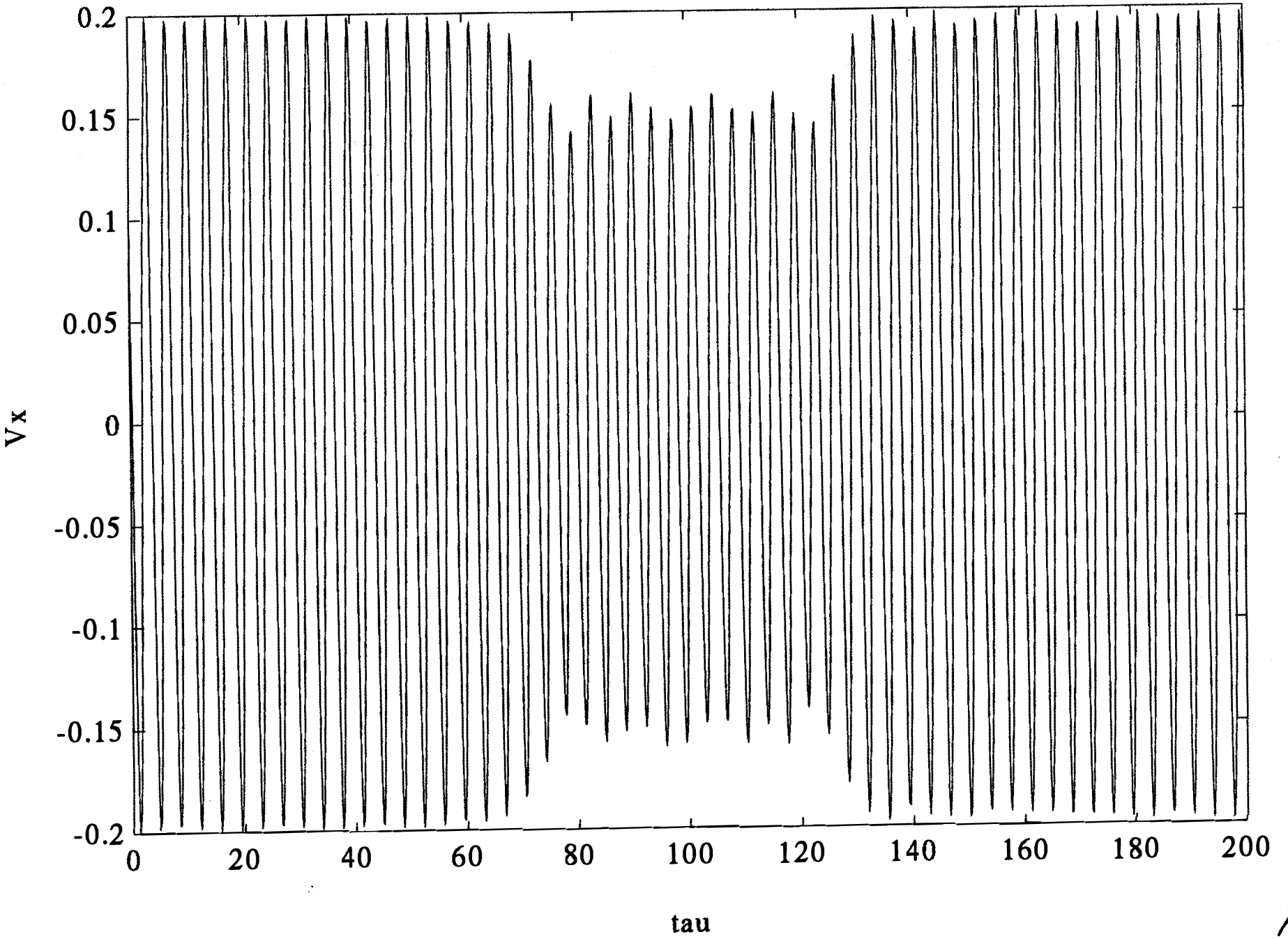
0.2
0.15
0.1
0.05
0
-0.05
-0.1
-0.15
-0.2
Vx
0
20
40
60
80
100
120
140
160
180
200
tau

Fig. V.10

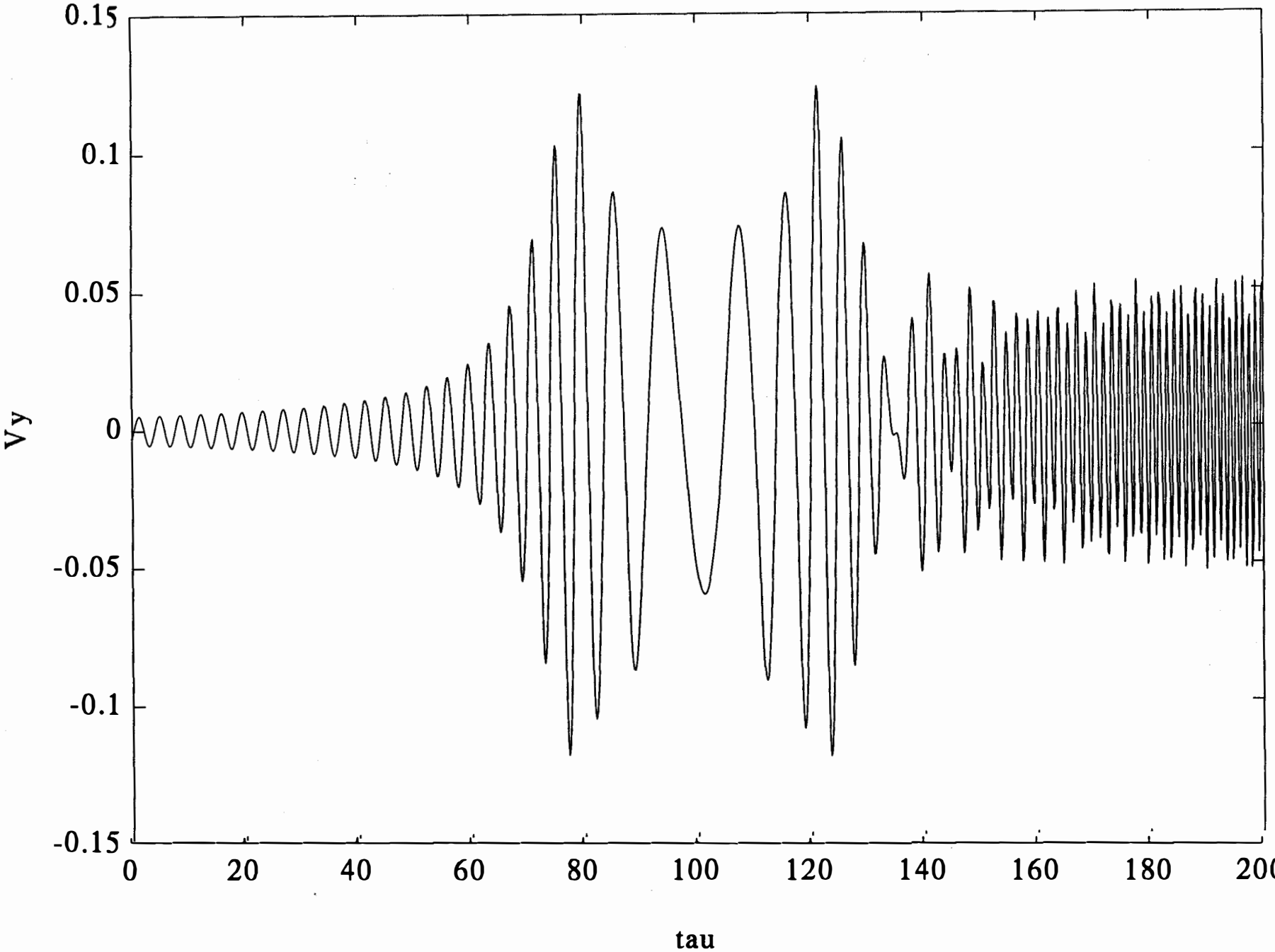

Fig. V.11

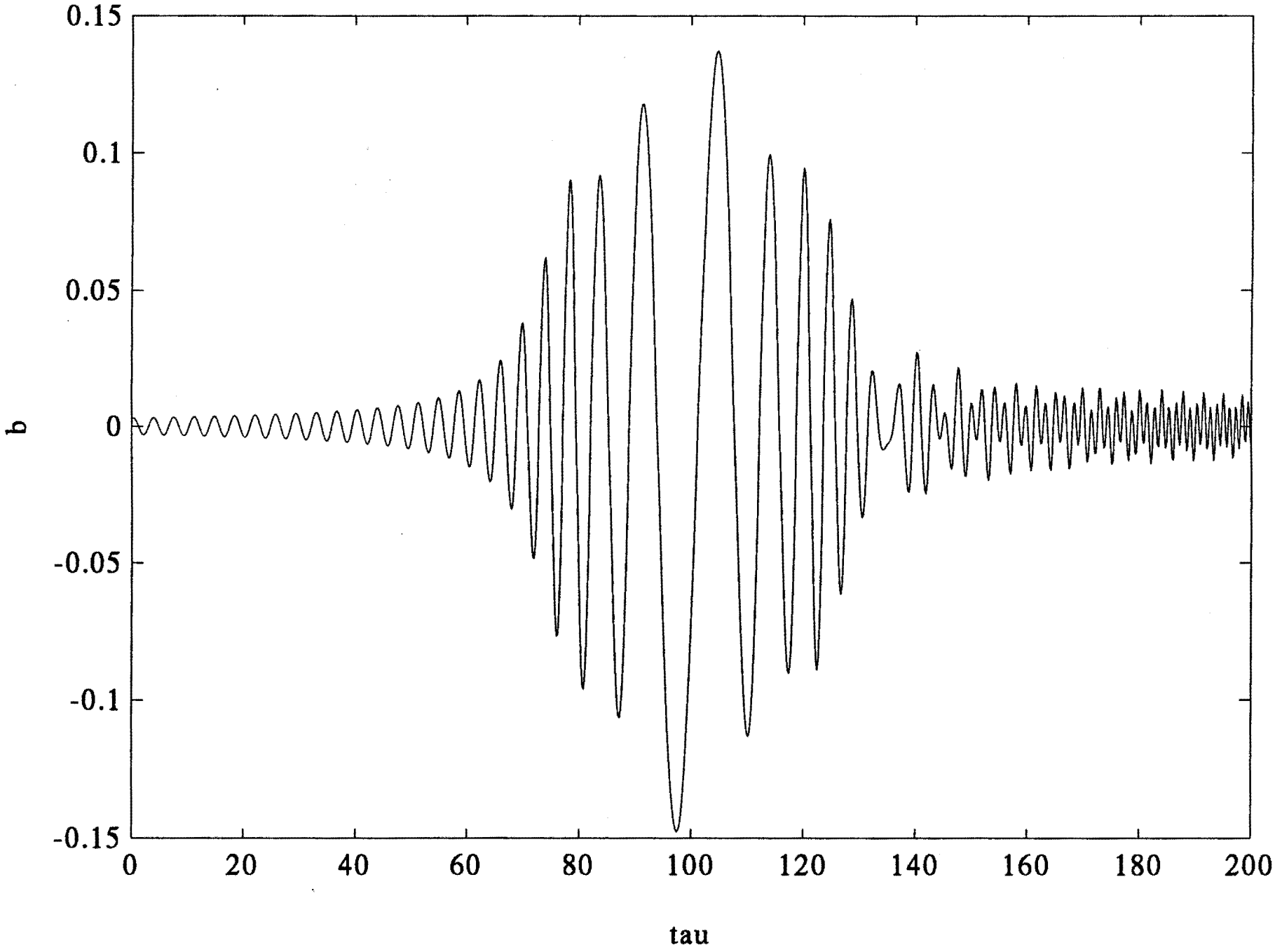

Fig. V. 12

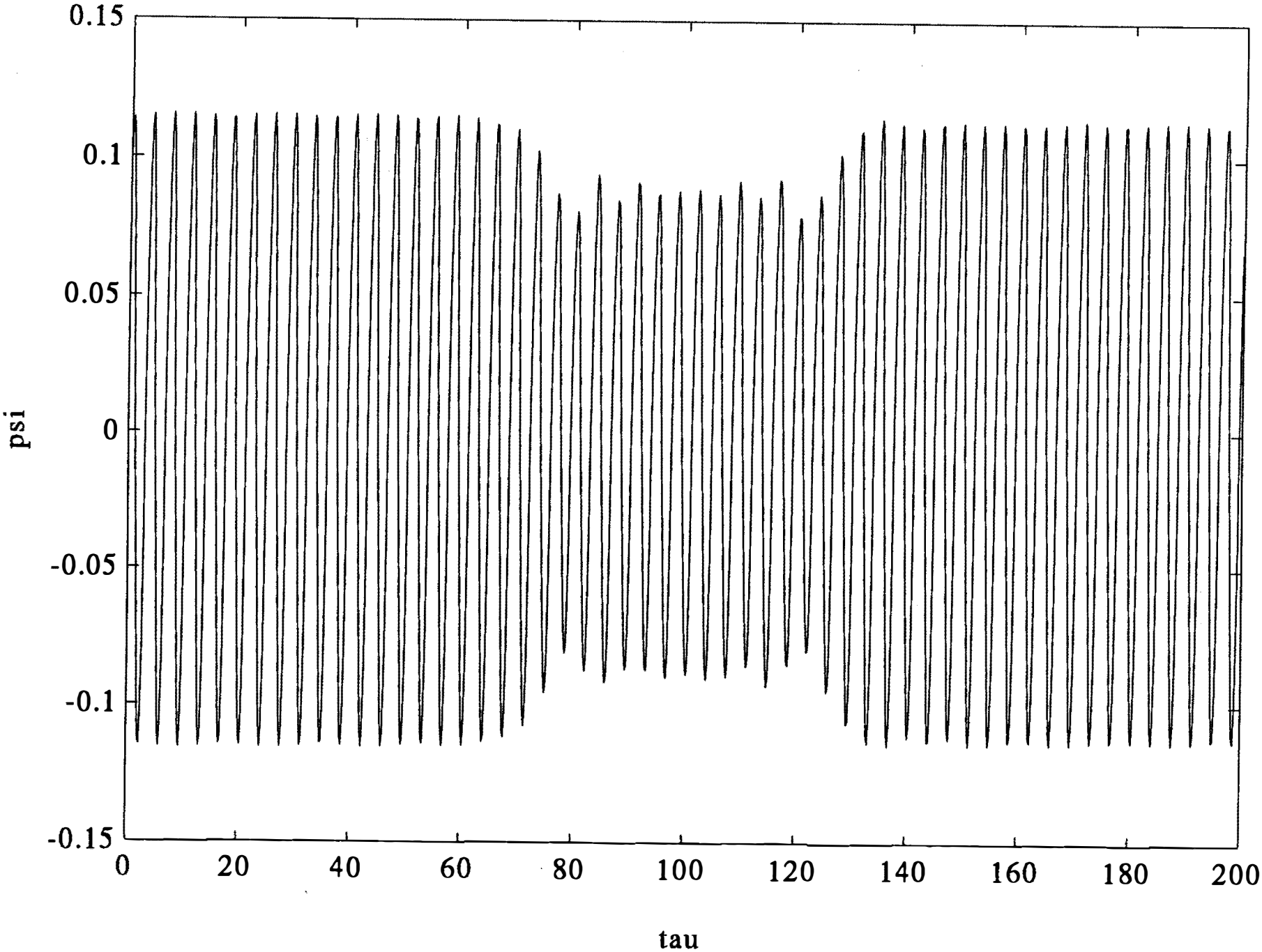
0.15
0.1
0.05
0
-0.05
-0.1
-0.15
psi
0
20
40
60
80
100
120
140
160
180
200
tau

Fig. V. 13

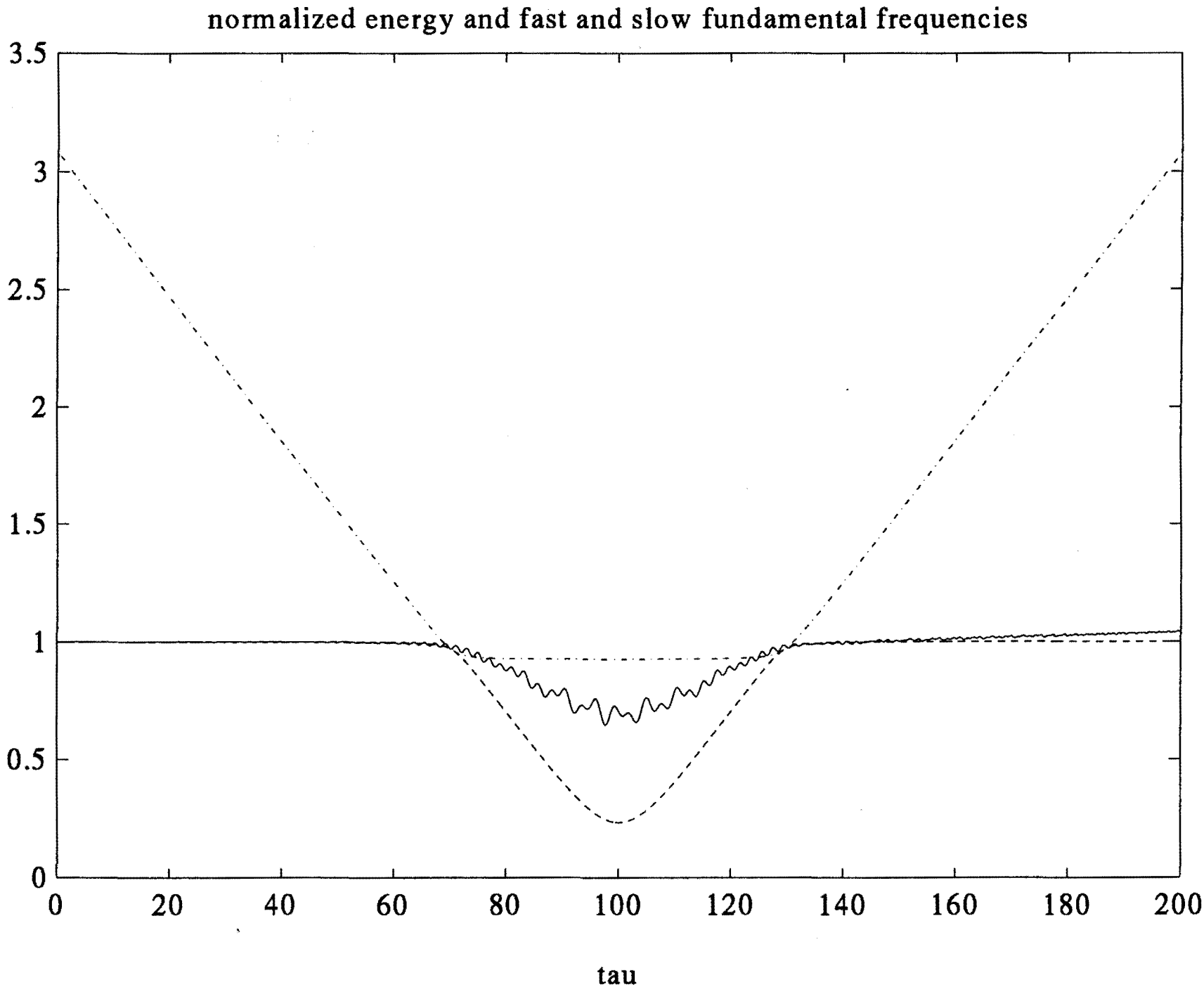
normalized energy and fast and slow fundamental frequencies
3.5
3
2.5
2
1.5
1
0.5
0
0
20
40
60
80
100
120
140
160
180
200
tau

Fig. V. 14

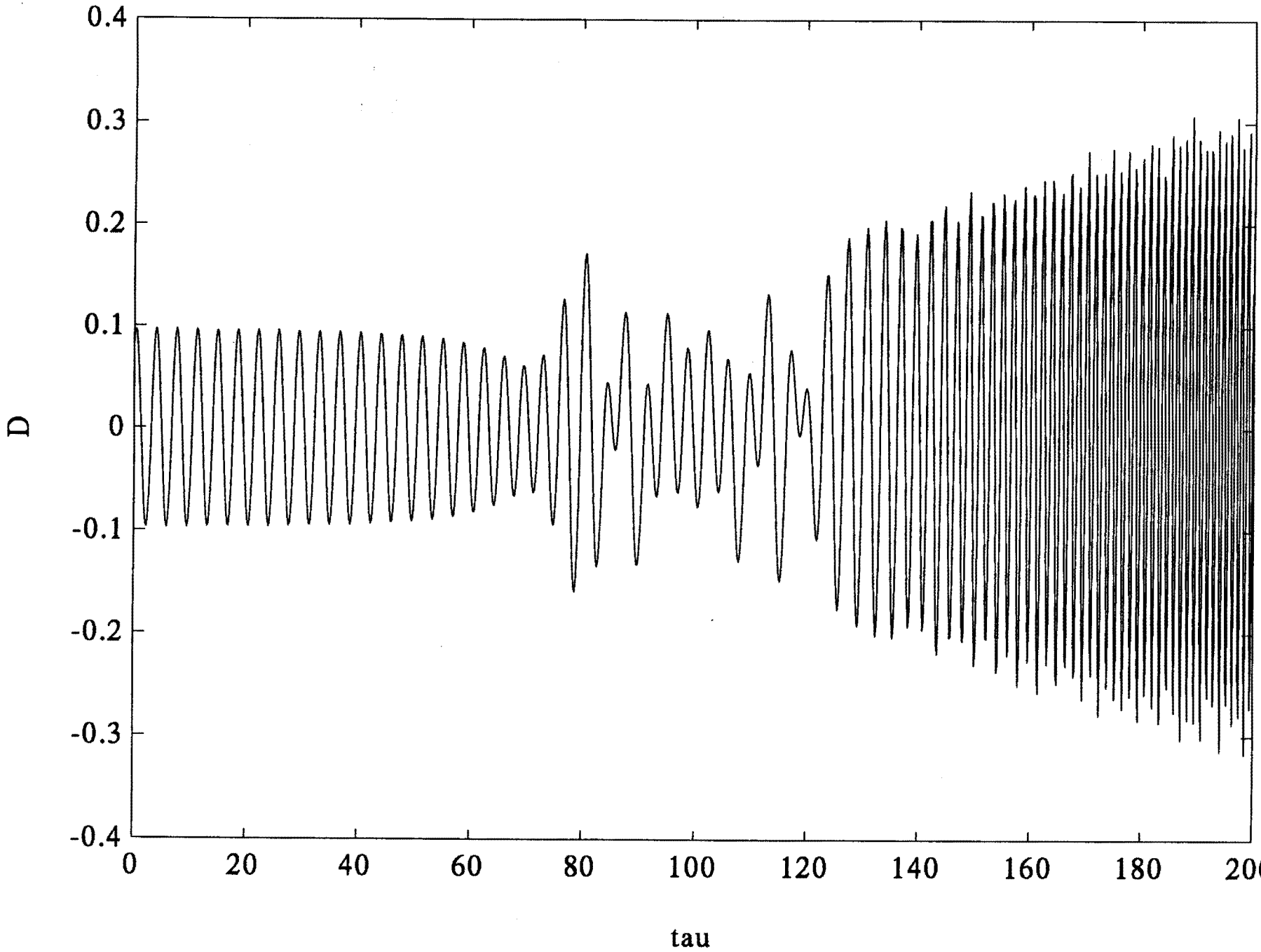

Fig. V.15

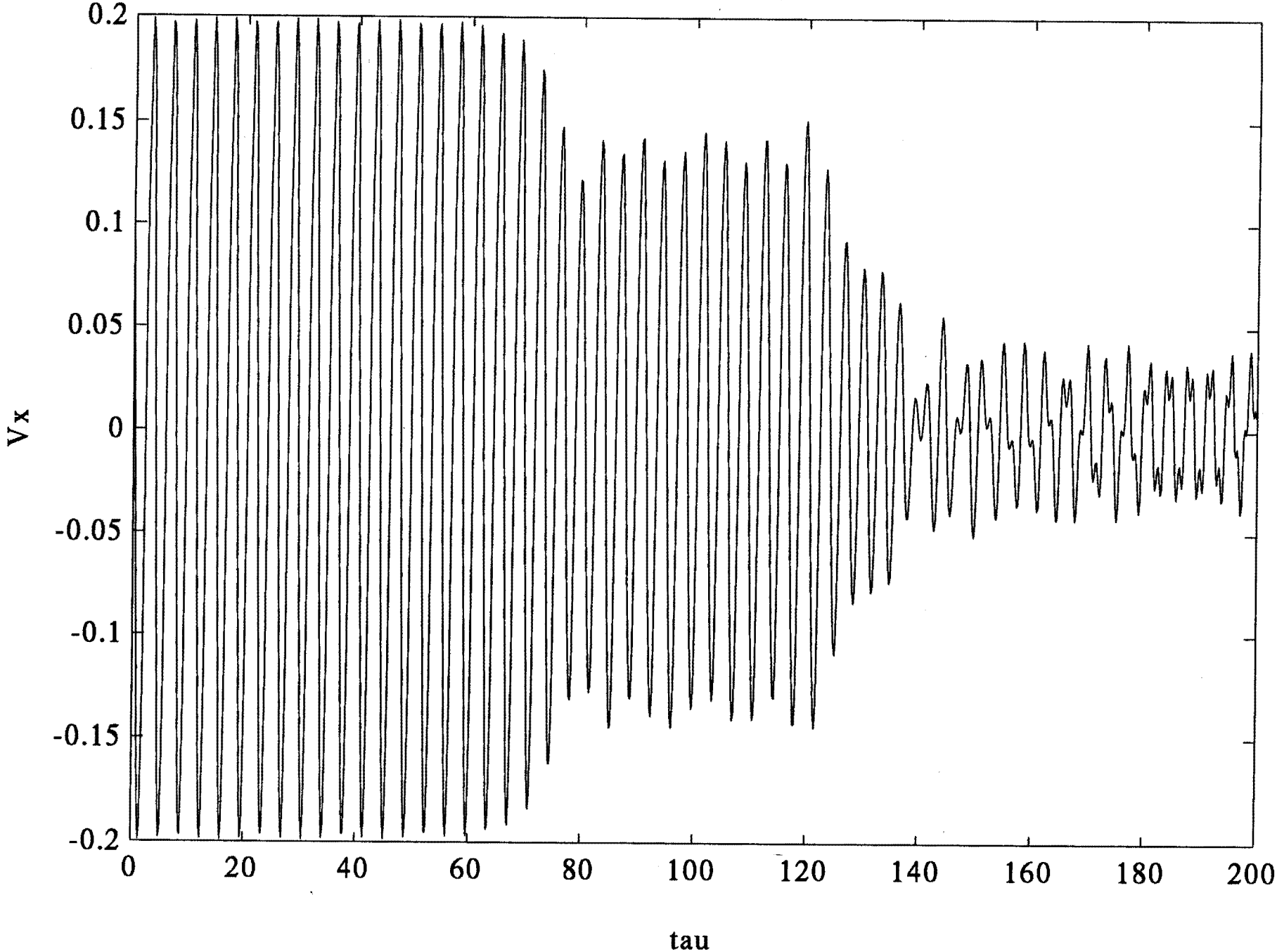
0.2
0.15
0.1
0.05
0
-0.05
-0.1
-0.15
-0.2
Vx
0
20
40
60
80
100
120
140
160
180
200
tau

Fig. V.16

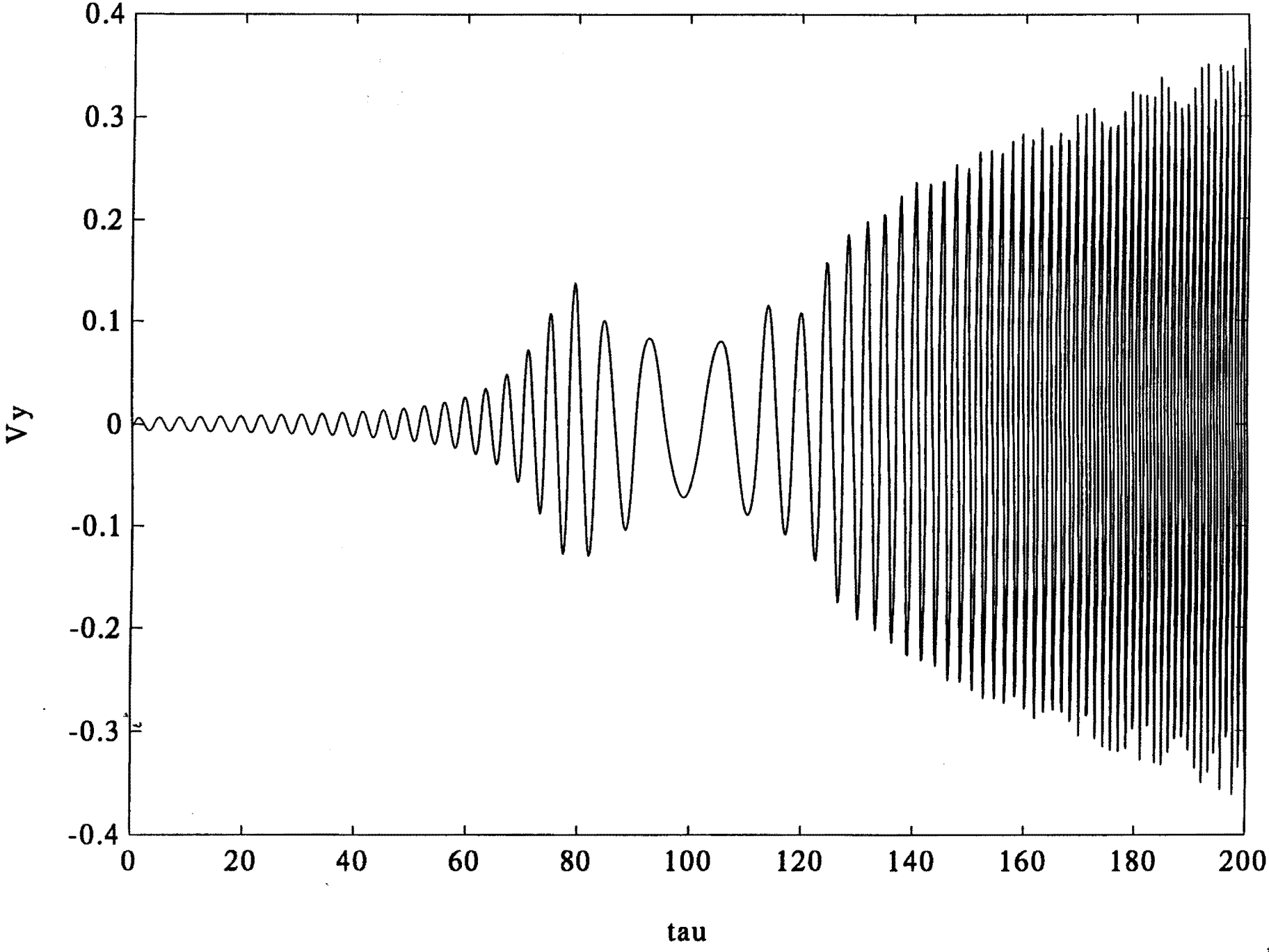

Fig. V. 17

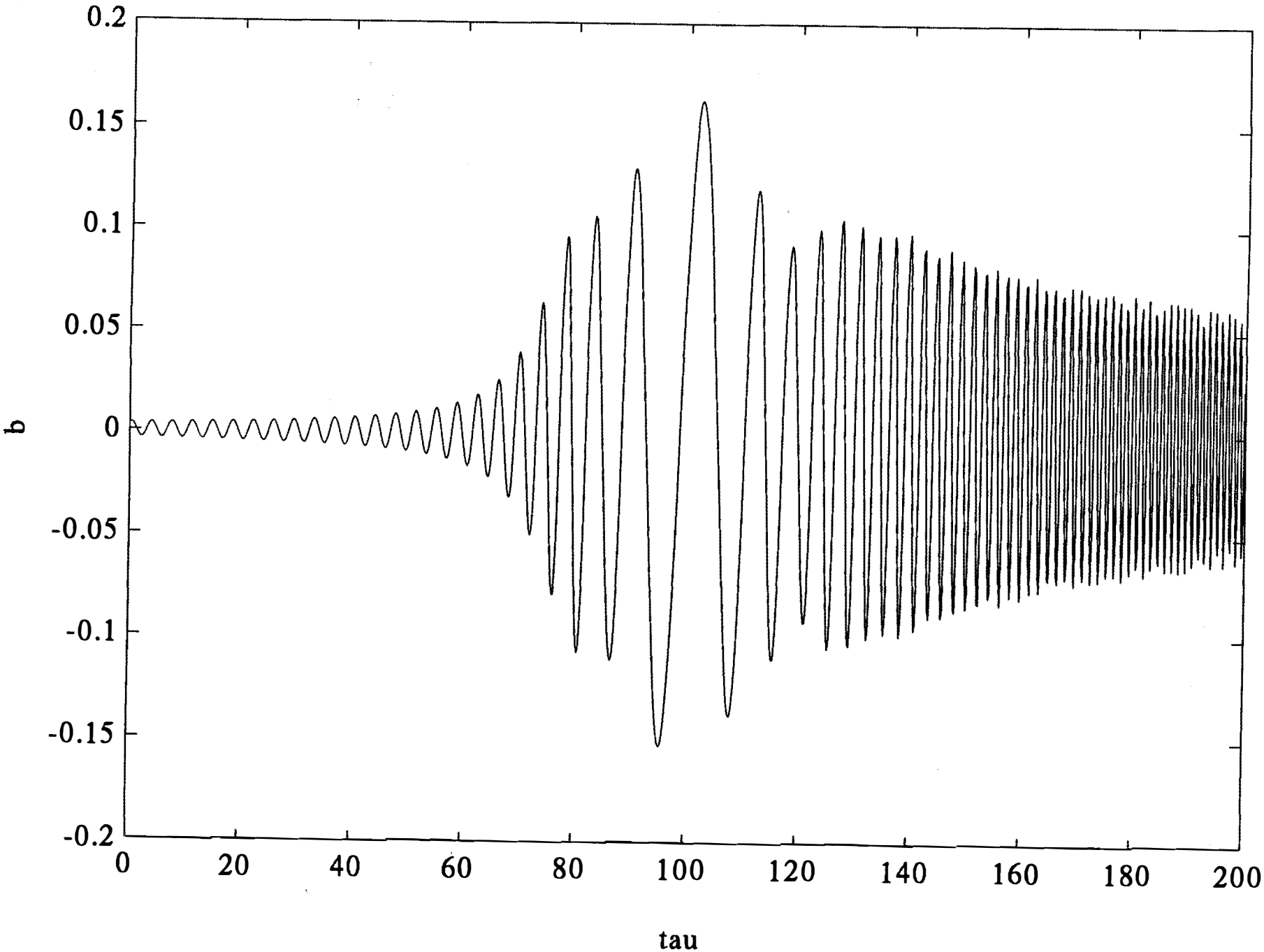
0.2
0.15
0.1
0.05
0
-0.05
-0.1
-0.15
-0.2
b
0
20
40
60
80
100
120
140
160
180
200
tau

Fig. V.18

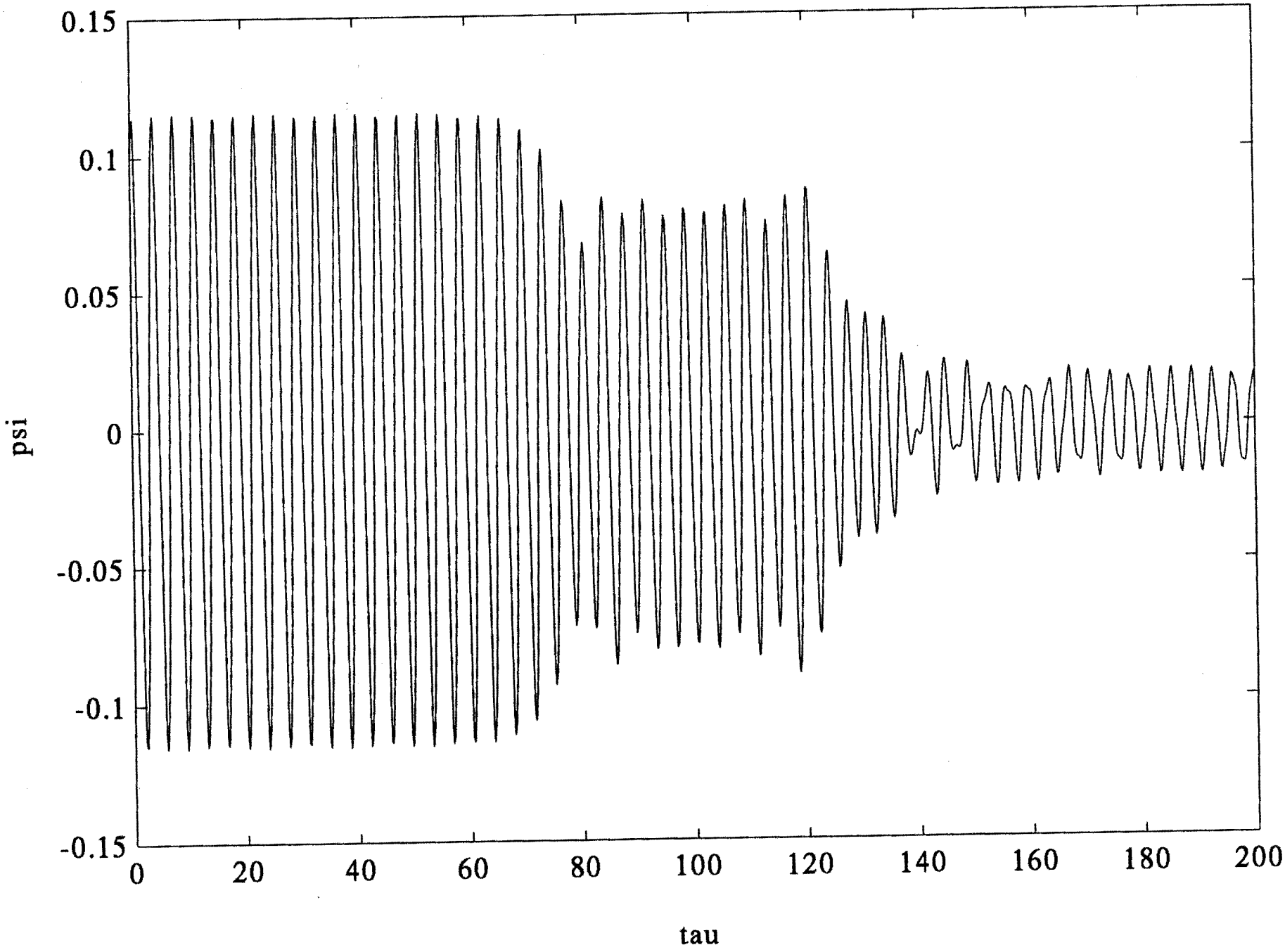
0.15
0.1
0.05
0
-0.05
-0.1
-0.15
psi
0
20
40
60
80
100
120
140
160
180
200
tau

Fig V 19

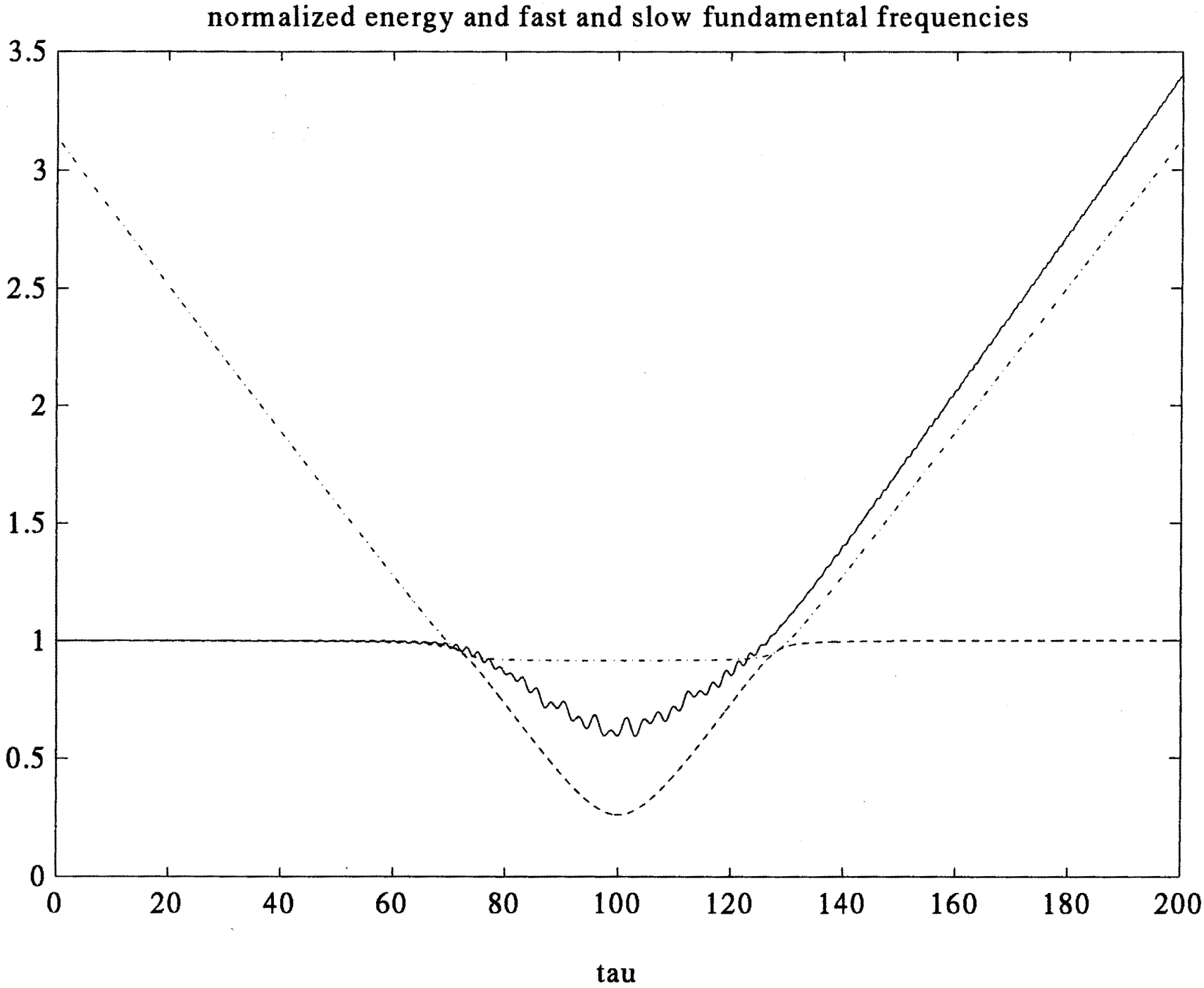
normalized energy and fast and slow fundamental frequencies
3.5
3
2.5
2
1.5
1
0.5
0
0
20
40
60
80
100
120
140
160
180
200
tau

Fig. V.20

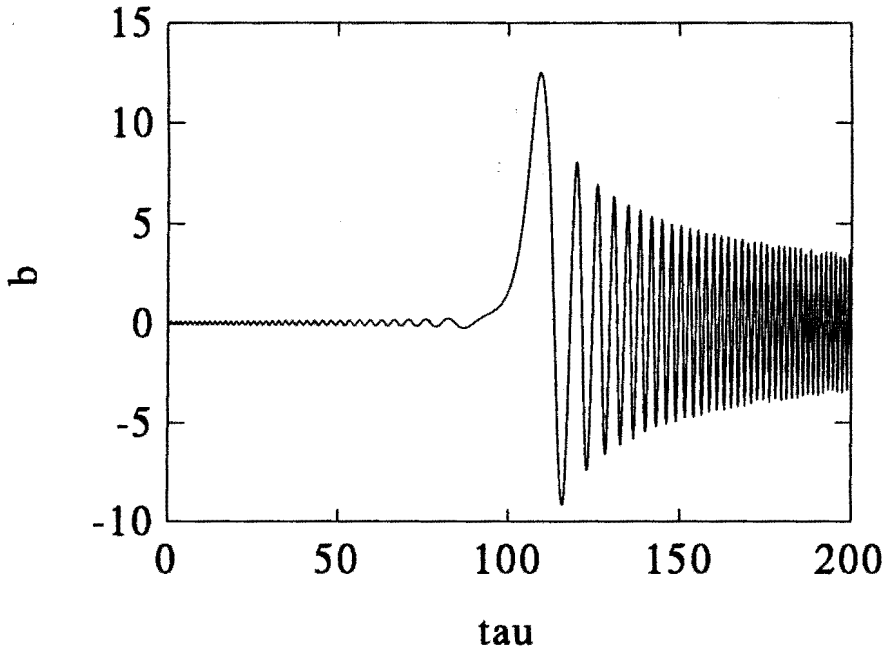
b
15
10
5
0
-5
-10
0
50
100
150
200
tau

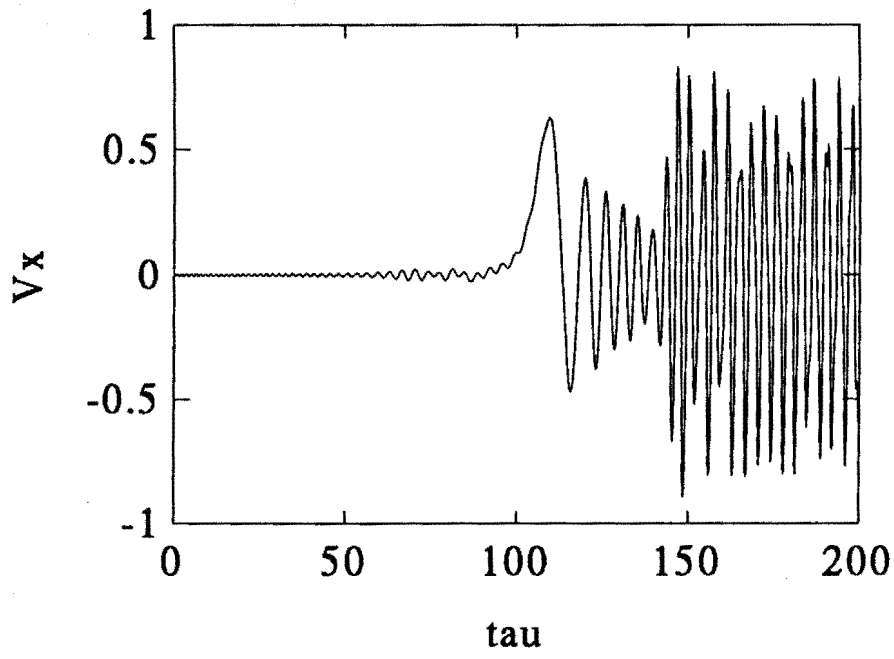
Vx
1
0.5
0
-0.5
-1
0
50
100
150
200
tau

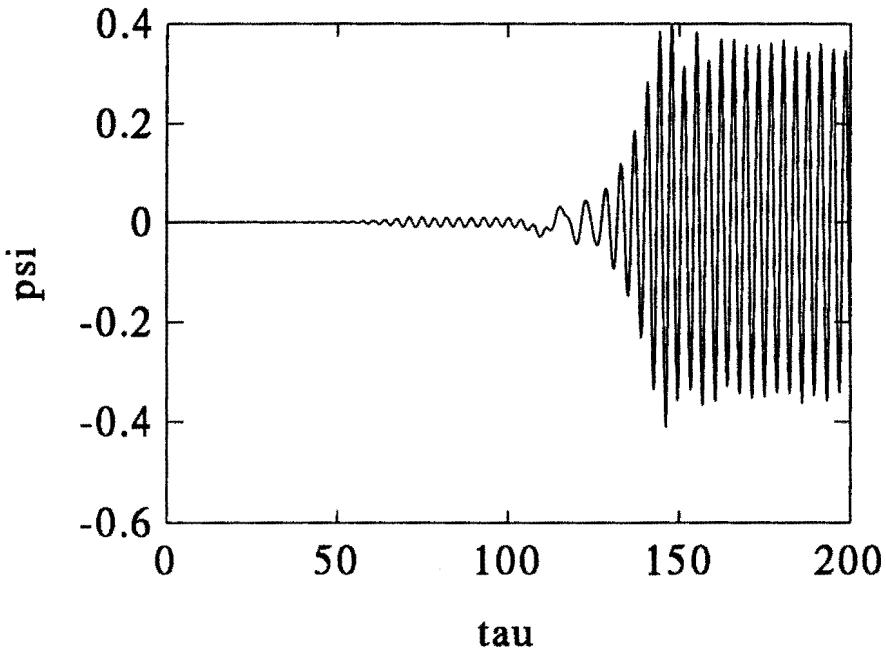
psi
0.4
0.2
0
-0.2
-0.4
-0.6
0
50
100
150
200
tau

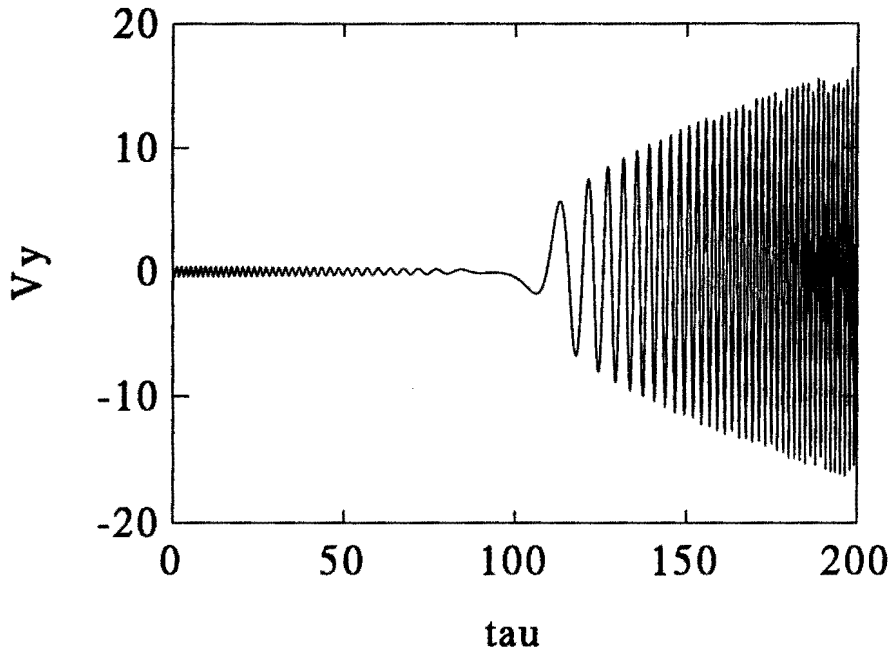
Vy
20
10
0
-10
-20
0
50
100
150
200
tau

Fig. V.21

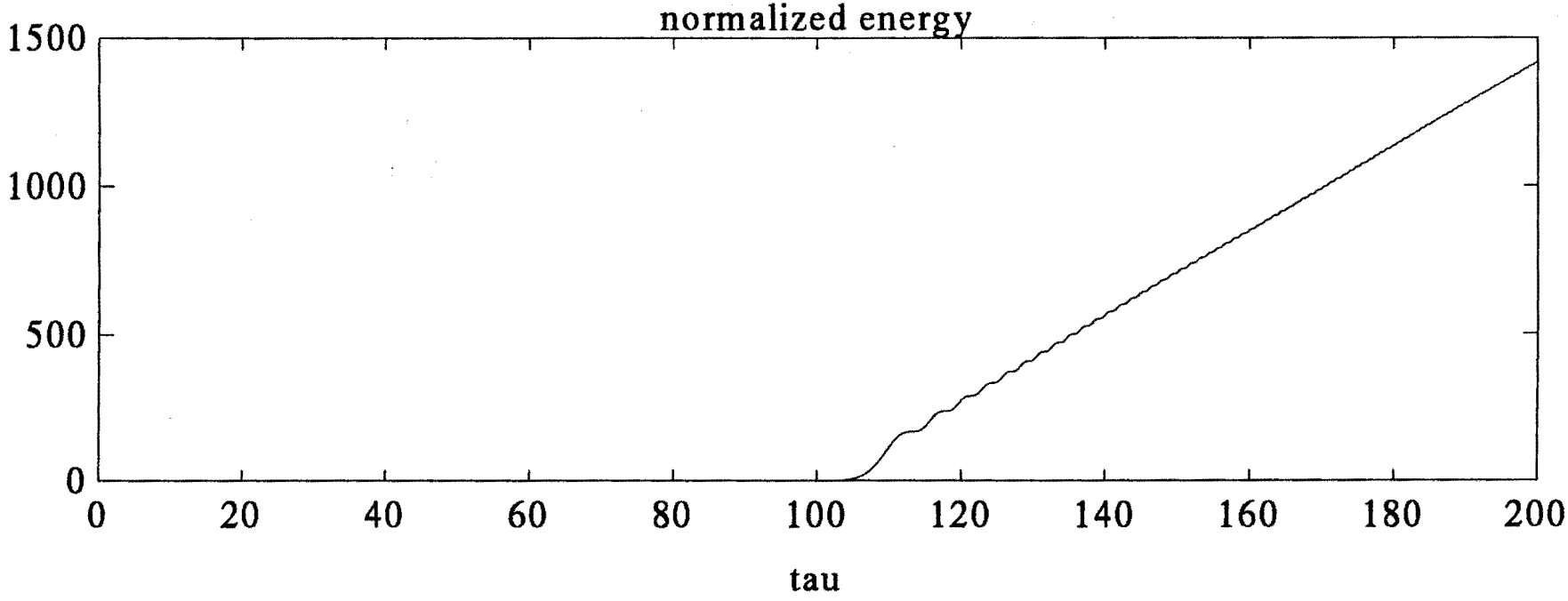
normalized energy
1500
1000
500
0
0
20
40
60
80
100
120
140
160
180
200
tau

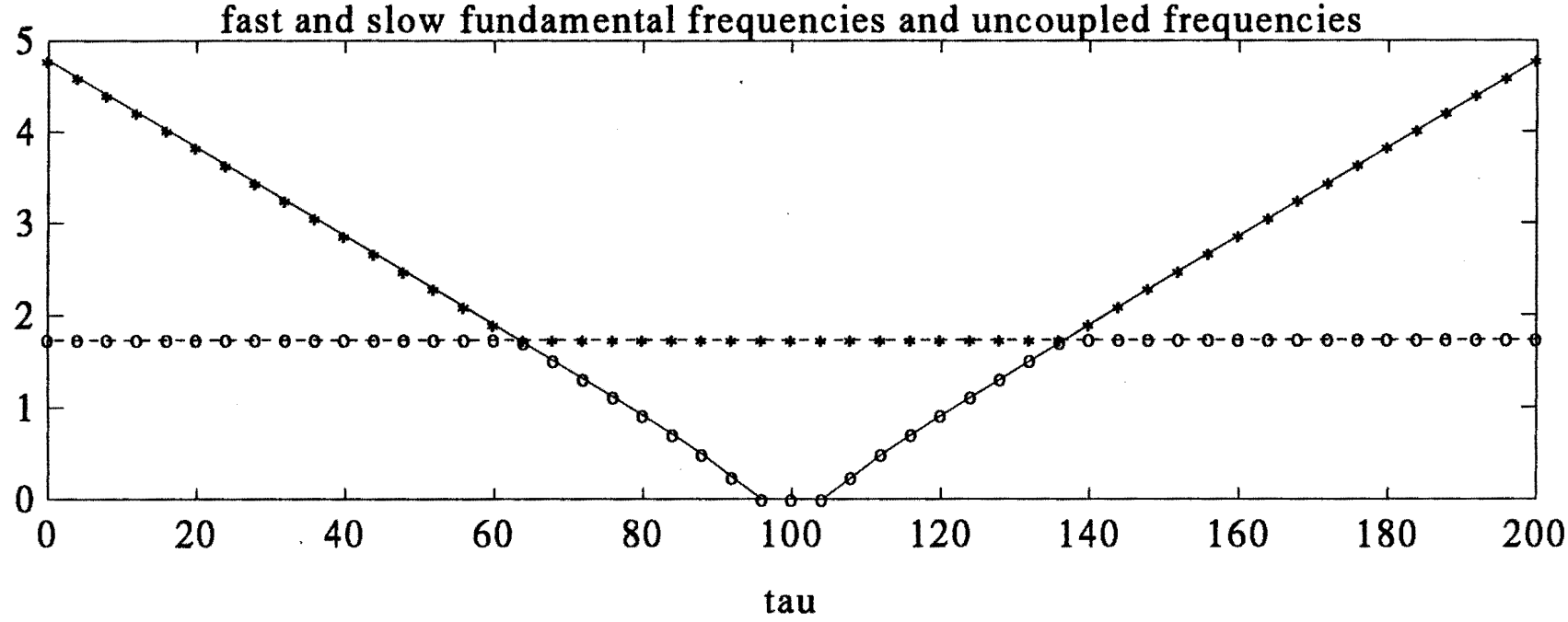
fast and slow fundamental frequencies and uncoupled frequencies
5
4
3
2
1
0
0
20
40
60
80
100
120
140
160
180
200
tau

Fig. V.22

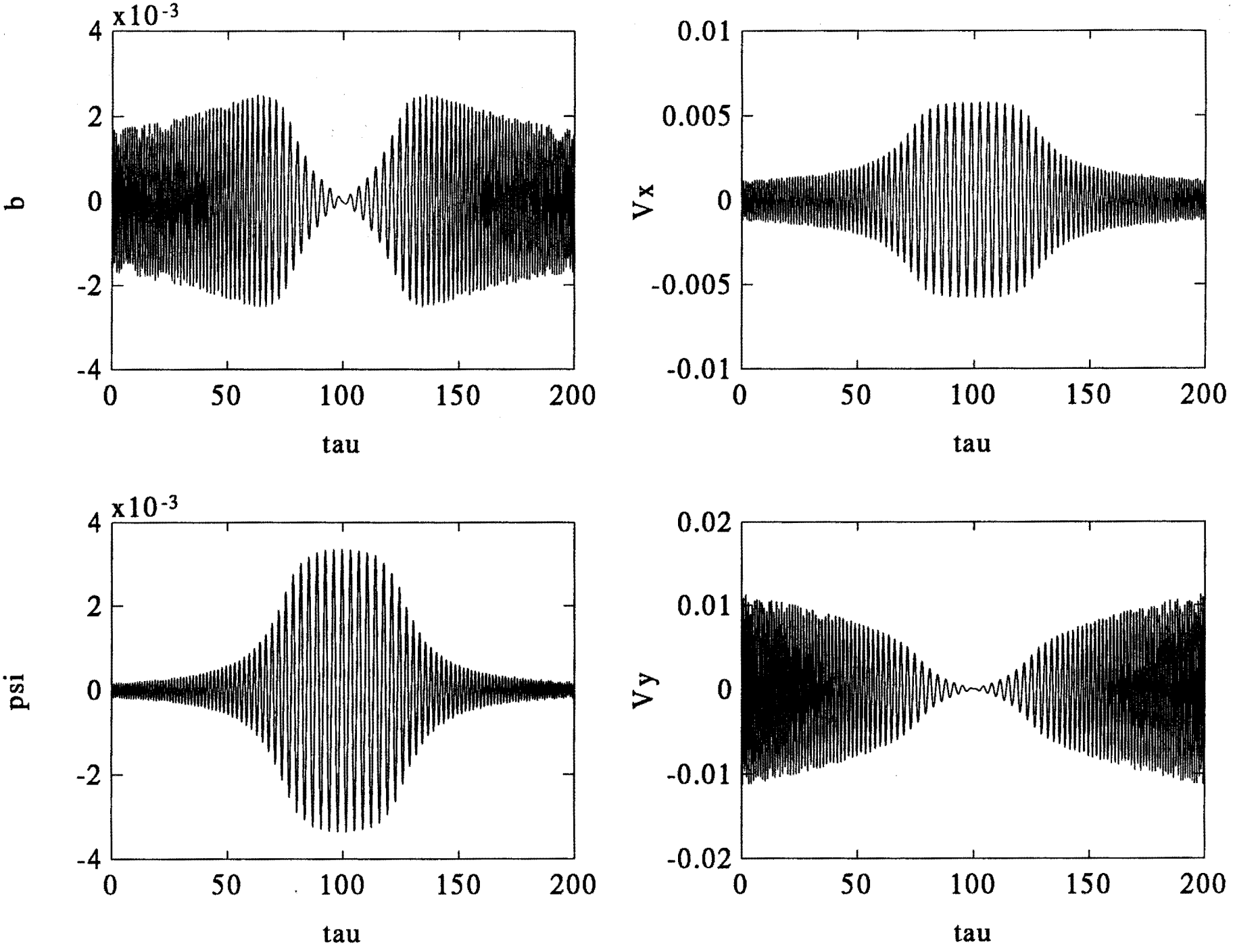
x10-3
4
2
0
-2
-4
b
0
50
100
150
200
tau
0.01
0.005
0
-0.005
-0.01
Vx
0
50
100
150
200
tau
x10-3
4
2
0
-2
-4
psi
0
50
100
150
200
tau
0.02
0.01
0
-0.01
-0.02
Vy
0
50
100
150
200
tau

Fig. V.23

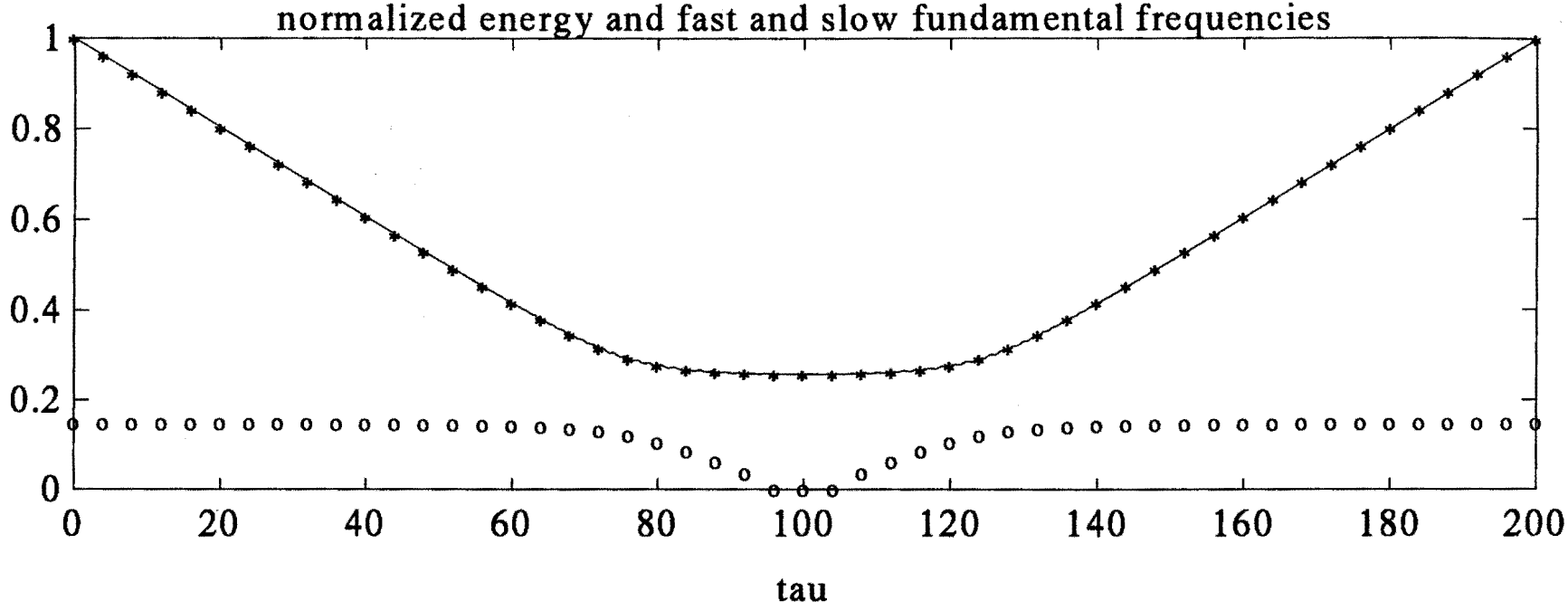
normalized energy and fast and slow fundamental frequencies
1
0.8
0.6
0.4
0.2
0
0
20
40
60
80
100
120
140
160
180
200
tau

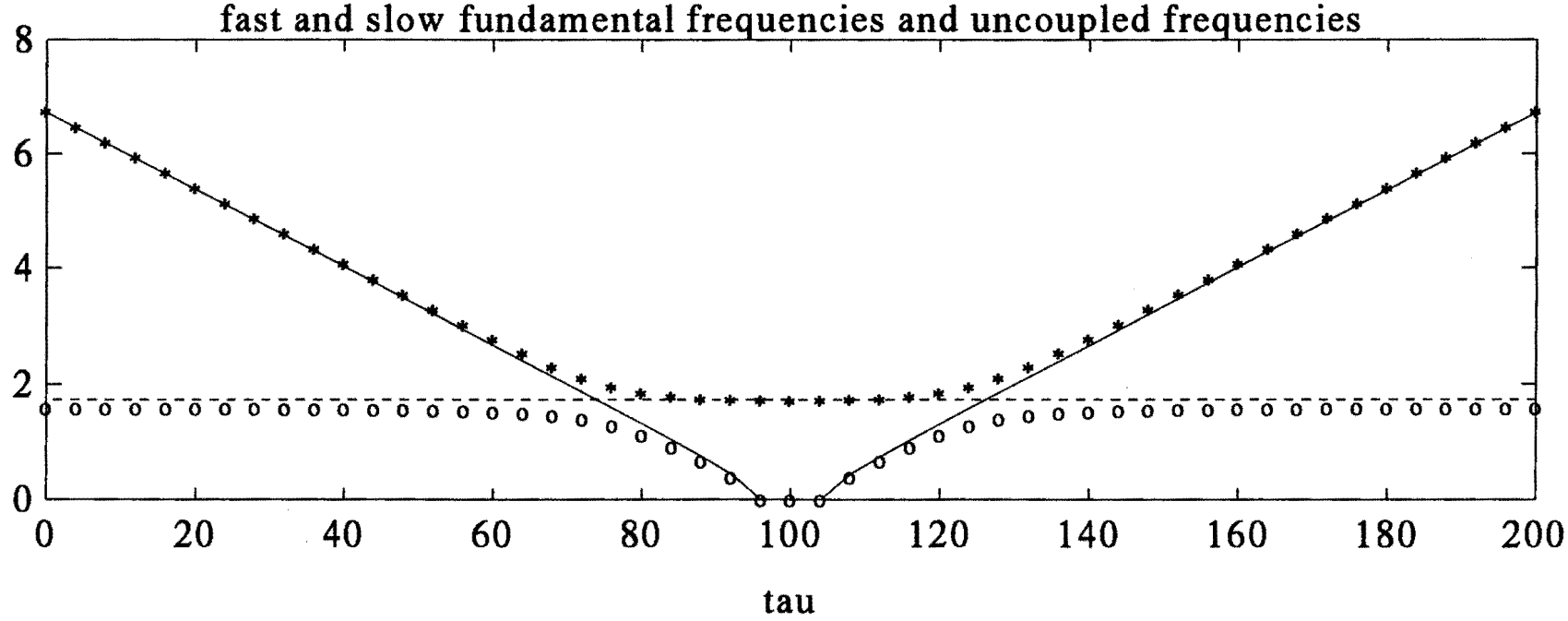
fast and slow fundamental frequencies and uncoupled frequencies
8
6
4
2
0
0
20
40
60
80
100
120
140
160
180
200
tau

Fig. V. 24

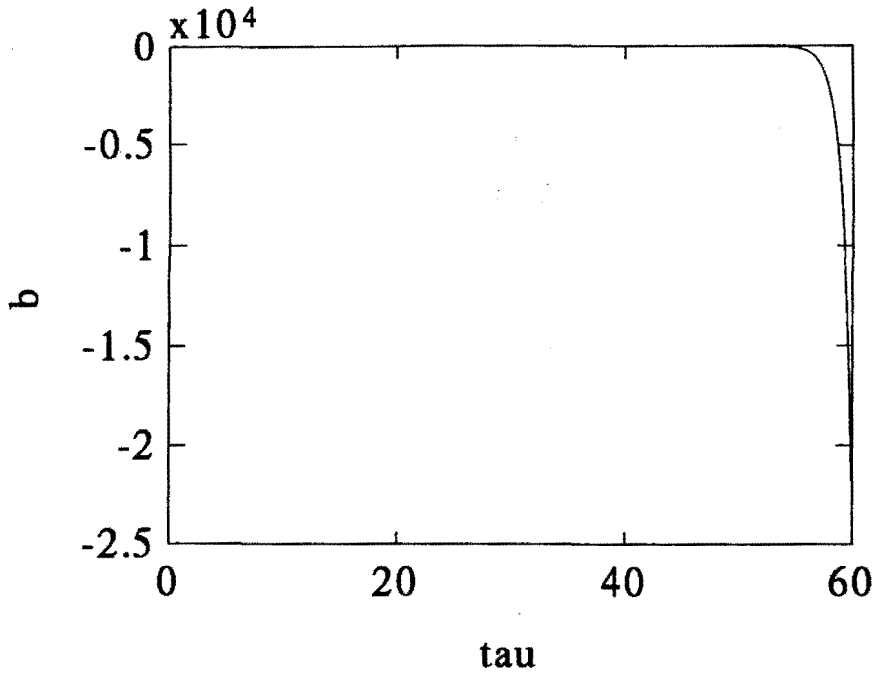
x10^4
0
-0.5
-1
-1.5
-2
-2.5
b
0
20
40
60
tau

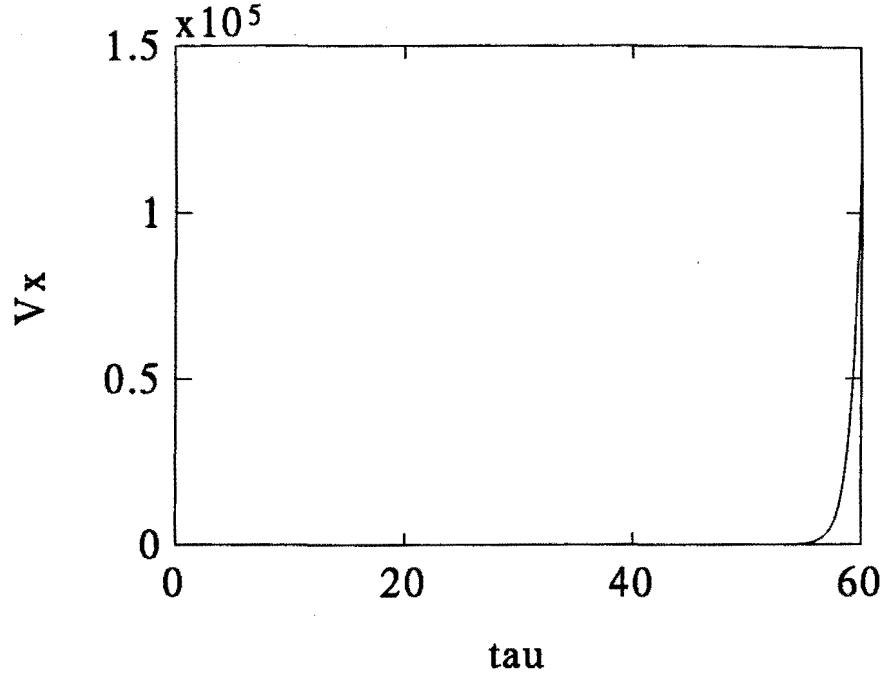
x10^5
1.5
1
0.5
0
Vx
0
20
40
60
tau

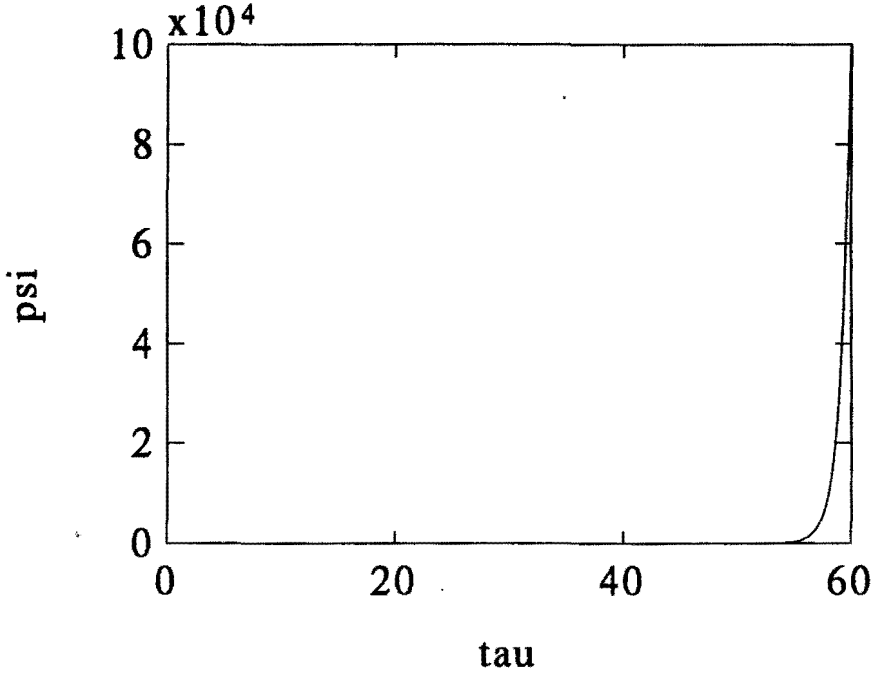
x10^4
10
8
6
4
2
0
psi
0
20
40
60
tau

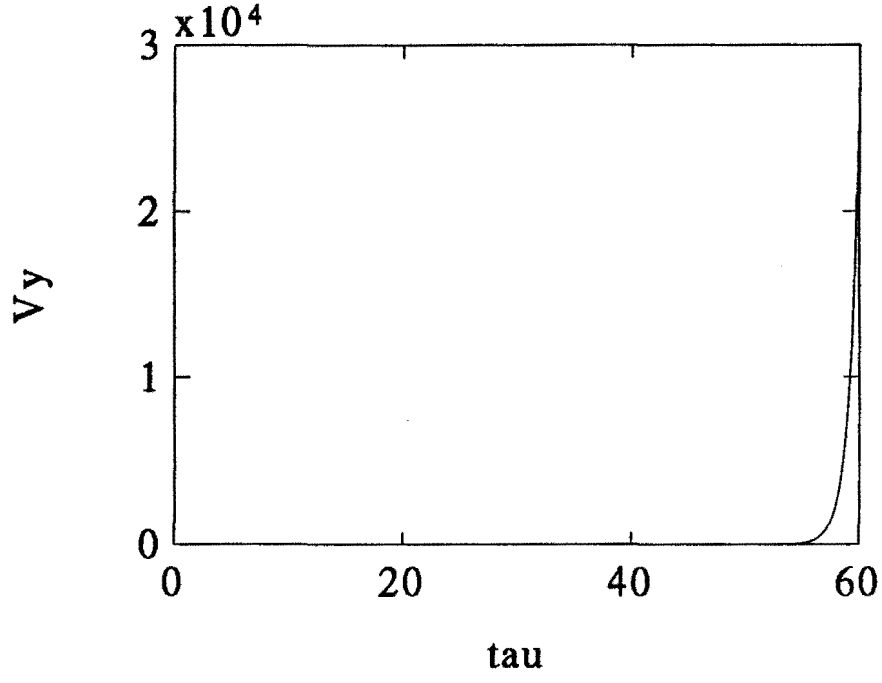
x10^4
3
2
1
0
Vy
0
20
40
60
tau

Fig. V.25

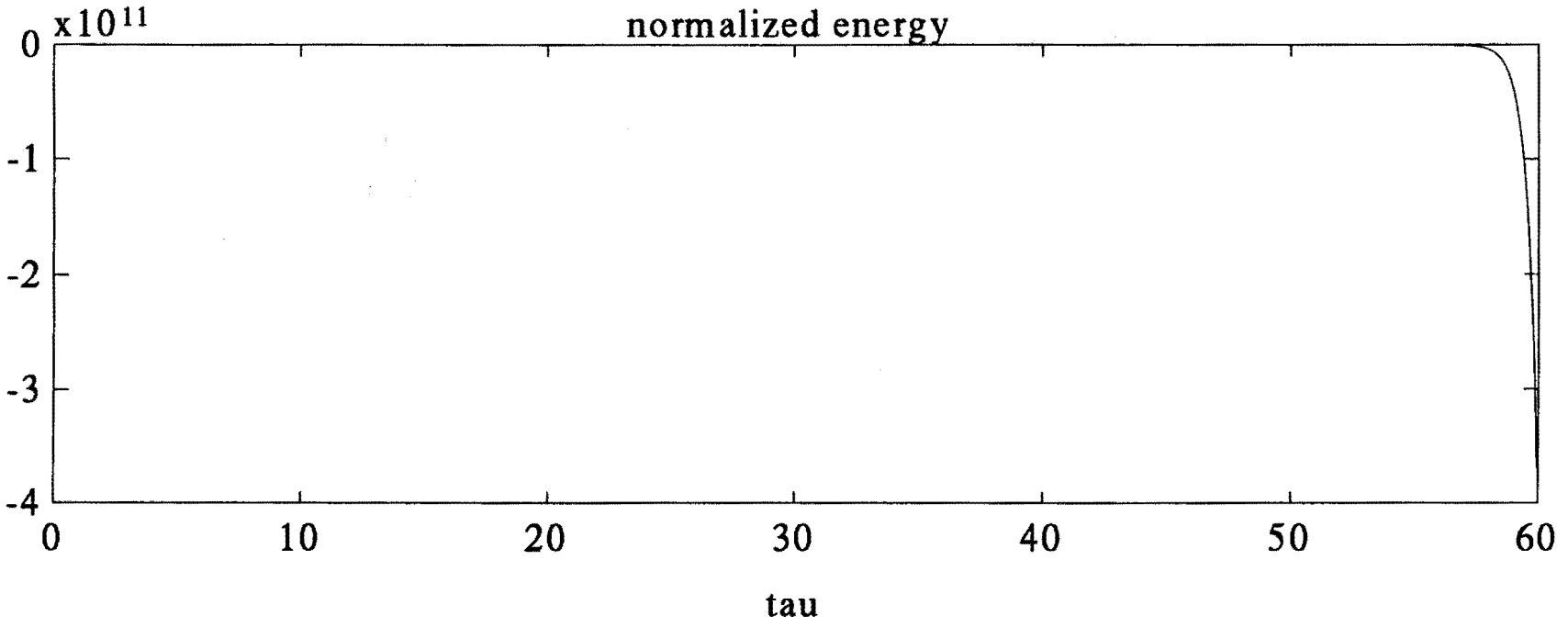
x10^11
normalized energy
0
-1
-2
-3
-4
0
10
20
30
40
50
60
tau

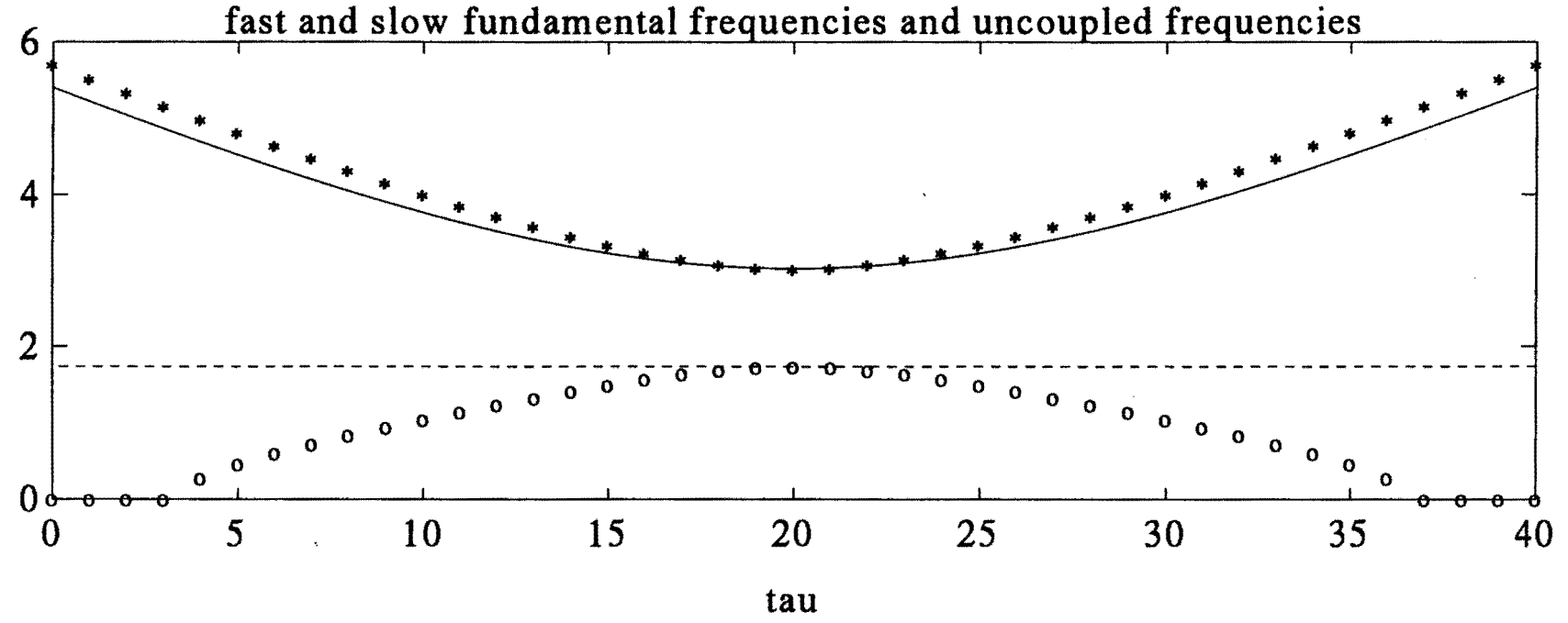
fast and slow fundamental frequencies and uncoupled frequencies
6
4
2
0
0
5
10
15
20
25
30
35
40
tau

Fig. V.26

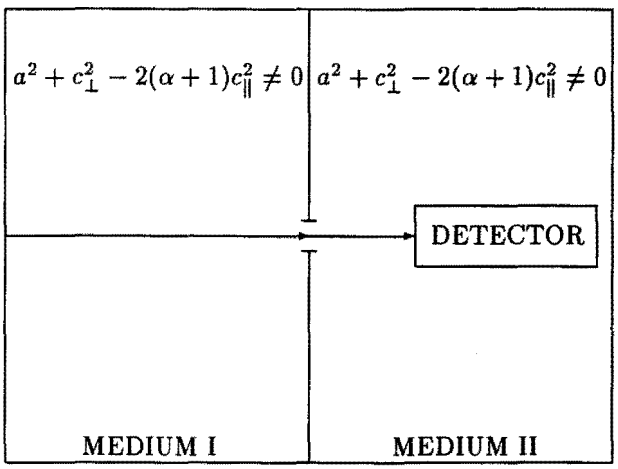
$a^2 + c_\perp^2 - 2(\alpha+1)c_\parallel^2 \neq 0$
$a^2 + c_\perp^2 - 2(\alpha+1)c_\parallel^2 \neq 0$
DETECTOR
MEDIUM I
MEDIUM II

Fig. VI.1

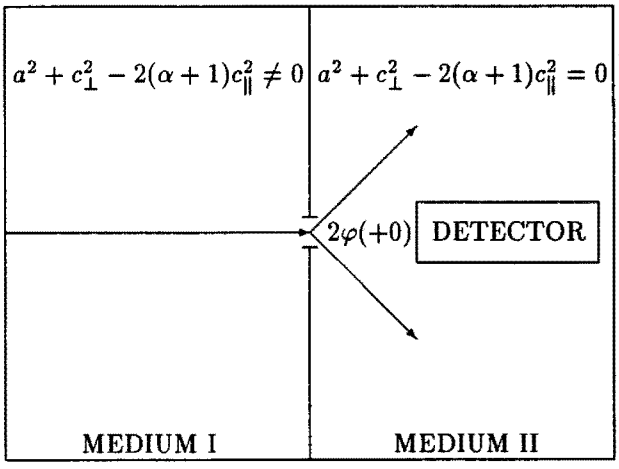
$a^2 + c_\perp^2 - 2(\alpha+1)c_\parallel^2 \neq 0$
$a^2 + c_\perp^2 - 2(\alpha+1)c_\parallel^2 = 0$
$2\varphi(+0)$
DETECTOR
MEDIUM I
MEDIUM II

Fig. VI.2